An Axisymmetric Linear/High-Order Finite Element for Filament Wound Composite Structures

by

Craig A. Rogers

Dissertation submitted to the Faculty of the

Virginia Polytechnic Institute and State University

in partial fulfillment of the requirements for the degree of

Doctor of Philosophy

in

Mechanical Engineering

APPROVED:

Charles E. Knight, Jr., Chairman

Norman S. Eiss, Jr.

Larry D. Mitchell

Robert M. Jones

Robert A. Comparin, Dept. Head

September 1987

Blacksburg, Virginia

An Axisymmetric Linear by High-Order Finite Element for Filament-Wound Composite Structures

by

Craig A. Rogers

Charles E. Knight, Jr., Chairman

Mechanical Engineering

(ABSTRACT)

The development of an axisymmetric linear by high-order finite element to model filament-wound structures is presented. The primary objective of this work was to develop a 'design code' to analyze filament wound spherical pressure vessels. In order to develop a design-oriented analysis capability which can produce accurate results rather quickly with reduced input-data requirements, the total number of system equations must be reduced. To accomplish this task, a linear by high-order element was formulated which uses a single high-order displacement field finite element to model the total thickness of an axisymmetric composite structure. The displacement order for the in-plane direction remains linear, while the transverse order is user selectable. Numerical integration for stiffnesses is evaluated with respect to varying material properties and lamina thicknesses in each individual element. Results from a computational economy study are presented showing potential time savings of 40 percent when compared to the conventional modeling scheme of using bi-linear elements. Actual test cases indicate that computation time savings may be as great as 55 percent when using linear by fourth-order elements and 45 percent when using linear by sixth-order elements. The accuracy of the element was evaluated by comparing the finite element results to elasticity solutions for isotropic, orthotropic, and filament-wound cylindrical pressure vessels. Most of the finite element results indicated a ± 3 percent maximum error of the stresses compared to the elasticity results. The new linear by high order element stress results were nominally within ± 2 percent of stresses calculated with conventional bi-linear elements. Comparisons of finite element results for an actual filament-wound spherical pressure vessel showed that linear by third- or fourth-order elements may be adequate for preliminary design purposes while the higher-order elements generally correlated better with the conven-

tional bi-linear elements. Also presented is an outline of the design code and sample results for spherically wound pressure vessels.

Acknowledgements

Whenever a task of the magnitude of a Ph.D. is finally realized, there are many people to whom a great deal of thanks must be expressed. First, I would like to thank Martin-Marietta Energy Systems, Fabrication System Development, Oak Ridge Y-12 Plant for their support of this work and in particular . I would also like to thank all my colleagues, the faculty, and the staff in the Mechanical Engineering Department for their assistance and support during all of my graduate years at Virginia Polytechnic Institute and State University. Especially the secretarial staff has been extremely patient and helpful with all of my last-minute requests.

I am most grateful for the encouragement, assistance, guidance, and patience of my major advisor, Dr. Charles E. Knight, Jr. Not only has he been the source of my inspiration during my six years at Virginia Tech and the reason I desired to pursue a Ph.D, but he has also been more than supportive to me during some difficult times. I will never be able to express the sincere appreciation my whole family wishes to offer to him for the understanding and support he has given me. Dr. Knight represents to me the type of engineer and gentleman that I will strive to become in the many years ahead in my career. I would also like to thank the other members of my committee for their assistance, Dr. N. S. Eiss, Dr. L. D. Mitchell, Dr. R. M. Jones, and Dr. R. A. Comparin.

Often times when one has completed a major milestone in his career, it is easy to forget the beginning. In my case, I owe a great deal of thanks to Dr. J. B. Jones for my beginning. Without

the assistance and encouragement he gave me five years ago, this dissertation never would have been begun. I am sincerely thankful for the opportunity to become an instructor in the Mechanical Engineering department. This experience has matured me as an engineer and as an educator. Dr. Jones represents the excellence in teaching that I hope to acheive.

The last faculty member that I would like to express my deepest appreciation to is Dr. H. H. Mabie. Dr. Mabie took me 'under his wing' when I first became an instructor and I have felt that he has been my mentor. While taking several graduate classes from Dr. Mabie, I developed a great deal of respect for him and I have always been impressed with the patience and respect that he reserves for his students. I hope that I will be able to foster those traits in my own teaching style. Dr. Mabie has been a inspiration to me, and I am proud to claim that I am a student of Dr. Mabie.

Naturally, over the course of six years of graduate study I owe a great deal of thanks to the many friends that have helped me and my family in numerous ways, especially

and . I will always be indebted to for all the time and effort he contributed to helping me finish my dissertation on time. help in debugging code in the last critical moments is appreciated more than I can express. I am particularly thankful to my friends; for his many insightful words of wisdom on how to live life and for giving me the ability to experience life from the world above the Earth, for being my motivation and role model during the time that I learned how to balance all parts of my life, and for the long runs, marathon training and friendship that helped me cleanse my mind and soul for a short time each day so that I could be more productive (you have all changed and enriched my life), and the many graduate students that I have had the pleasure of becoming acquainted with over the years. Lastly my whole family is grateful for the friendship and love that we share with . Their Christian way of life has been enlightening and refreshing to my wife and I, and especially our children. We will always hold a special place in our hearts for the Godparents of our daughter and hope that our paths will again meet in the future. To , I will always think of these Ph.D. years as the time I made my dearest friend. I wish you the best in the future and may God bless you.

Seldom are works of this magnitude solo endeavors. In this case, at least one other name deserves to be on the title page, the name of my dear wife, . I cannot express the love and respect I have for all her efforts in keeping our home and lives together, and I hope that over our lifetime together that she will always be aware of the most sincere admiration that I hold for her. Lastly, I need to thank and apologize to my two children, both born during my Ph.D years. I thank them for their uncanny understanding when Daddy had to go to work in the evenings instead of playing with them. I apologize to you both for not spending the amount of time with you that I wanted to during your early years. I offer to you, a promise that I will work as diligently to become a good daddy as I have to receive my Ph.D.

Table of Contents

List of Illustrations

List of Tables

1.0 Introduction and Background

1.1 Introduction

The analysis of filament-wound composite structures is typically very complex, and in order to accomplish a reasonable analysis, considerable detail of the fabrication pattern of the winding process usually must be incorporated. The application of the finite element method to the analysis and design of filament-wound composite structures makes what would normally be an intractable problem one that can be solved. The typical analysis scheme is to use relatively simple elements, i.e. linear, to model each layer of the composite structure, thereby necessitating the use of numerous elements to model the total thickness of a multi-layer laminate. Considering the number of elements needed along the in-plane direction, this technique results in a large number of elements needed to sufficiently model the structure and thus generates a large set of system equations. Because of the large number of equations, the data input and computer computational time are consequently large also.

The motivation for initiating this research program was the desire for a 'design-oriented' analysis program for filament-wound spherical pressure vessels. The conventional finite element modeling scheme and analysis algorithms require such a large amount of computer computation

time that it essentially prohibits its use as a design tool. The typical finite element mesh utilizing conventional finite elements for a spherically wound pressure vessel involves several hundred elements and nodes in order to sufficiently model the detailed winding pattern and generate the stress resolution necessary to make engineering judgments about the performance of the structure. If the computation time could be reduced significantly, a design engineer could investigate numerous design alternatives, i.e., different size structures, different winding patterns, different materials, and different loadings on the structure in order to create the most desirable design. This research program was concerned primarily with the computation time involved in analyzing this particular class of structures. The current finite element technique and modeling scheme that utilizes conventional quadrilateral elements performs the stress analysis satisfactorily and generate results that are sufficiently accurate. Therefore, the objective is simply to investigate a novel concept of formulating a 'high-order composite element' that could be incorporated into a new program to perform the same functions as the current analysis code but to do so more efficiently and without seriously sacrificing accuracy.

The concept that was proposed is to use a high-order finite element, one with enough side nodes along the element to sufficiently model the transverse elastic behavior of a composite laminate, to design filament-wound spherical pressure vessels with a finite element program and do so more efficiently than with conventional finite element techniques. The element would have to be able to account for the various material properties (fiber orientations) and layer thicknesses of the individual laminae. This single high-order finite element could then replace a large number of linear elements that are currently needed to model the total thickness of composite laminates and do so with fewer nodes and therefore fewer system equations. The element that is to be developed for this purpose will be linear in the in-plane direction and higher-order in the transverse direction, however, the element will be referred to as simply a 'high-order element' realizing that the displacement fields are different in the two directions. The high-order composite elements will be specified with reference to the order of the transverse displacement field only, i.e., a linear by fourth-order element is referred to as a 'fourth-order element'.

In the initial stage of this research program, a theoretical computational study is needed to determine the potential efficiency of the high-order formulation. The theoretical study will concentrate on two of the most important computational phases of the finite element solution method; i) the generation of the element stiffness matrices, and ii) the subsequent solution of the structure stiffness equations. The formulation and development of the high-order element and supporting finite element processor will begin once the computational studies indicate the potential for computational savings with the new element. After implementation of the composite element in a useable finite element program, the theoretical computational study will be verified by a numerical computational study that utilizes the actual element and finite element program to solve carefully selected problems. The computational study using the newly developed finite element program will determine the Central Processing Unit (CPU) time associated with the four main portions of the solution method; i) input phase, ii) generation and assembly of the structure stiffness matrix, iii) triangularization of the structure stiffness matrix and the calculation of the nodal point displacements, and iv) calculation of the stresses.

An accuracy study to follow the development of the element is needed to fully understand the applicability of the newly developed element. The accuracy study should be designed to verify the results of the finite element program with i) elasticity solutions for internal pressure-loaded cylinders and ii) conventional four-noded isoparametric finite element solutions. The models selected for this study should included geometries and materials that have some practical significance as well as known elasticity solutions, namely; i) homogeneous isotropic cylinders, ii) homogeneous orthotropic cylinders, iii) non-homogeneous orthotropic cylinders (filament-wound cylinders), and iv) non-homogeneous isotropic cylinders.

Lastly, upon completion of the computational study which will demonstrate the level of the potential economy of the element and the accuracy study which will show the effectiveness and limitations of the element, the high-order element can then be incorporated in a 'design code'. The design code shall be constructed so that comparisons of the high-order element models and the conventional model can be made. The mesh generator will be created so that the same user defined input variables are needed as with the existing mesh generator and only two additional pieces of

information will be needed, i) order of the radial displacement field and ii) the internal pressure (the existing mesh generator does not create the applied nodal load data). By using the same data format as used with the existing code, anyone with experience with the existing code will be able to use the new program and all the existing data files used with the existing finite element analysis code may be used without modification in the new, more efficient, design-analysis code.

1.2 Overview

Presented in this dissertation are the formulation, evaluation and implementation of an axisymmetric high-order finite element for modeling filament-wound composite structures. The approach used in this research effort is explained above. Each phase of the research program is presented beginning with the theoretical formulation of the element in Chapter 2. The formulation of the stiffness and system equations for the high-order element is presented along with the classical displacement-based formulation for conventional bi-linear elements for comparison and background. The unique features of the new formulation are explained in detail.

The computational time study is presented in Chapter 3. The computational studies consisted of both a theoretical and actual finite element study. The theoretical study was used as the basis for begining the formulation and continuing to the implementation stage. The results from the finite element study show precisely where the computational savings are being made and present some interesting possibilities for future work which will be discussed in Chapter 7.

The results from two accuracy studies are presented in Chapter 4. The high-order element was evaluated with respect to elasticity solutions and conventional bi-linear finite elements. Models with varying levels of complexity were used in the accuracy studies, all of which had known elasticity solutions. The theoretical development of the elasticity solutions is also presented for plane-stress and plane-strain multi-layer pressure-loaded cylinders.

Implementation of the high-order element in a 'design code' for filament-wound spherical pressure vessels is discussed in Chapter 5. The finite element program was created by modifying a relatively simple finite element program which will also be described in Chapter 5. This base program and the solution scheme used to solve the system equations are discussed in some detail. The pre-processing code which consists of two separate programs, a mesh generator and a coupling program which creates the data file for the finite element processor, is also presented. Lastly, the actual finite element processor HICOM (HIgh-order COMposite finite element program) and the novel high-order axisymmetric composite element are discussed along with several of the unique algorithms used in its implementation. Several of the algorithms used in implementation of the composite element can be used in conventional finite element programs and may lead to increased capabilities and/or efficiencies. Contained in Chapter 7 are the conclusions and recommendations for future work.

1.3 Literature Review

The development of a high-order element capable of modeling axisymmetric composite laminates requires certain aspects of several technical areas be incorporated, i.e., finite elements, composite materials, and filament-wound structures. Therefore, this literature review will consist of four separate parts, i) Historical, ii) Full Field Solutions, iii) Filament Wound Structure Analysis, and iv) High-Order Theories (Shear Deformation Plate Theories and Finite Elements), each highlighting past and present work. The advances that have been made over the years in the analysis of composite laminates are briefly described in the historical section. The relative infancy of the science is particularly striking.

The finite element method is a numerical technique that is sometimes referred to as a 'full-field solution' method. Because of the complexities that often accompany stress analysis of laminated structures, i.e., non-homogeneous material and anisotropic material properties, finite el-

ement solutions have become increasingly more common. Very few theoretical solutions exist for laminated structures and those that do are for relatively simple geometries, e.g., plates and shells. Again, a brief presentation of some of the finite element formulations used to analyze composite structures is given along with a few applications of the technique.

The axisymmetric high-order composite element that will be described in Chapter 2 was developed in order to design and analyze filament-wound spherical pressure vessels. The third section of the literature review will show the range of activity and interests in analyzing filament-wound structures. The high-order composite element, or a variation of it, could be used in any of the studies that are presented.

The concept that is incorporated in the formulation of the high-order composite element is to use a high-order displacement field in a single finite element to simulate the transverse displacement of a composite laminate. This basic idea has been used with several variations to better analyze composite laminates. A significant amount of work in the literature can be found on high-order shear deformation theories relating to plates and shells. This work will be reviewed as it represents the foundation on which the 'continuum approach' used in this study was created. Only one paper was found with a description of a solution method similar to the one used in formulating the high-order composite element presented in this dissertation. The continuum-based finite element method paper was published in 1985, the same year that first paper based on the work presented in this dissertation was published, and will be reviewed in some detail.

Included in the last literature review section is some relatively recent work directed towards high displacement order finite elements. Even though none of the work presented in this section of the literature review considers composite or nonhomogeneous materials, several of the results and conclusions parallel the results that will be presented in Chapter 4 concerning the accuracy of the element.

1.3.1 Historical

The early work in the analysis of composite laminates was prompted by the desire and need to design efficient plywood structures. In 1953, Smith [1] [1] presented a technique to compute the effective shear modulus of plywood when a state of plane stress was assumed. One of the earliest complete works with detailed solutions to a wide class of orthotropic and anisotropic problems is the monograph *Anisotropic Plates* (1947) written by Lekhnitskii [2]. In the preface to his first edition, he outlines the utility of his work as he perceived it at the time.

> As structural elements, anisotropic plates, i.e., plates in which resistance to mechanical actions is different for different directions, find wide application in modern technology. Such plates include aircraft plywood, delta wood, textolite and other materials. The experimental studies of a material such as plywood show a great difference in elastic moduli and flexural rigidities between the principal directions, i.e., parallel and perpendicular to the grain of the external layer. ... Not only will civil engineers need to calculate stresses and strains in anisotropic plates, but also physicists who deal with plates made of crystals (for example, quartz crystals). ...

His work included solutions to bending of plane anisotropic bars and curved beams, stress distribution in an elastic body, stress distribution in plates with holes, bending of thin plates, transverse vibration of anisotropic plates, and stability of reinforced plates, to name but a few. The work of Lekhnitskii is truly remarkable and insightful when one considers the time and environment in which he developed many of the solutions that are now considered classical. Other classical works include Reissner and Stavsky's [3] technique which included coupling between the in-plane extension and transverse bending of plates. This work represents the foundation of the so-called 'lamination theory'. Ashton and Whitney [4] present a detailed description of lamination theory and an extension to dynamic and stability analysis. Jones [5] also discusses lamination theory in complete detail.

---

[1] Numbers in brackets refer to references at the end of this dissertation.

1.3.2 Full-Field Solutions (Finite Element Solutions)

The solutions referred to here as 'full field' are so called because the problem is not limited by assumptions such as those imposed in lamination theory. Thus, the full set of stresses may be solved for, as well as the displacements for the complete physical structure that is modeled by some mathematical means. Even though these solutions have been dominated by finite element work, some of the early finite difference investigations are also noteworthy.

Pipes and Pagano [6] and Pipes [7] utilized a finite difference technique to solve the quasi-three-dimensional elasticity equations for composite laminates. Interlaminar stresses were evaluated.The capability for thermal effects was also included.

Isakson and Levy [8] used the finite element method to model a laminate in a state of plane stress. The plies were modeled as orthotropic layers separated by isotropic shear layers. Interlaminar normal stresses were omitted from the study. The technique of using an isotropic shear layer had been previously reported by Puppo and Evenson [9], but not in conjunction with the finite element method. Subsequently, Levy, Armen, and Whiteside [10] extended the work of Isakson and Levy for plastic deformation of the shear layer. A Ramberg-Osgood representation for boron-epoxy was used as a model for the nonlinearity of the shear layer. Results were presented for the interlaminar stresses around holes and the effects of stacking sequence were discussed.

Herakovich and Brooks [11] used the finite element method to examine the stress distribution in uniaxial and cross-ply laminates subjected to thermal and uniaxial strain loading. Interlaminar stresses were shown to be significant near the free edge. Herakovich [12] later showed the effects of stacking sequence on interlaminar thermal stresses. His analysis also indicated that the overall strength of a laminate is dependent on the stacking sequence. Lin[13], Dana [14], and Dana and Barker [15] all used a 72 degree-of-freedom, three-dimensional orthotropic isoparametric finite element to model composite laminates. All results were linear elastic, and no thermal effects were included in the analysis. Stresses were calculated near holes and free edges. Comparisons of hole shapes and sizes were made with respect to the resulting interlaminar stresses.

Rybicki, et al. used several variations of the finite element method to examine the behavior of composite structures. They include i) complementary energy methods [16], ii) stress function methods [17], and iii) the standard displacement formulation [18,19]. Rybicki and Schmueser [20] used the three-dimensional finite element program SAP IV to predict stress distributions near holes in linear elastic laminates. Stanton, et al. used a parametric cubic modeling system [21] to analyze nonlinear behavior in laminates.

Various non-displacement finite element formulations have also been used to study the behavior of composite structures and laminates. Wang, Mandell and McGarry [22] have all used the hybrid stress formulation of Pian [23]. Several problems exist with this approach. In the boundary layer, steep stress gradients are known to be present, therefore, in the hybrid stress approach a significant number of high-order terms must be included in the assumed stress polynomial. The analysis is also complicated by the fact that a large number of unknowns per element are created by the need to include the high-order stress polynomial in the analysis. This approach does seem to have some utility for investigations of fracture mechanics and laminates containing initial flaws, although treatment of nonlinearities may be difficult.

Very recently, some work has begun to be published on the use of high-order finite elements to model composite laminates and in particular the transverse elastic behavior of laminates. At this time, most of the effort reported in the literature is directed towards elements that are based on high-order transverse shear plate or shell theories (discussed in section 1.3.4.1). One notable exception is presented in reference [24] which uses a continuum approach similar to the method used in this development of the high-order composite element and is also explained in section 1.3.4.1.

1.3.3 Filament-Wound Structure Analysis

Filament winding has been an active growing manufacturing process for more than thirty years. Filament-wound composites have ranged from rocket motor cases and launch tubes in the early years to automotive leaf springs and drive shafts today. A large amount of emphasis has been placed on modeling the fabrication process in order to predict the residual stress and strain state upon completion of construction. These models generally involve the use of finite element analysis, static and thermo-mechanical, as well as other mathematical techniques to model the flow of resin, etc.. This review of the literature is intended to provide a sampling of the range of activities in the field of filament-wound structure analysis.

In a filament-wound composite structure, the effects of varying winding tension during the fabrication process on the overall strength of the structure was examined by Portnov and Spridzans [25]. They showed that the cure modulus of elasticity and the burst pressure of rings increased with higher winding tension until cracks were formed because of the increasing radial stresses. The interaction between winding tension, mandrel stiffness, and shell thickness for filament-wound cylinders has also been studied by Dobie, Leavesly and Knight [26].

Leavesley's Ph.D. dissertation [27] represents a unique approach to analyzing the fabrication stresses of filament-wound spheres. Leavesley created a program to predict the potential strength degradation of filament-wound spherical pressure vessels during the fabrication process. The pre-processing capabilities that he used for his analysis were taken with slight modifications to become a part of the design program that is described in Chapter 5.

The thickness profile of the spherical pressure vessel's composite layers were calculated using a thickness profile/pattern simulation program (which will be described in detail in Chapter 5). The thickness profile was then used by a finite element mesh generating program to model the composite structure with four-noded isoparametric quadrilateral elements, in which each layer of the structure is modeled with at least one element through its thickness. The main feature of the finite element program was the incremental construction and loading of the model. However, the

final model is typical of finite element models used to analyze filament wound spherical pressure vessels.

1.3.4 High-Order Theories

1.3.4.1 Transverse Shear Deformation Plate and Shell Theories

The shear deformation theories found in the literature can be grouped into two classes; i) stress-based theories, and ii) displacement-based theories. The stress-based transverse shear deformation plate theory is credited to Reissner [28-30]. The theory is based on a linear distribution of the in-plane normal and shear stresses through the thickness. The distribution of the transverse normal and shear stresses across the thickness of the plate is determined from the equilibrium equations.

The early work in the formulation of displacement-based theories was done by Basset [31], who represented the displacement field across the plate thickness with a high-order polynomial function. Based on Bassset's representation of the displacement field, Hildebrand, Reissner and Thomas [32] developed a variational consistent first-order theory for shells.

By using the displacement representation for a first-order theory, Mindlin [33] extended Hencky's theory of isotropic plates to the dynamic case. The basic idea of the displacement-based first-order shear deformation theory came from Hildebrand, Reissner and Thomas [32] and Hencky. Many extensions and applications of the two classes of theories followed these works and have been reported in the literature.

Gol'denveizer [34] has generalized Reissner's theory [28-30] by replacing the linear distribution of stresses through the thickness by a distribution represented by an arbitrary function. Librescu [35,36] made the first attempt to formulate a higher order theory of anisotropic plates and shells of general shape.

The second- and higher order displacement-based shear deformation theories have been presented by several investigators. Levinson [37] and Murthy [38] presented a third-order theory that assumes transverse inextensibility. However, both authors used the equilibrium equations of the first-order theory in their analysis, so they were variationally inconsistent. As a consequence,

the higher order terms of the displacement field are accounted for only in the calculation of the strains but not in the governing differential equations or in the boundary conditions.

Recently, Reddy [39-41] corrected these theories by deriving the governing differential equations by means of the virtual work principle. The theory presented in [39] accounts for the von Karman strains but is limited to orthotropic plates, while that in [40] deals with the small deflection theory of laminated plates. The third-order theory presented in [41] accounts for moderately large rotations in the same manner as described by Librescu and Schmidt [42].

With the advent of the numerous theoretical treatments of high-order shear-deformable laminated plate and shell theory, the same concepts were then applied to finite element formulations. Murakami [43,44] presented a refinement of the theory which improved the accuracy of the in-plane response by including a zig-zag function to approximate the thickness variation of the in-plane displacements. This technique allowed for somewhat of a simplification in that the in-plane displacement response was modeled with a linearly varying function within each layer which, in turn, was approximating a high-order variation through the entire thickness of the laminate. A comparison of the in-plane displacements and stresses predicted by the proposed theory with Pagano's [45] exact solution of laminated plates in cylindrical bending indicates that inclusion of the zig-zag function predicts the in-plane responses more efficiently then the inclusion of smooth non-linear functions.

A variation of this method has also been presented by Natarajan [24] which is based on continuum principles rather plate or shell theory. The difference between the two classes of solutions is that the plate and shell theories utilize the laminate properties, i.e., extensional stiffness, bending-extension coupling, and bending stiffness, which in essence, gives a homogeneous representation of the elastic behavior of the laminate and the displacement field then becomes a function of only the laminate properties. The continuum approach, however, accounts for the influence of each layer on the stiffness and the displacement field is based on this effect. Natarajan's [24] work published in 1985, uses a similar method to that described in Chapter 2 and published by Rogers, Knight, and Dodge in 1985 [46]. The continuum approach to the finite element formulation means that the evaluation of the volume integral to determine the element stiffness matrix is performed

on a layer-by-layer basis. The unique feature of Natarajan's work is the method used to evaluate the volume integral. The integral that defines the element stiffness is a function of the material properties which may change from layer to layer and, therefore, creates a discontinuous function. The element stiffness matrix is calculated by evaluating the integral on a layer-to-layer basis rather than integrating over the entire thickness of the laminate. Through the use of a transformation of the variable of integration, a local coordinate representing the transverse direction of the laminate, the integral is written in terms of a summation of the integrals over each layer which accounts for the varying material properties and the various layer thicknesses. No information was given as to the order of the element used except that it was a 20 noded three-dimensional element. It was also unclear as to the order of the integration. It was stated in the paper that a "27 point rule" was used but it was unclear if that was on an element or layer basis.

1.3.4.2 High-order Finite Elements

A basic concept used in the finite element method for elastic continua is that the solution represents the minimum potential energy with respect to the set of system equations that are written in terms of nodal point displacements and the assumed displacement field approximations. The accuracy of the solution is dependent on the approximations made in modeling the structure which is related to the size of the mesh and the order of the assumed displacement functions. A particular choice of mesh size and polynomial order may not yield a solution to within the desired accuracy level. Thus, it is necessary to have the ability to improve the quality of the approximations made. This is generally accomplished by increasing the number of degrees-of-freedom either by using more elements and thus more nodes (more refined mesh) or by keeping the mesh size constant and increasing the number of nodes that comprise an element (increased polynomial order of the assumed displacement field).

There are three basic approaches that can be used to increase the number of degrees of freedom. The first approach, called the *h*-version, is where the order of the assumed displacement

field is held constant and the mesh size h is reduced to obtain the desired accuracy. The h-version has been investigated theoretically and practically for many years. In the p-version, the mesh is fixed, and the order of the polynomial p that describes the assumed displacement field is increased in order to reduce the approximation error. The development of the p-version is very recent. The h-p version combines the h- and p-versions.

The first known theoretical study of the p-version element was published by Babuska, Szabo and Katz in 1981 [47]. The h-p version was first discussed by Babuska and Dorr [48] also in 1981. The main concept being addressed in those early works was the hypothesis that it was possible to achieve an exponential rate of convergence with the combined efforts of h and p refinements to the finite element method.

The p-version in three-dimensions was studied by Dorr and his work presented in 1984 [49]. Implementation aspects of the p- and h-p version techniques are discussed by Babuska, Gui, Guo, and Szabo [50]. It has been shown by Babuska, Szabo, and Katz [47] that the rate of convergence for the p-version cannot be worse than that of the h-version with a quasi-uniform mesh. However, the most efficient means of achieving convergence is with the h-p version which displays an exponential rate of convergence with respect to the number of degrees-of-freedom. The h- and p-versions have only a polynomial rate of convergence [51,47] with the p-version generally converging at least twice the rate of the h-version.

The implementation of the p-version element solution method can be coupled with near optimal control of the error when feedback information is created [52]. With information generated from p convergence data, decisions can be made which indicate if the mesh should be refined or the polynomial degree of the elements should be increased.

The discussions that are included in the presentation of the formulation and implementation schemes of the p-, h-, and h-p version solution techniques center on the efficiency of this solution method. The definition of efficiency in the references cited is related to the convergence rate of the solution. In order to appreciate the effect of this method, a relatively coarse mesh with relatively low-order elements are used and the program then solves for the state of stress and computes several quantities related to accuracy. Based on these results, the mesh, order of the elements, or

both are refined and another solution created. This process continues until 'convergence' has been achieved. This is an extremely useful technique. However, for very large structures the computation time for a single static analysis may be hours which would probably make this approach less attractive. The *p*- and *h*-version techniques are 'designed' to save the engineer time in the modeling phase and in the process 'charge' that time to the solution phase.

The work that is presented in the remainder of this dissertation is based on the opposite philosophy, which is to force the engineer to make sound judgements about the refinement needed in the model and select the appropriate order element to efficiently solve the static analysis (minimum computation time). All of the work published on *p*-order elements has dealt solely with homogeneous isotropic materials which is a significant departure from the utility of the element developed and presented in this dissertation which is intended for (but not limited to) nonhomogeneous orthotropic laminates. However, there are some parallels between these efforts, primarily in the accuracy evaluation of the elements. Some of the accuracy concepts presented in the references relating to *p*- and *h*-version techniques will be presented in Chapter 3.

2.0 Element Formulation

Most common elements that have been used in finite element programs are based upon the assumption of a simple displacement field for the continuum within the element. This assumed displacement field is typically linear for the simplest of all elements and the literature does not contain a great deal of information on elements using polynomials of order greater than three. Recently Babuska, Szabo, and others [47-52] have contributed greatly to the literature concerning higher order elements (see section 1.2.4.2). The use of higher order elements have advantages over their lower order counterparts [53]. In common usage, the term 'higher order element' includes elements with 'extra degrees-of-freedom' as well as elements with corner and side nodes and only the essential degrees of freedom at each node. The primary advantage of higher order elements is that they provide good accuracy in a coarse mesh. They also have certain disadvantages [53]. The input data that describes element shape can be cumbersome. By enforcing a higher order of inter-element continuity than is necessary, the structure appears to be more stiff than reality, which somewhat negates their benefit. However, it appears that higher order elements have begun to be very popular for the analysis of composite structures.

The use of higher order finite elements to model composite structures is essentially a numerical equivalent to the higher order transverse shear plate theories discussed in section 1.2.4.1. Higher order theories are needed so that relatively thick plates and shells can be evaluated properly.

The linear theories (first order shear deformation theory or a single linear finite element through the thickness) are adequate for thin plates and shells. Finite element analysis of thick composite plates was first accomplished by using several linear elements through the thickness of the structure. If a sufficient number of linear elements were used through the thickness of the laminate, the nonlinear displacement variation that actually exists through the thickness is approximated. In order to reduce the error of this approximation, a large number of elements and degrees-of-freedom is necessary. This approach is costly from a computational standpoint. Higher order elements are of interest for analyzing composite structures because the nonlinear transverse displacements that are caused by the shear deformation effects are more closely approximated. Utilizing the higher order elements will allow for a more accurate approximation of the transverse displacement field than acheived with fewer degrees-of-freedom.

In this chapter, the formulation of the high-order composite element will be presented. The formulation of the composite element is displacement based and uses the Lagrangian family of interpolation functions. In order to illustrate the unique features of this element and its formulation, the classical displacement formulation will be presented. A more complete discussion and explanation of the specifics involved in the classical formulation can be found in several finite element texts [53-57]. The classical formulation that follows is precisely that which Leavesly [27] used in his 'fabrication process analysis program' (see section 1.2.3). and is referred to as the 'conventional' approach throughout this dissertation.

2.1 Classical Finite Element Formulation

The basic concept of the finite element technique, as in most numerical procedures, is to discretize a complicated continuous system into well-defined portions for which the elastic behavior is known and may be expressed analytically by exact or approximate functions. There are several approaches used in solving a continuum problem by the finite element method. The majority of

finite element approaches are based on the principle of virtual work (or its equivalent, the principle of minimum potential energy). In solid mechanics problems the continuum is divided into a finite number of sections called elements. The elements are assumed to be interconnected at a discrete number of nodal points situated on their boundaries. The displacement of these nodal points are the unknown parameters of the problem. A set of functions is chosen to define uniquely the state of displacement within each element in terms of its nodal displacements. The constitutive properties of the material are used to determine the stress state throughout the element from the strains caused by displacements plus any initial strains. A degree of freedom of a finite element is defined to be a displacement or rotation of each node of the element. Thus, an element with n degrees of freedom will have n equations which relate nodal forces to nodal displacements through the stiffness of the element coefficients. The equations relating the nodal forces to the nodal displacements may then be written as:

$$\begin{aligned} K_{11}d_1 + K_{12}d_2 \ldots K_{1n}d_n &= F_1 \\ K_{21}d_1 + K_{22}d_2 \ldots K_{2n}d_n &= F_2 \\ &\ldots \\ &\ldots \\ &\ldots \\ K_{n1}d_1 + K_{n2}d_2 \ldots K_{nn}d_n &= F_n \end{aligned} \qquad [2.1]$$

where

d_i = i^{th} degree of freedom nodal displacement

F_i = i^{th} force or moment applied to the element

K_{ij} = stiffness coefficients

The equations of 2.1 are gathered into matrix form to give the relationship

$$[K]\{d\} = \{F\} \qquad [2.2]$$

where $[K]$ = structure stiffness matrix

$\{d\}$ = vector of nodal displacements

$\{F\}$ = vector of element nodal forces

In this approach, some approximations are involved. In general, there are six basic assumptions, approximations or consequences of these assumptions that are made. It is important to note that the significance of each of these approximations varies for different types of finite elements. An element that performs well in one situation may be unsatisfactory in another area. The six approximations are [53]:

1. Equilibrium is usually not satisfied within an elements unless it is in a state of constant-strain. In a varying strain field and for a given number of degrees-of-freedom, a mesh of rectangles usually gives more accurate results than a mesh of triangles.

2. Equilibrium is usually not satisfied between elements.

3. Equilibrium of nodal forces and moments is satisfied. The structural equations given in Eq. 2.2 represent the nodal equilibrium equations. Therefore, the solution vector $\{d\}$ is such that the resultant forces and moments (if some are allowed as a degree-of-freedom) applied to each node are zero.

4. Compatibility is satisfied within elements if the assumed displacement field is continuous.

5. Compatibility may or may not be satisfied along interelement boundaries.

6. Compatibility is enforced at nodes which simply means that adjoining elements are connected to one another at the nodes.

"In general, the objective is to select an element realizing that it may violate the equilibrium and compatibility requirements of an exact solution but by modeling the structure with more and more

elements or degrees-of-freedom the violations will tend toward zero" [47]. Convergence is typically guaranteed by elements that have a continuous displacement field within the element and the element must be able to assume a constant state-of-strain. The choice of the undeformed element shape and the form of the displacement function will affect the degree of approximation for each specific case.

The most common element generally chosen to be used in finite element models of spherical pressure vessels is an axisymmetric, four-noded, two-dimensional, isoparametric element capable of handling both isotropic and orthotropic materials. The term isoparametric refers to the class of finite elements that use the same interpolation function for i) geometrical mapping transformations from the global coordinate system to the natural coordinate system and ii) the assumed displacement field. The isoparametric element maps the arbitrarily shaped (within reasonable bounds) quadrilateral in the r-z plane of the axisymmetric coordinates (r,z,t) to a square element in a natural coordinate system (ξ,η) as shown in Fig. 1. The mapping parameters are called shape functions. When mapping parameters are the same for the geometry mapping as for the displacement mapping of displacements within the element, the element is called isoparametric.

The chosen displacement function for the 'bi-linear' element is a polynomial in terms of the local or natural coordinates, ξ and η. Equation 2.3 can be used to relate the actual global coordinates to the natural coordinate system or to calculate the displcements, u and v, at any point within the element (locations ξ,η) when the nodal point displacements are known. The displacement functions are formed by using linear displacement functions in each of the two directions within the element, thereby assuring compatibility along adjoining element boundaries.

$$u = a_1 + a_2\xi + a_3\eta + a_4\xi\eta$$
$$v = a_5 + a_6\xi + a_7\eta + a_8\xi\eta \qquad [2.3]$$

where u and v = displacements in the global coordinate system

ξ and η = natural coordinates

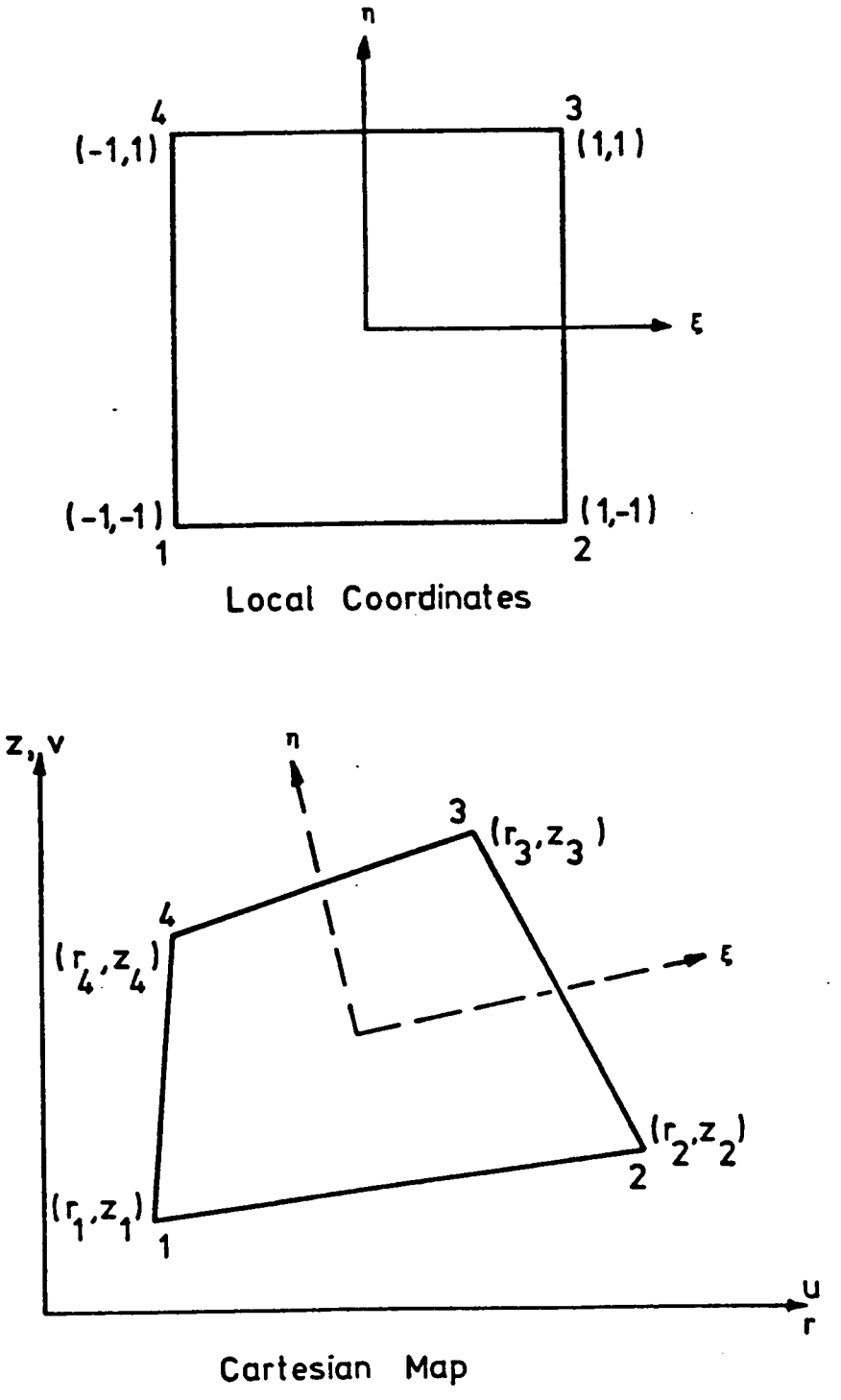

Figure 1. Mapping of an Element from the Global Coordinate system to the Natural Coordinate System

Since the element is square in the ξ, η coordinate system, for the displacement function given in Eq. 2.3, compatibility is also satisfied along interelement boundaries as the element sides remain straight when the element is deformed. This displacement function satisfies the equations of equilibrium at the nodes of the element and within the element, but not along the element boundaries.

The shape functions are defined in the natural, or local, coordinate system and represent surfaces defined over the isoparametric element such that each shape function has unit value at one node and zero at all other node points. The relationships between the *r-z* coordinates and natural coordinates are

$$r(\xi, \eta) = \sum_{i=1}^{4} N_i r_i$$
$$z(\xi, \eta) = \sum_{i=1}^{4} N_i z_i \qquad [2.4]$$

where $r(\xi, \eta)$, $z(\xi, \eta)$ = *r-z* coordinates of any point located in natural coordinates

r_i , z_i = node point coordinates in *r-z*coordinates

N_i = Lagrangian shape function

The relationships for the displacements between the two coordinate systems are similarly stated

$$u(\xi, \eta) = \sum_{i=1}^{4} N_i u_i$$
$$v(\xi, \eta) = \sum_{i=1}^{4} N_i v_i \qquad [2.5]$$

where $u(\xi, \eta)$, $v(\xi, \eta)$ = displacements of any point located in natural coordinates

u_i , v_i = node point displacements in cartesian coordinates

Expressed in matrix form

$$\begin{Bmatrix} u(\xi,\eta) \\ v(\xi,\eta) \end{Bmatrix} = \begin{bmatrix} N_1 & 0 & N_2 & 0 & N_3 & 0 & N_4 & 0 \\ 0 & N_1 & 0 & N_2 & 0 & N_3 & 0 & N_4 \end{bmatrix} \begin{Bmatrix} u_1 \\ v_1 \\ u_2 \\ v_2 \\ u_3 \\ v_3 \\ u_4 \\ v_4 \end{Bmatrix} \quad [2.6]$$

$$\{u\} = [N]\{d\} \quad [2.7]$$

where $\{u\}$ = vector of displacement components in the element field

$[N]$ = matrix of shape functions

$\{d\}$ = vector of nodal displacements

The original development of the displacement-based finite element method was carried out using physical considerations and was basically an extension of the matrix displacement analysis of truss and beam structures. However, the important difference between a general finite element analysis and the matrix analysis of a truss or beam structure is that, in general, only approximate results can be obtained. The general finite element analysis process, however, should be understood to be a numerical procedure used to obtain approximate solutions to problems in continuum mechanics. The approximations of this method were described earlier and are dependent on the characteristics and the number of elements that are used to idealize the continuum or structure. A major advancement was achieved once it was recognized that the finite element analysis procedure is a specific form of the Ritz analysis [53-57], which had been used many years in the solutions of general variational problems. The importance of realizing that the finite element method is a form of Ritz analysis lies in that, automatically, all theorems regarding Ritz solutions are also applicable to finite element solutions.

With the use of the minimum potential energy finite element formulation, which is derived from variational principles, the potential energy for an element in this system neglecting initial stresses and strains is

$$I^e = 1/2 \int_{vol} \sigma_{ij} \varepsilon_{ij} \, dvol \qquad [2.8]$$

where I^e = potential energy of the element

σ_{ij} = stress tensor

ε_{ij} = strain tensor

vol = volume of the element

or in matrix form, Eqn. 2.8 can be expressed as

$$I^e = 1/2 \int_{vol} \{\sigma\}^T \{\varepsilon\} \, dvol \qquad [2.9]$$

where $\{\sigma\}^T$ = transpose of the stress tensor

$\{\varepsilon\}$ = matrix form of the strain tensor

The stress tensor can be replaced by using the stress-strain relationship for orthotropic (or isotropic) materials and the strain tensor

$$\{\sigma\} = [D]\{\varepsilon\} \qquad [2.10]$$

where $[D]$ = stress-strain relationship matrix. Now, Eq. 2.9 can be written as

$$I^e = 1/2 \int_{vol} \{\varepsilon\}^T [D] \{\varepsilon\} \, dvol \qquad [2.11]$$

where $\{\varepsilon\}^T$ = transpose of the strain tensor.

The stress-strain relationship for the axisymmetric case is

$$[D] = \frac{1}{Div}\begin{bmatrix} E_r(1 - \nu_{zt}\nu_{tz}) & E_z(\nu_{rz} + \nu_{tz}\nu_{rt}) & E_t(\nu_{rt} + \nu_{rz}\nu_{zt}) & 0 \\ & E_z(1 - \nu_{rt}\nu_{tr}) & E_t(\nu_{zt} + \nu_{zr}\nu_{rt}) & 0 \\ \text{(Symmetric)} & & E_t(1 - \nu_{rz}\nu_{zr}) & 0 \\ & & & G_{rz} \end{bmatrix} \qquad [2.12]$$

where $Div = (1 - \nu_{rz}\nu_{zr} - \nu_{zt}\nu_{tz} - \nu_{tr}\nu_{rt} - 2\nu_{rz}\nu_{zt}\nu_{tr})$ and

E_r = Young's modulus in the radial (r) direction

E_z = Young's modulus in the axial (z) direction

E_t = Young's modulus in the tangential (t) direction

G_{rz} = Shear modulus between the r and z direction

$-\nu_{zt}$ = Poisson's ratio of t strain to z strain for a z load

$-\nu_{rz}$ = Poisson's ratio of z strain to r strain for a r load

$-\nu_{rt}$ = Poisson's ratio of t strain to r strain for a r load

$-\nu_{tz}$ = Poisson's ratio of z strain to t strain for a t load

$-\nu_{tr}$ = Poisson's ratio of r strain to z strain for a z load

The strain tensor in terms of the displacements is

$$\{\varepsilon\} = \begin{Bmatrix} \varepsilon_r \\ \varepsilon_z \\ \varepsilon_t \\ \varepsilon_{zr} \end{Bmatrix} = \begin{Bmatrix} \frac{\partial u}{\partial r} \\ \frac{\partial v}{\partial z} \\ \frac{u}{r} \\ \frac{\partial u}{\partial z} + \frac{\partial v}{\partial r} \end{Bmatrix} = \begin{bmatrix} \frac{\partial}{\partial r} & 0 \\ 0 & \frac{\partial}{\partial z} \\ \frac{1}{r} & 0 \\ \frac{\partial}{\partial z} & \frac{\partial}{\partial r} \end{bmatrix} \begin{Bmatrix} u \\ v \end{Bmatrix} \qquad [2.13]$$

where r = radial coordinate

ε_r = radial strain

ε_z = axial strain

ε_t = tangential (hoop) strain

ε_{rz} = transverse shear strain

The relationship between the derivatives in the natural coordinate system and the derivatives in the *r-z* coordinate system are

$$\begin{Bmatrix} \frac{\partial}{\partial \xi} \\ \frac{\partial}{\partial \eta} \end{Bmatrix} = \begin{bmatrix} \frac{\partial r}{\partial \xi} & \frac{\partial z}{\partial \eta} \\ \frac{\partial r}{\partial \eta} & \frac{\partial z}{\partial \xi} \end{bmatrix} = [J] \begin{Bmatrix} \frac{\partial}{\partial r} \\ \frac{\partial}{\partial z} \end{Bmatrix} \qquad [2.14]$$

Where $[J]$ is called the Jacobian matrix. $[J]$ can be written in terms of the shape functions and the $r - z$ node point coordinates as

$$[J] = \begin{bmatrix} \sum_{i=1}^{4} (\frac{\partial N_i}{\partial \xi}) r_i & \sum_{i=1}^{4} (\frac{\partial N_i}{\partial \xi}) z_i \\ \sum_{i=1}^{4} (\frac{\partial N_i}{\partial \eta}) r_i & \sum_{i=1}^{4} (\frac{\partial N_i}{\partial \eta}) z_i \end{bmatrix} \qquad [2.15]$$

Taking the inverse

$$\begin{Bmatrix} \frac{\partial}{\partial r} \\ \frac{\partial}{\partial z} \end{Bmatrix} = [J]^{-1} \begin{Bmatrix} \frac{\partial}{\partial \xi} \\ \frac{\partial}{\partial \eta} \end{Bmatrix} \qquad [2.16]$$

where

$$[J]^{-1} = \begin{bmatrix} J_{11}^* & J_{12}^* \\ J_{21}^* & J_{22}^* \end{bmatrix} \qquad [2.17]$$

is called the inverse Jacobian matrix. Rewriting the strain tensor in natural coordinates results in

$$\begin{aligned} \frac{\partial u}{\partial r} &= J_{11}^* \frac{\partial u}{\partial \xi} + J_{12}^* \frac{\partial u}{\partial \eta} \\ \frac{\partial v}{\partial z} &= J_{21}^* \frac{\partial v}{\partial \xi} + J_{22}^* \frac{\partial v}{\partial \eta} \\ \frac{\partial r}{\partial z} &= J_{21}^* \frac{\partial u}{\partial \xi} + J_{22}^* \frac{\partial u}{\partial \eta} \\ \frac{\partial v}{\partial r} &= J_{11}^* \frac{\partial v}{\partial \xi} + J_{12}^* \frac{\partial v}{\partial \eta} \end{aligned} \qquad [2.18]$$

where each partial derivative in the global coordinate system can be written as

$$\begin{aligned}
\frac{\partial u}{\partial r} &= J_{11}^{*}\frac{\partial u}{\partial \xi} + J_{12}^{*}\frac{\partial u}{\partial \eta} \\
\frac{\partial v}{\partial z} &= J_{21}^{*}\frac{\partial v}{\partial \xi} + J_{22}^{*}\frac{\partial v}{\partial \eta} \\
\frac{\partial u}{\partial z} &= J_{21}^{*}\frac{\partial u}{\partial \xi} + J_{22}^{*}\frac{\partial u}{\partial \eta} \\
\frac{\partial v}{\partial r} &= J_{11}^{*}\frac{\partial v}{\partial \xi} + J_{12}^{*}\frac{\partial v}{\partial \eta}
\end{aligned} \qquad [2.19]$$

Substituting the equations of Eq. 2.19 in Eq.2.13 and expressing in matrix form yields

$$\{\varepsilon\} = \begin{bmatrix} (J_{11}^{*}\frac{\partial}{\partial \xi} + J_{12}^{*}\frac{\partial}{\partial \eta}) & 0 \\ 0 & (J_{21}^{*}\frac{\partial}{\partial \xi} + J_{22}^{*}\frac{\partial}{\partial \eta}) \\ \frac{1}{r} & 0 \\ (J_{21}^{*}\frac{\partial}{\partial \xi} + J_{22}^{*}\frac{\partial}{\partial \eta}) & (J_{11}^{*}\frac{\partial}{\partial \xi} + J_{12}^{*}\frac{\partial}{\partial \eta}) \end{bmatrix} \begin{Bmatrix} u \\ v \end{Bmatrix} \qquad [2.20]$$

rewritting Eq. 2.13, the element strain is

$$\{\varepsilon\} = [B]\{d\} \qquad [2.21]$$

where $[B]$ is the matrix of strain-node displacement functions. The potential energy of Eq. 2.8 for the element becomes

$$I^{e} = 1/2 \int_{\text{vol}} \{d\}^{T}[B]^{T}[D][B]\{d\}\, d\text{vol} \qquad [2.22]$$

Then by summing over all the elements, the potential energy for the whole structure is

$$I = \sum_{n=1}^{m} 1/2 \int_{\text{vol}} \{d\}^{T}[B]^{T}[D][B]\{d\}\, d\text{vol} + P.E. \qquad [2.23]$$

where m = total number of elements in the structure

$P.E.$ = potential energy of external loads

The variation with respect to $\{d\}$ of the potential energy when set to zero can be expressed as

$$\partial I = 0 = \sum_{n=1}^{m} \left[\int_{\text{vol}} [B]^T [D][B] d\text{vol} \right] \{d\} + \{F\} \qquad [2.24]$$

where $\{F\}$ is the vector containing the external loads. The volume integral can be replaced by $r\, d\theta\, dz\, dr$ which can also be replaced by $r\,(\det|J|)\, d\theta\, d\xi\, d\eta$ in natural coordinates [54].

$$\sum_{n=1}^{m} \left[\int_{\theta} \int_{-1}^{1} \int_{-1}^{1} [B]^T [D][B] r(\det|J|) d\theta\, d\xi\, d\eta \right] \{d\} = -\{F\} \qquad [2.25]$$

Evaluating Eq. 25 for one radian of arc in the tangential direction yields

$$\sum_{n=1}^{m} \left[\int_{-1}^{1} \int_{-1}^{1} [B]^T [D][B] r(\det|J|) d\xi d\eta \right] \{d\} = -\{F\} \qquad [2.26]$$

The element stiffness matrix may now be defined as

$$[K^e] = \int_{-1}^{1} \int_{-1}^{1} [B]^T [D][B] r(\det|J|) d\xi d\eta \qquad [2.27]$$

The integral is a complicated polynomial in ξ and η and cannot be readily evaluated explicitly. Therefore, the element stiffness matrices are evaluated using numerical integration techniques which will be explained in section 2.2.2.

2.2 *High-Order Elements*

The displacement-based formulation presented above for linear elements represents the foundation of the high-order formulation that is to be presented. However, for the most part, every facet of the formulation required slight and sometimes major modifications, if not in the formulation itself then in the numerical implementation of the concept. All of the important aspects of the high-order element will be described.

2.2.1 Displacement Interpolation Functions

Shape functions are commonly derived using Lagrangian interpolation polynomials. The Lagrange interpolation polynomials are defined by [53]:

$$N_k(x) = \prod_{i=0}^{n}\left[\frac{(x - x_i)}{(x_k - x_i)}\right] = \frac{(x - x_0)(x - x_1)...(x - x_{k-1})(x - x_{k+1})...(x - x_n)}{(x_k - x_0)(x_k - x_1)...(x_k - x_{k-1})(x_k - x_{k+1})...(x_k - x_n)} \qquad [2.28]$$

where n is the number of stations or points where the polynomial is calculated. The Lagrange interpolation polynomials defined for one-dimensional problems can be used to construct interpolation functions for two- or higher dimensional problems. The technique for a two-dimensional problem is to simply multiply the Lagrange interpolation polynomial in the two coordinate directions to represent the interpolation functions of a rectangular element.

For a four-noded isoparametric bi-linear element, each of the interpolation functions, N_i, is the product of the one-dimensional interpolation function in the ξ and η directions.

$$N_i(\xi, \eta) = L_i(\xi) \bullet L_i(\eta) \quad ; \quad i = 1,2,3,4 \qquad [2.29]$$

where $L_i(\xi)$ and $L_i(\eta)$ denote the Lagrangian interpolation polynomial in the ξ and η direction corresponding to node i (refer to Fig. 1).

$$L_1(\eta) = \frac{\eta - \eta_4}{\eta_1 - \eta_4} \; ; \; L_2(\eta) = \frac{\eta - \eta_3}{\eta_2 - \eta_3} \; ; \; L_3(\eta) = \frac{\eta - \eta_2}{\eta_3 - \eta_2} \; ; \; L_4(\eta) = \frac{\eta - \eta_1}{\eta_4 - \eta_1}$$
$$L_1(\xi) = \frac{\xi - \xi_2}{\xi_1 - \xi_2} \; ; \; L_2(\xi) = \frac{\xi - \xi_1}{\xi_2 - \xi_1} \; ; \; L_3(\xi) = \frac{\xi - \xi_4}{\xi_3 - \xi_4} \; ; \; L_4(\xi) = \frac{\xi - \xi_3}{\xi_4 - \xi_3} \qquad [2.30]$$

Thus

$$N_1 = \left(\frac{\xi - \xi_2}{\xi_1 - \xi_2}\right)\left(\frac{\eta - \eta_4}{\eta_1 - \eta_4}\right) = \left[\frac{\xi - (1)}{(-1) - (1)} \bullet \frac{\eta - (1)}{(-1) - (1)}\right] \qquad [2.31]$$

or

$$N_1 = \frac{1}{4}(1 - \xi)(1 - \eta) \qquad [2.32]$$

and similar operations will produce N_2, N_3, and N_4.

The high-order elements can be formulated precisely the same way by taking products of the Lagrange interpolation polynomials, which are linear in the meridian direction and higher order in the transverse or radial direction. This technique of generating high-order interpolation functions has been incorporated in an algorithm which requires only the order of the desired polynomial from which it generates all the shape functions and their partial derivatives (which are used to calculate the Jacobian). This algorithm allows the order of the element that is used in the finite element model to be bounded only by the dimension statements in the code without having to manually derive the shape functions for every order element possible. The Lagrangian shape function and Jacobian algorithm is presented in section 5.3.2.2.

2.2.2 Numerical Integration

One of the requirements of this newly formulated high-order composite finite element is that it have the capability to model multiple layers of a laminate by accounting for the effect of each layer (thickness and material properties) on the overall stiffness of the element. The effect of each layer of the laminate is best accounted for by performing the necessary numerical integrations (see Eq. 2.27) in the element on a layer-by-layer basis.

The most common numerical integration scheme used in finite element formulations is Gauss quadrature. This technique involves evaluating a function within the region of interest at specified locations called Gauss points. The sampling points are located symmetrically with respect to the center of the interval or the element when mapped in the natural coordinate system. The location of the Gauss points is determined to achieve the maximum accuracy in evaluating the integral of any continuous function as determined by a Taylor series analysis. Evaluation of the in-

tegral consists of determining the value of the function at these specified Gauss points and multiplying the functional values by the appropriate weighting factors. Symmetrically paired points have the same weighting factors. The weighted functional values are then summed to produce the value of the integral. A two-dimensional integration is performed by summing the weighted functional values in the ξ-direction and then repeating the process in the η-direction. The addition of the two one-dimensional integrations yields the result of the two-dimensional integration. Therefore, a typical four-point Gauss quadrature integration that would be used in a bi-linear finite element is performed with the following expression:

$$I = (W_\xi) \bullet (W_\eta)[f(\xi_1, \eta_1) + f(\xi_2, \eta_2) + f(\xi_3, \eta_3) + f(\xi_4, \eta_4)] \qquad [2.32]$$

where W = Weighting factor associated with appropriate direction

$f(\,)$ = Functional value in the local coordinate system

For a four-point Gauss quadrature, the locations of the sampling points are specified as $\xi, \eta = \pm 0.577350$ and the corresponding weighting factors are $+1.000$. Because the Gauss quadrature method specifies the location of the integration points, they would not in general lie within each of the layers of the laminate. One reason the Gauss quadrature procedure is so widely used is that a polynomial (or assumed displacement function) of degree $2n - 1$ is integrated exactly by a n-point integration. Thus, for a bi-linear element, a single integration point is sufficient for an exact integration of a four-noded quadrilateral element. However, using a single integration point may also produce zero-energy deformation modes. Therefore, two-by-two point integration is typically used and is in fact the method used in the conventional analysis code. If a layer does not contain an integration point or the integration point is not properly weighted for the thickness of the layer, the material properties and geometry will not be correctly modeled. For this reason, a different integration scheme is required for the implementation of the high-order composite element.

The integration method used currently in the code to perform the accuracy study presented in Chapter 4 is a zeroth-order integration (rectangular integration). This results in the weighting

factors being proportional to the thickness fraction of each layer in which the integration points reside. A $2 \times n$ point integration is used for the high-order element as shown in Fig. 2, where n is twice the number of layers. The locations of the integration points are specified so that there are four points within each layer of the laminate. The number of integration points within each layer in both the ξ and η directions is user definable in the design code (see section 5.3.2.3). Four integration points within each layer were used for most of the work to be presented so that the results generated by the high-order element could be compared to those generated by a conventional bilinear element that uses a 2×2 Gauss quadrature integration scheme. A zeroth-order integration is employed on the continuous high-order interpolation polynomial. Presently, any number of layers may be specified for each element provided the program array dimensions are large enough. This means that the larger the number of layers in each element, the larger the number of integration points that must be specified. Because the number of integration points is not defined in the code as a function of the interpolation order (order of the element's displacement field), the user must be aware of the importance of having a minimum appropriate number of integration points to accurately integrate the high-order interpolation function. As an example, if a fourth-order interpolation function is specified, i.e., an element with five side nodes, but only one material layer is defined, the integration can not be done accurately with a 2×2 integration grid.

When Gauss quadrature is used to perform the numerical integration it is possible to declare the minimum number of Gauss points needed to model a n^{th}-order interpolation function. As stated earlier, in general a polynomial of degree $2n - 1$ is integrated exactly by a n-point Gauss quadrature. The zeroth-order integration scheme has no such relationship and in fact an exact evaluation of the integral is not assured for any function of order two or greater. This creates another variable in the accuracy of the finite element method that the designer/engineer must gain experience with in order to consistently generate accurate results. However, for now it seems that at least as many integration points as interpolation order should be used. This additional variable is simply one of the many which include selecting the order of the element, creating a reasonable mesh and selecting the number of plies that the design engineer will have to become familiar with in order to consistently generate accurate results.

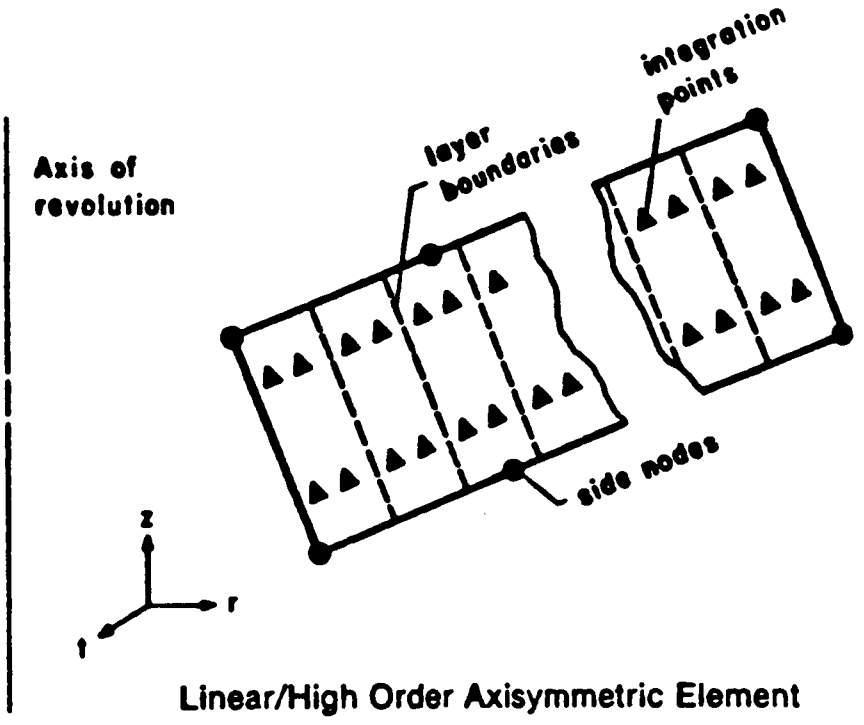

Figure 2. High-Order Axisymmetric Finite Element

2.2.3 Material Stiffness

The material properties of the fiber-reinforced composite structure are orthotropic, with each layer of the filament wound structure being transversely isotropic. The principal directions of each layer are oriented such that the 1-direction is along the fibers' wrapping path and the 2- and 3- directions are perpendicular to the fiber path. The spheres that are to be analyzed and designed with the aid of this program are wrapped with a delta axisymmetric winding pattern, as is shown in Fig. 3, and consist of numerous fiber directions depending on the location within the sphere's structure. A delta axisymmetric winding pattern is a variation of the common polar wind which uses filament tape rather than creating the bands with the actual wrapping process with continuous fibers. The delta axisymmetic winding pattern also use an incremental technique to create the polar wind which is not necessary with the more common tape winding technique. However, the fiber angle at any given point in the structure is known from the carefully described winding pattern. These angles are determined by use of the program NTHICK which will be described in section 5.2.2 and then used by the finite element program, HICOM (see section 5.3.1), to specify the angles and material properties of each layer of the laminate within the high-order element.

The element stiffness is calculated in the *r-z-t* or global coordinate system for all the elements of the model. This means that the material properties of the composite will have to be transformed to the *r-z-t* or global coordinate system from the prescribed fiber orientation or local wrapping coordinate system. The local wrapping coordinate system, denoted as the 1-2-3 coordinate system, and the global coordinate system which is denoted as the *r-z-t* coordinate system are shown in Fig. 4. The fiber coordinate system, 1-2-3, has the 1-axis aligned along the fibers and the 2-axis being in the band plane and perpendicular to 1. The 3-axis is, of course, orthogonal to 1 and 2 and is in the outward radial direction of the sphere to complete the right-hand coordinate system.

The transformation from the fiber, 1-2-3, coordinate system to the global coordinate system, *r-z-t*, can be most easily accomplished with the use of two fourth-order tensor transformations. The transformation matrix is shown in Fig. 5 and may be obtained from any one of several refer-

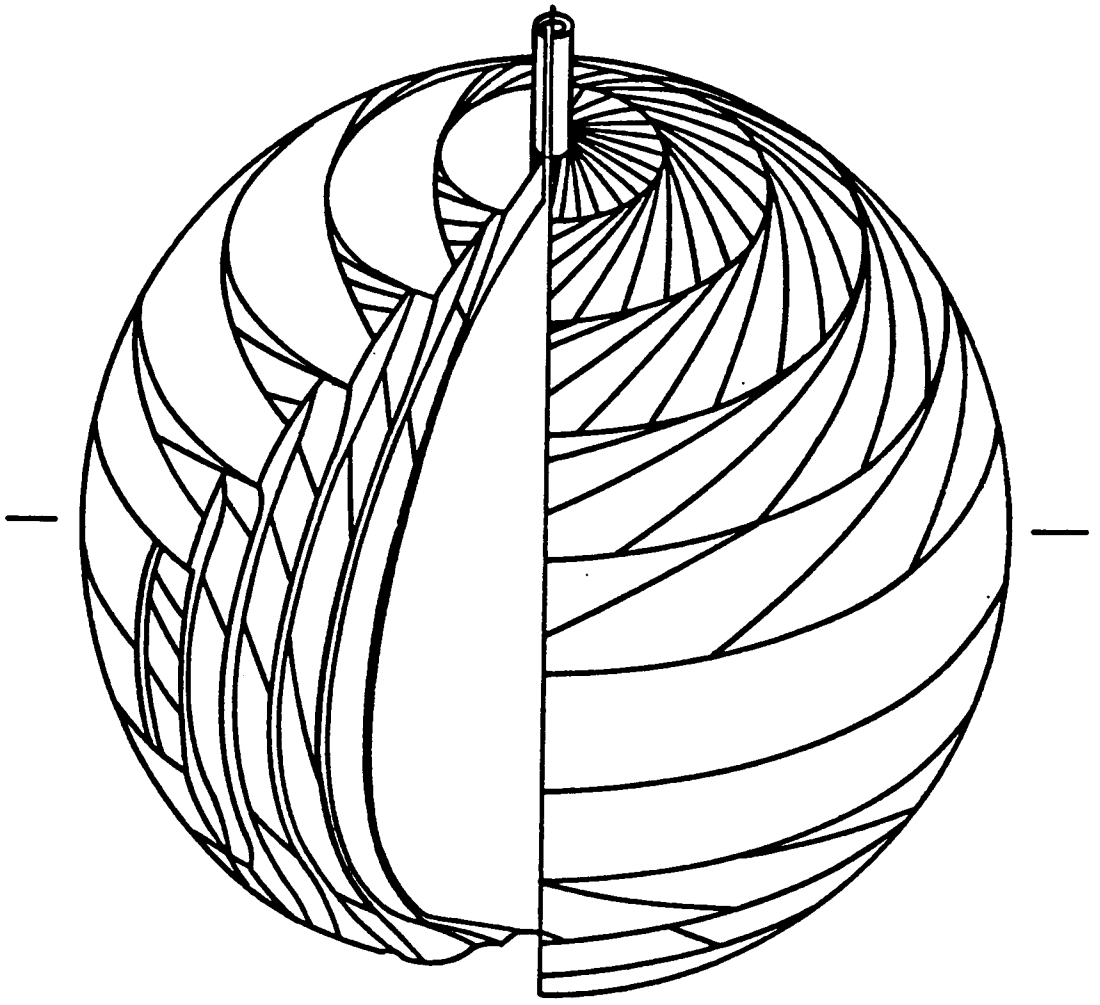

Figure 3. Delta-Axisymmetric Pattern on a Sphere; after Leavesley [27]

BETA View along spherical radius or n and 3 axis.

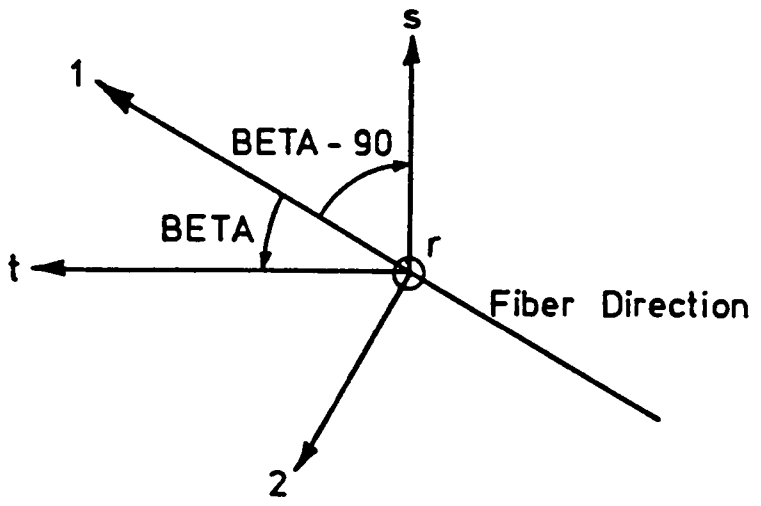

SETA View in tangential direction along the t axis.

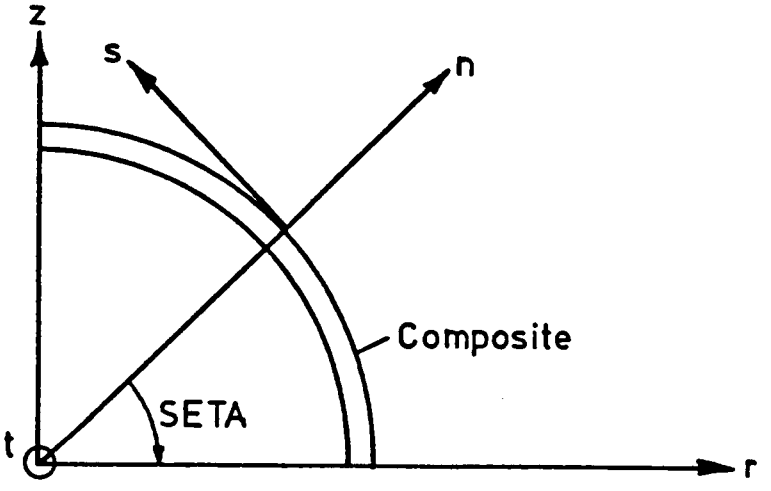

Figure 4. Three Dimensional View of the Transformation Angles BETA and SETA; after Leavesley [27]

$$[T_m] = \begin{bmatrix} N^2 & M^2 & 0 & 0 & 0 & -2MN \\ M^2 & N^2 & 0 & 0 & 0 & 2MN \\ 0 & 0 & 1 & 0 & 0 & 0 \\ 0 & 0 & 0 & N & M & 0 \\ 0 & 0 & 0 & -M & N & 0 \\ MN & -MN & 0 & 0 & 0 & M^2-N^2 \end{bmatrix}$$

where M - sine of the rotation angle between the 1-axis and the 1′-axis.

N - cosine of the rotation angle between the 1-axis and the 1′-axis.

where the transformation is from the unprimed to the primed coordinate system.

Figure 5. Material Transformation Matrix

ences pertaining to composite materials [5]. The fourth-order transformation is most easily accomplished by post-multiplying the material property matrix by a second-order transformation matrix (shown in Fig. 5) and then pre-multiplying again by the transpose of the transformation matrix as shown below.

$$[D]_r = [T_m]^T[D]_1[T_m] \qquad [2.33]$$

where $[D]_1$ = matrix of material properties

$[D]_r$ = matrix of transformed material properties

$[T_m]$ = second order transformation matrix

$[T_m]^T$ = transpose of the transformation matrix

The two transformation angles that are present because of the geometry of a sphere, BETA and SETA, are shown in Fig. 6. The first transformation angle is a negative rotation about the 3-*n* axis to the s-t-n coordinate system through the angle (BETA − 90) . The *s-t-n* coordinate system has the *s*-axis aligned along a longitudinal line with the *t*-axis being tangent to the latitude line in the band plane. The *n*-axis coincides with the 3-axis to again complete the right-hand coordinate system. The second transformation is a negative rotation about the *t*-axis . This negative transformation through the angle *SETA* gives the material properties in the *r-z-t* or global coordinate system.

2.2.4 Stress Computation

Stresses for every layer within an element are calculated in both the local and global coordinate systems. The layer stresses in the global coordinate system are calculated by using Eq. 2.10 and Eq. 2.21 which are repeated below.

$$\{\sigma\} = [D]\{\varepsilon\} \qquad [2.10]$$

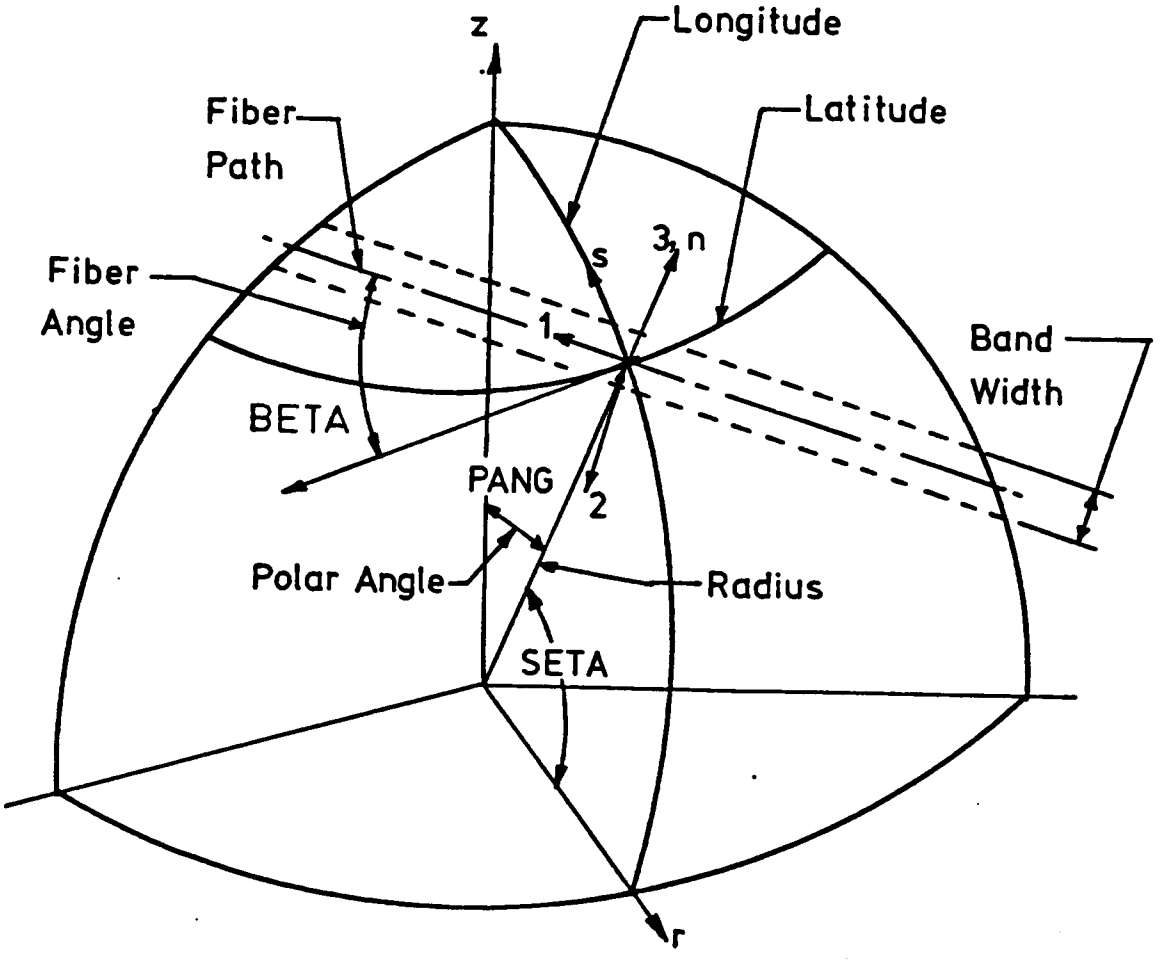

Figure 6. Transformation Angles - BETA and SETA; after Leavesley [27]

where

$$\{\varepsilon\} = [B]\{d\} \qquad [2.21]$$

which results in

$$\{\sigma\} = [D][B]\{d\} \qquad [2.34]$$

The stresses are calculated at each integration point within each layer of the element and averaged together to output the layer stresses.

The output of layer stresses in fiber coordinates involves a transformation from the global coordinate system to the fiber coordinate system as the finite element program calculates the displacements and resulting stresses and strains in the global structure coordinate system. This transformation is carried out by first transforming the layer strains rather than transforming the layer stresses directly. The element strains are transformed since the fiber direction within a 'layer' is assumed to be made-up of an equal number of + and - fiber orientations due to bands crossing. The bands cross the equator at a set angle, as shown in Fig. 3, and each band set contains two layers of coverage at the equator. This means that any point on the equator has two bands crossing it at opposite angles within every band set as shown in Fig. 7. At this point, the strain components in any direction within the two bands must be the same. However, the stress components in any given direction in the two bands would generally be different. Therefore, transformation of the global layer stress components would give the average stress for the two bands. This averaged stress of the two bands is not the correct fiber direction stress. However, transforming the layer strains from the global to fiber coordinate system does yield the correct fiber direction strains as continuity must be assured. The fiber direction stresses are obtained by multiplying the transformed (fiber direction) strains by the material stiffness matrix in the material's principal directions.

$$\{\sigma\}_1 = [D]\{\varepsilon\}_1 \qquad [2.35]$$

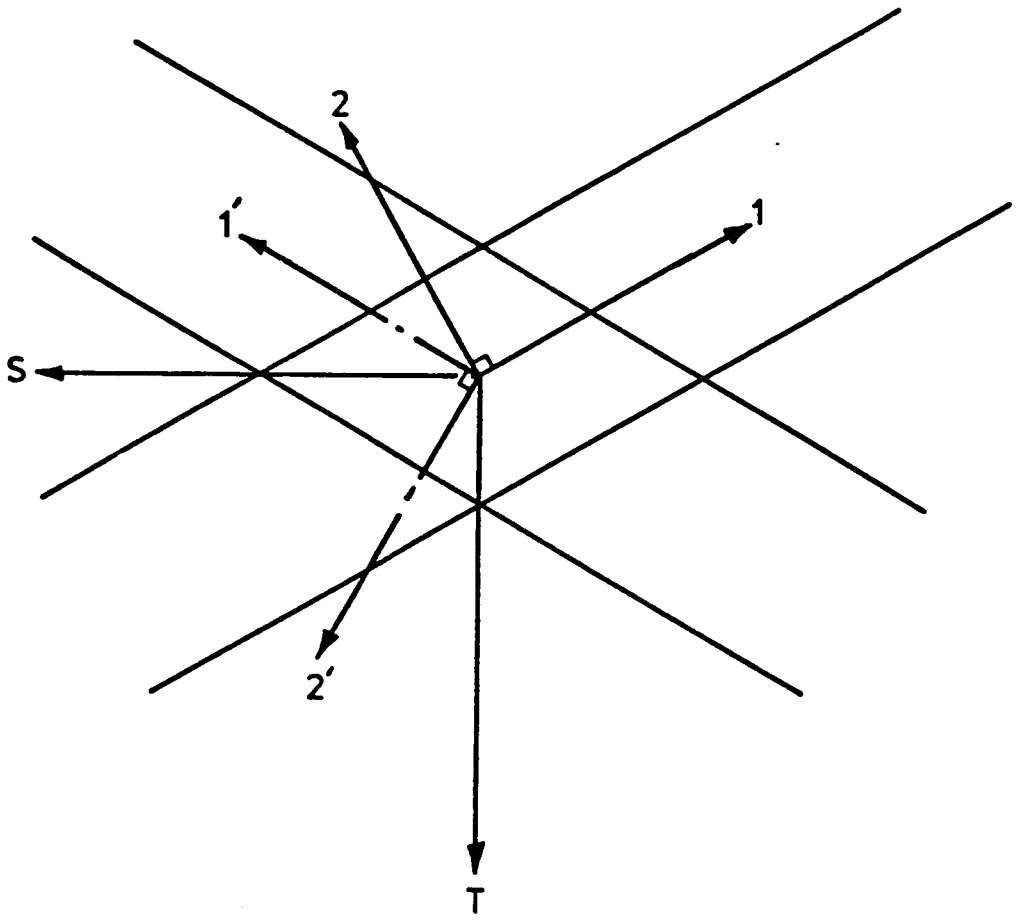

Figure 7. Crossing of Bands Within a Layer; after Leavesley [27]

2.2.5 Strain Transformation

Stresses are the primary quantities that are of interest to design engineers and are also the preferred quantity for many failure criteria. To calculate the fiber-direction stresses, the 'layer' stresses must be transformed from the global coordinate system to the fiber, (1-2-3), coordinate system. The finite element method calculates the strains and stresses based on the nodal displacements of the structure. The nodal point displacements are, of course, calculated in the structure's global coordinate system which in this case is axisymmetric, (r,z). These displacements are multiplied by the strain-displacement matrix [B], which is evaluated at each of the integration points in order to calculate the strains in the global (r-z-t) coordinate system. The strains at each integration point that lie within each layer of the composite structure are then averaged together to get the average layer strains in the global coordinate system. Strains are transformed from one coordinate system to another by a second-order transformation.

$$\{\varepsilon\}_1 = [T_s]\{\varepsilon\}_r \qquad [2.36]$$

where $\{\varepsilon\}_1$ = strain tensor in the fiber-coordinate system, 1-2-3

$\{\varepsilon\}_r$ = strain tensor in the global-coordinate system, r-z-t

$[T_s]$ = second-order strain transformation matrix

The transformation from the global (r-z-t) system to the fiber-coordinate system, (1-2-3), again requires two transformations as the strains must be rotated through the two angles, BETA and SETA. It is also important to note that the strain transformation matrix is slightly different than the transformation matrix that is used to transform the material properties because the angle of transformation is now positive resulting in sign changes to some of the terms. The strain transformation matrix, or the positive angle rotation transformation matrix, can be found in reference [27].

The transformation angles BETA and SETA between the two coordinate systems are shown in Fig. 6. The first transformation is a positive rotation about the t-axis to the n-s-t coor-

dinate system and is then permutated to make a *s-t-n* coordinate system. The second transformation is a positive rotation about the *n*-axis to fiber or 1-2-3 coordinate system.

The individual layer strains are now defined in the fiber-coordinate system. The principal material direction stresses are then calculated by multiplying the strains by the fiber's material property matrix, [D] defined in the 1-2-3 or fiber-coordinate system.

3.0 Computational Time Study

3.1 Review of Solution Methods

In Chapter 2, the basic formulation of the finite element method was presented which showed that the primary objective is to represent a complicated structure by a set of simultaneous equations relating internal and external loads to the nodal point displacements.

$$[K]\{d\} = \{F\} \qquad [3.1]$$

where $[K]$ = the stiffness matrix

$\{d\}$ = the displacement vector

$\{F\}$ = the load vector

In practice, this expression may easily contain thousands of equations. In a linear static analysis the time for solution of the equilibrium equations can be a large percentage of the total solution time, depending on the kind and number of elements used in the assemblage and on the topology of the finite element mesh. In dynamic analysis or in nonlinear analysis, this percentage may be

still larger [54]. Therefore, if inappropriate techniques for the solution of the equilibrium equations are used, the total cost of analysis is affected a great deal.

In addition to considering the actual computer effort that is spent on the solution of the equilibrium equations, it is important to realize that an analysis may in fact, not be possible if inappropriate numerical procedures are used. In this particular study the cost associated with the solution is not nearly as important as the real time of the solution that currently renders the conventional analysis finite element program inadequate for 'design purposes' because the solution time is too long to allow for numerous evaluations of design alternatives. But, even more important is the fact that some solution methods may be unstable and not converge to the correct solution. This is more common in dynamic analysis then static analysis however and is sometimes a problem in nonlinear solutions such as elastic-plastic material response.

There are two general classes of solution methods for the set of equations in Eq. 3.1; direct solution techniques and iterative solution methods. Each method has certain advantages over the other, however, the direct methods are almost always used for linear elastic static analysis as they are more efficient for this class of problem. The most effective direct solution techniques currently used are basically applications of Gauss elimination. However, although the basic Gauss solution scheme can be applied to almost any set of simultaneous linear equations, the effectiveness in finite element analysis depends on the specific properties of the finite element stiffness matrix, i.e., symmetric, positive definite, and bandedness.

The basic procedure of the Gauss elimination solution is to reduce the coefficient matrix, [K], of the linear simultaneous equations, to an upper triangular matrix from which the unknown displacements, $\{d\}$, can be calculated by back-substitution.

Basically, the matrix operations used to reduce the stiffness matrix to an upper triangular form can be expressed as

$$L_{n-1}^{-1}...L_2^{-1}L_1^{-1}K = S \qquad [3.2]$$

where S is the final upper triangular matrix and L is a decomposition matrix that is explained in many references [54,58].

Decomposing the stiffness matrix in this fashion and performing like operations on the load vector results in the following steps that can be very easily incorporated into a finite element algorithm to efficiently solve large sets of linear simultaneous equations.

$$K = LDL^T \qquad [3.3]$$

Which leads to

$$\begin{aligned} LV &= F \\ DL^T d &= V \end{aligned} \qquad [3.4]$$

where the load vector F is reduced to obtain the vector V by using the same decomposition matrices as used in Eq. 3.2.

One of the positive aspects to solving the large set of equations often generated by models to simulate complicated structures in the finite element method is that the stiffness matrix is positive definite (a condition for a Gauss elimination solution), symmetric and banded. This last characteristic depends on the nodal point numbering of the finite element mesh, and it is important to exploit this trait to create the most efficient algorithm possible. An algorithm to automatically generate and number the nodes of the mesh to insure the most efficient solution time is incorporated into the program SPHMESH described in section 5.2.3.

The coefficient pattern of a typical stiffness matrix is shown in Fig. 8. As noted earlier, the stiffness matrix is symmetric, therefore, only the upper triangular portion of the matrix will be stored and worked upon. Further more, only the coefficients that 'fall under the skyline' as shown in Fig. 8 will be stored. The half bandwidth of the matrix is denoted by, m_k. The half-bandwidth is defined by the value for which no elements within the coefficient matrix are zero and that are defined by the following expression:

$$j > i + m_k \qquad [3.5]$$

where i and j are row and column indices of the stiffness matrix. The half-bandwidth, m_k is also equal to the maximum difference in global degrees of freedom pertaining to any one of the finite

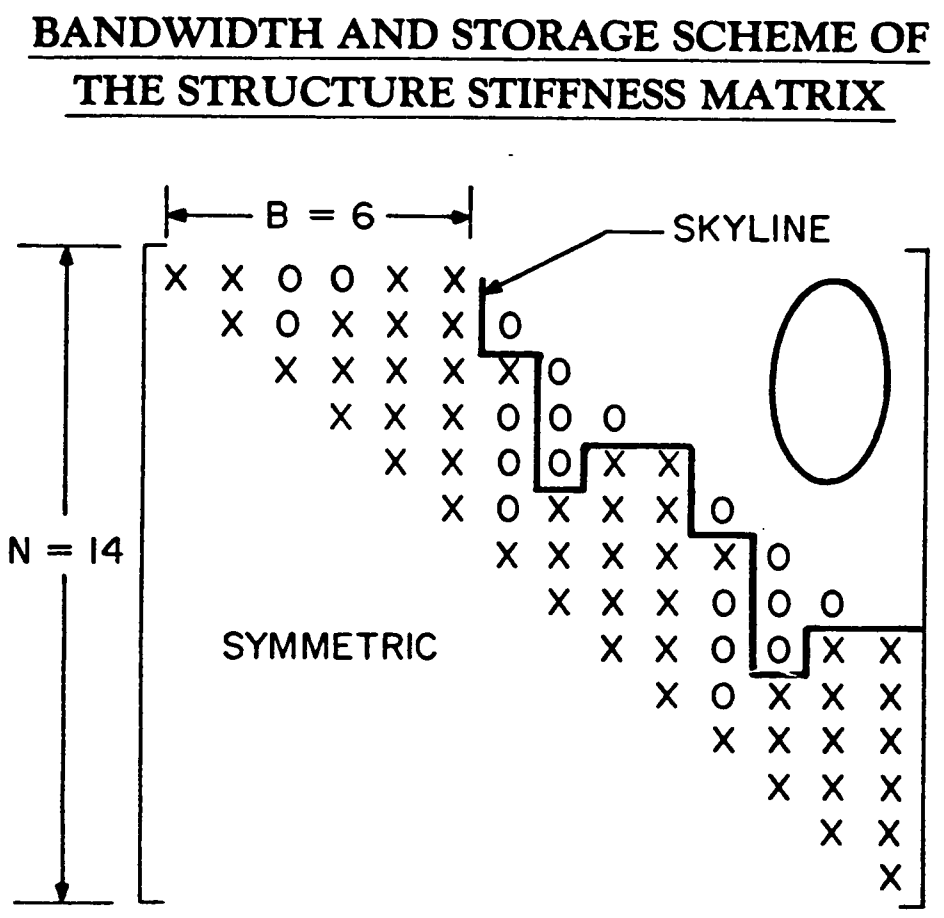

Figure 8. Storage Scheme Used for a Typical Stiffness Matrix

elements in the mesh and, therefore, explains the significance of nodal numbering in reducing the half-bandwidth and consequently the number of operations to solve the set of equations. The effectiveness of this solution scheme lies simply in the fact that only elements below the skyline are stored and processed in the decomposition of the stiffness matrix and the load vector.

In addition to the LDL^T decomposition described above, various other schemes are used that are closely related. One of the more common methods is Cholesky factorization [54,55]. In this technique, the stiffness matrix is decomposed in a manner very much like that described above but in which

$$K = \bar{L}\bar{L}^T \qquad [3.6]$$

and where

$$\bar{L} = LD^{1/2} \qquad [3.7]$$

Therefore, the Cholesky factors could be calculated from the D and L factors, but more generally, the elements of $\bar{L}$ are calculated directly. An operation count shows that slightly more operations are required in the equation solution if the Cholesky factorization is used rather than the LDL^T decomposition. For this reason, the LDL^T decomposition method will be used in all further discussions of solution methods and is the solution method incorporated in the finite element program HICOM.

3.2 *Theoretical Computational Time Study*

The primary objective of this work is to illustrate the potential of a new algorithm to reduce the computation time to solve a general class of spherical filament-wound pressure vessel problems. However, because the computation time will vary greatly from machine to machine, the efficiency

and time savings of a novel algorithm is best illustrated by estimating the number of mathematical operations that must be performed. In the preliminary stages of this work, the working thesis was that if the number of nodes was reduced in a model without sacrificing accuracy, then the computation time to solve the system equations would be likewise reduced and would constitute the majority of the time savings.

3.2.1 Computations to Solve Equilibrium Equations

In order to estimate the number of mathematical operations that are carried out in the solution of the equilibrium system equations, a mathematical operation is defined as one multiplication (or division), which is nearly always followed by an addition [54]. For an operation count estimate, consider a system with a half-bandwidth, m_k , that is full and constant across the stiffness matrix. In this case the number of operations required for the LDL^T decomposition of the stiffness matrix, K, is approximately [55]

$$n\{m_k + (m_k - 1) + \ldots + 1\} = \frac{1}{2}nm_k^2 \qquad [3.7]$$

and for the reduction and back-substitution of a load vector, an additional number of multiplications is required, which is approximately

$$2nm_k \qquad [3.8]$$

Seldom in practical problems will the half-bandwidth be constant across the stiffness matrix, however, the above relationships can still be used for approximations if m_k is defined as the 'mean half-bandwidth'.

The objective of this high-order element, with the ability to account for numerous different materials internally, is to reduce the number of system equations and, therefore, the computation time to generate an accurate solution. In particular, the objective is to create a computer code to

be used for the design of the filament-wound spherical pressure vessel of the type shown in Fig. 9. To evaluate the potential of the element to reduce the number of system equations and consequently the computation time, an analysis of the number of mathematical operations used to generate a finite element method solution was performed. An actual finite element model of a typical filament-wound spherical pressure vessel for which this element is ultimately to be used is shown in Fig. 10. Therefore, this model was used as the standard in order to judge the expected efficiency and time savings that the new high-order element may provide in solving the system equations.

In these studies designed to evaluate the total number of mathematical operations associated with the finite element method of solution, only the formulation of the element stiffness matrices and the subsequent solution of the system equations for the nodal point displacements were analyzed. The analysis did not account for any pre- or post-processing, which constitutes a considerable portion of the total time. However, heuristic evaluations point clearly to the fact that using the newly developed element will require less pre-processing time and input-phase time (formulating the element connectivity arrays, etc.) because of the fewer number of nodes. There are however, other areas that may prove to be important in evaluating the actual efficiency of this new element formulation. It is possible that a greater number of computer operations will be necessary to store material and integration point information for the high-order element than for the conventional elements. There are several areas within the implementation of the finite element method in which it is hard to identify whether the new element formulation will be more efficient, less efficient or make essentially no difference in the computational time involved. For this reason the theoretical studies (section 3.2) only evaluated the 'heart' of the finite element technique, the formulation of the system equations and the subsequent solution of these equations. The finite element computation study (section 3.3) will be investigating the efficiency of the formulation in all phases and aspects of the solution method.

The evaluation of the number of mathematical operations was performed for both a high-order element and the conventional bi-linear element. When simply modeling the total transverse thickness of a twenty-five layer composite structure, the number of system equations are reduced from 104 to 20 which results in a reduction in the number of mathematical operations needed to

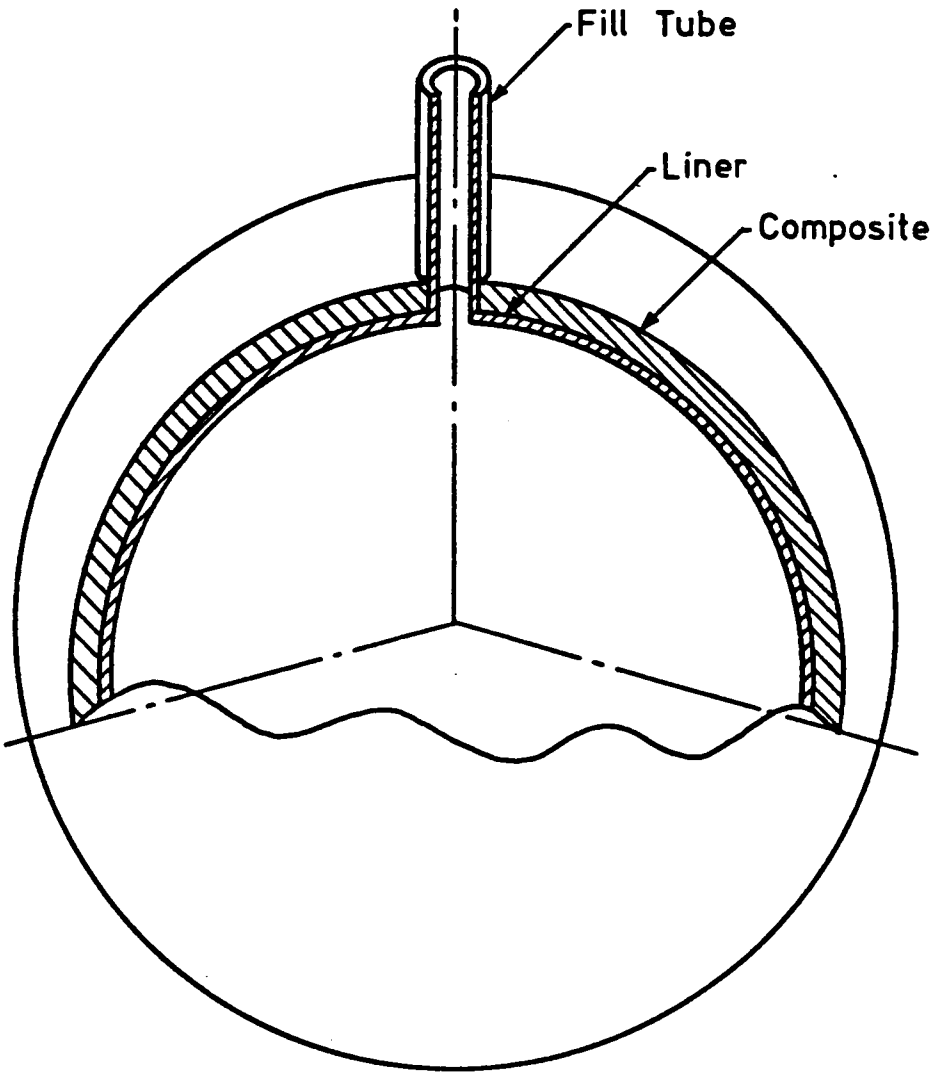

Figure 9. General Design of Filament-Wound Spherical Pressure Vessels; after Leavesley [27]

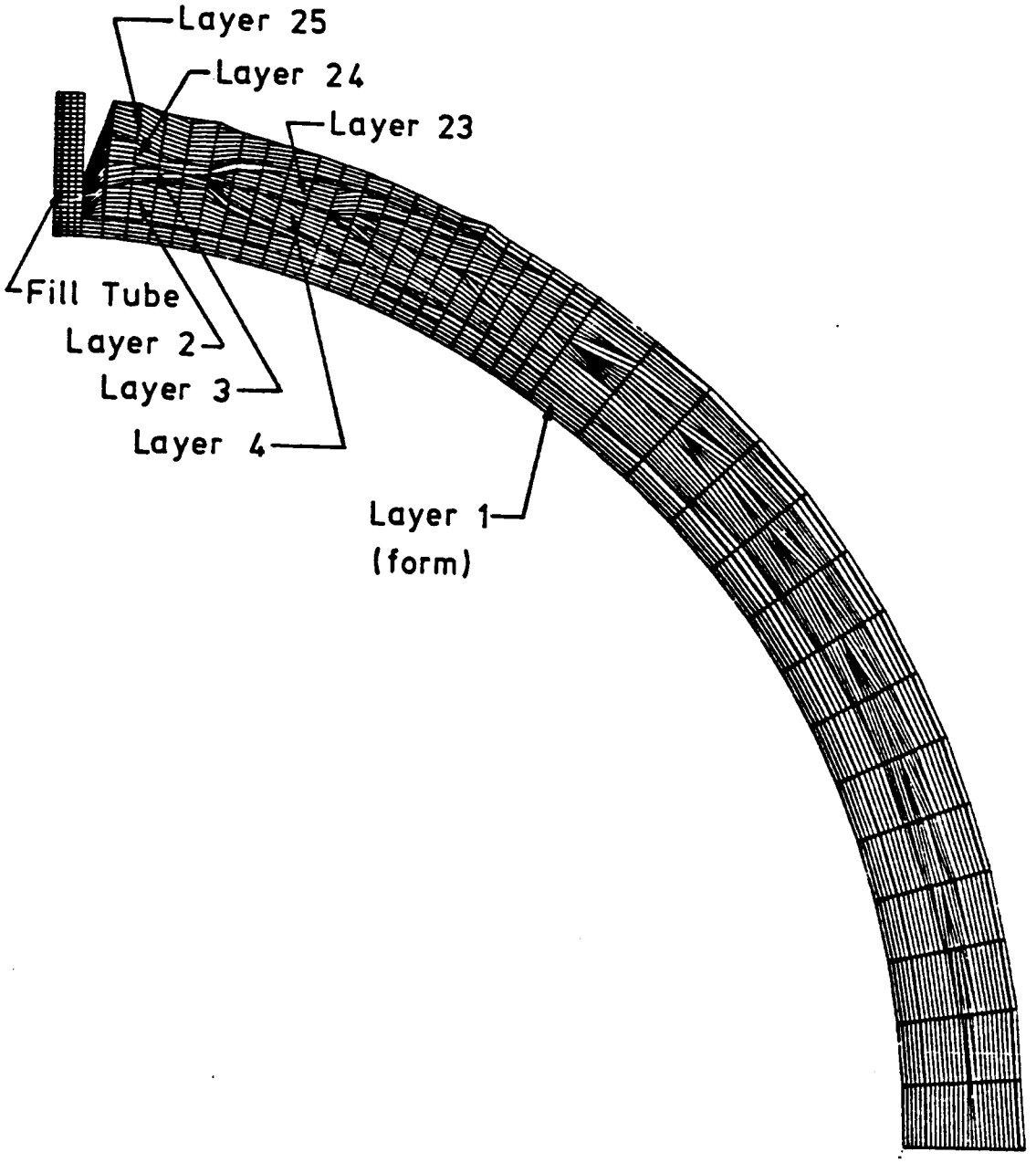

Figure 10. Full Generated Mesh for an Axisymmetric Quadrilateral Model

solve for the nodal point displacements by a factor of approximately 40. However, with the information needed for this part of the analysis, the resolution of the stress calculations is irrelevant. The resolution of the stress calculations is dependent on the number of integration points as that is where the stresses and strains are to be evaluated. Not only are the number of integration points important in determining the resolution of the results but also in the accuracy of the results and the accuracy of the element stiffness calculations. In the next section the importance of the stiffness matrix calculation on the economy of the element will be discussed.

3.2.2 Computations to Evaluate Stiffness Matrix

As explained in Chapter 2, the element stiffness matrix can be evaluated numerically by integrating the expression

$$K = \int_{\text{vol}} B^T D B \, d\text{vol} \qquad [3.8]$$

For the numerical integration, the weight coefficient associated with every point of integration is first multiplied into the material property matrix. The product $B^T D B$ is then evaluated at the integration points through the element. The individual terms are then added to give the elements of the stiffness matrix. The steps and the number of operations (additions and multiplications) for evaluating the stiffness matrix of a three-dimensional element are given in Table 1. If Σ and Π denote the number of additions and multiplications respectively, then

$$\begin{aligned} \Sigma &= \frac{1}{2}(63r^2 + 237r)I \\ \Pi &= (27r^2 + 117r + 36)I \end{aligned} \qquad [3.9]$$

where r = Number of nodes in the element

I = Number of integration points in the element

Table 1. Operations Required for the Evaluation of the Element Stiffness Matrix, Conventional Method

Assumption: 2-Dimensional
Numerical Integration by Gauss Quadrature

Notation: r = Number of Nodes per Element
i = Number of Integration Points per Element

Computation Step	Number of Additions	Number of Multiplications
1. For each point of Integration		
a) Product of Weight coefficients and material property matrix, D	6x6	
b) Obtaining the product DB	6x6x2r	6x6x2r
c) Obtaining B^TDB (upper triangular portion only)	1/2[6x2r(2r+1)]	1/2[6x2r(2r+1)]
TOTAL FOR STEP 1	$12r^2+78r$	$12r^2+78r+36$
2. Repeating the operation in Step 1 for i integration points	$(12r^2+78r)i$	$(12r^2+78r+36)i$
3. Summing up the individual elements of the stiffness matrix evaluated at i integration points	1/2[2r(2r+1)]i	
4. **TOTAL** number of operations to obtain the element stiffness matrix	$(14r^2+79r)i$	$(12r^2+78r+36)i$

With the results from Table 1, the number of computations needed to generate the respective structure stiffness matrix is calculated for a fourth-order composite element and shown in Table 2. The fourth-order composite element again contained 25 layers of an orthotropic material and 25 integration points that would result in output values for the stress state in each of the 25 layers thereby corresponding to the output resolution for the conventional bi-linear element model.

3.2.3 Summary

The results from Table 2 are used for a comparison of the conventional model, Fig. 10, versus a proposed model which contains only high-order elements that contain 25 different material layers was completed to evaluate the reduction in the number of operations to solve for the nodal displacements. The high-order element model contains only 48 elements as each element models the entire through-thickness of the filament winding. Both models would be subdivided along the meridian in a similar fashion. The high-order composite element being evaluated uses a fourth-order displacement function approximation, which requires five nodes on each side of the element. The high-order element is linear in the meridian direction. In order to produce the same number of stress values through the thickness of the filament winding, each layer of the filament winding must contain at least one integration point. The integration point, which is also the location for the stress calculations, is located in the center of the layer.

The results of Table 1, which indicate the number of multiplications needed to generate the element stiffness matrix and then solve the resulting set of equations, are used in the analysis that is displayed in Table 2. There is approximately a factor of four reduction between the number of operations for a single fourth-order composite element and 25 conventional bi-linear elements. The potential computation time savings between the two element types and modeling schemes certainly justifies pursuing the development and formulation of this element.

Table 2. Comparison of the Number of Multiplication Operations to Generate and Solve the System Equations

CONVENTIONAL ELEMENT	FOURTH-ORDER COMPOSITE ELEMENT
1. Generate the Element Stiffness Matrices	
25 Elements	1 Element
4 Integration Pts./Element	25 Integration Pts./Element
4 Nodes/Element	10 Nodes/Element
$[12(4^2)+78(4)+36]4$	$[12(10^2)+78(10)+36]25$
= 2160 / Element	= 50,400
Total = 2160/Element x 25 Elements	
TOTAL = **54,000**	= **50,400**
2. Solve the Structure System Equations - 2 D.O.F./Node	
Total Number of Nodes	
52	10
Total Degrees of Freedom	
104	20
[K]= 104x104	[K]=20x20
Number of Operations to solve [K]{d}={F} by LDL^T	
(m_k = 54)	(m_k = 20)
$1/2\ n\ m_k^2 + 2nm_k$	
TOTAL=**162,864**	TOTAL=**4,800**
TOTAL=216,864	**TOTAL=55,200**

m_k = average bandwidth
n = number of equations

3.3 *Finite Element Computation Time Study*

The potential for the high-order composite element to be significantly more economical than the conventional modeling scheme utilizing bi-linear quadrilaterals has been demonstrated in the previous section. The development of the finite element program using the high-order elements was begun based on these results. However, there were several aspects of the finite element solution method that were not considered in the theoretical computation study presented above. Upon completion of the finite element program with the high-order element in its library, another computational study was performed using the actual finite element programs (high-order and bi-linear) to investigate the actual economy of all phases of the solution method using the new element formulation. The following sections describe the test conditions used and present results of Central Processing Unit (CPU) time for four main portions of the solution method; i) input phase, ii) generation of the structure stiffness matrix, iii) solution of the system equations to determine the nodal point displacements, and iv) calculation of the stresses.

3.3.1 Test Conditions and Models

Evaluating the computational time of the high-order element and the conventional finite element method requires that two test conditions be carefully monitored before beginning. The first is that all tests cases be run in like conditions on the computer. The second is that the same relative problem be solved by both methods. This involves not only the geometry of the structure but also node numbering and other aspects of data input. The evaluation of the computational efficiency of the high-order elements will be based on the CPU time used in comparison with that used by the conventional technique.

CPU time is a measure of the time that the computer is actually expending to perform the tasks given it by the compiled program. Surprisingly, the CPU time to solve a given problem is

often not a constant for a given computer system. On time-sharing systems, the time used to exit and re-enter a process during the 'time sharing' activity is applied to the executing process. This additional CPU time is normally small depending on the actual computational system being employed and the execution time of the program. Variations of CPU time to perform identical operations have even been witnessed on personal computers.

The computer system chosen for this study was a VAX 11/780. The computation time for a process being run on the VAX is 'charged' for time associated with 'page faults' and 'swapping' that is done to allocate and rearrange sufficient memory for the process. The number of page faults and swapping that is done depends on many things, including the load on the system, size of the program, the amount of storage needed for arrays and matrices, and the efficiency of the code itself. The current system management philosophy for the particular VAX on which this computation study was carried out is to allow for relatively large amounts of memory to be allocated for executing processes so that relatively little time sharing is needed. Many of the variables that appear to influence the variation of CPU time in executing a process seem to change with the system management scheme that is employed on the VAX 11/780 such as the amount of virtual memory available for paging.

In order to generate a value for the CPU time for a given problem, an average of the CPU times for 20 solutions of the same problem run consecutively was used. All of the CPU times were generated when no other interactive users were on the VAX and the load factor indicated that the operator was not processing. With these conditions, the average of 20 consecutive runs were repeatable and deemed accurate for the purposes of this study.

The problems that were solved in order to create the CPU times were similar to those used in the accuracy study (Chapter 4). The majority of the results generated were for a pressure-loaded cylindrical pressure vessel as shown in Fig. 11. The cylinder was modeled with a single high-order element containing eleven 'layers' for which stresses are calculated. The conventional or bi-linear results were calculated with a finite element model consisting of one four-noded quadrilateral for each of the eleven 'layers' as shown in Fig. 11. The nodes of both models were numbered in the sequence that will correspond to the minimum bandwidth in the filament-wound spherical pressure

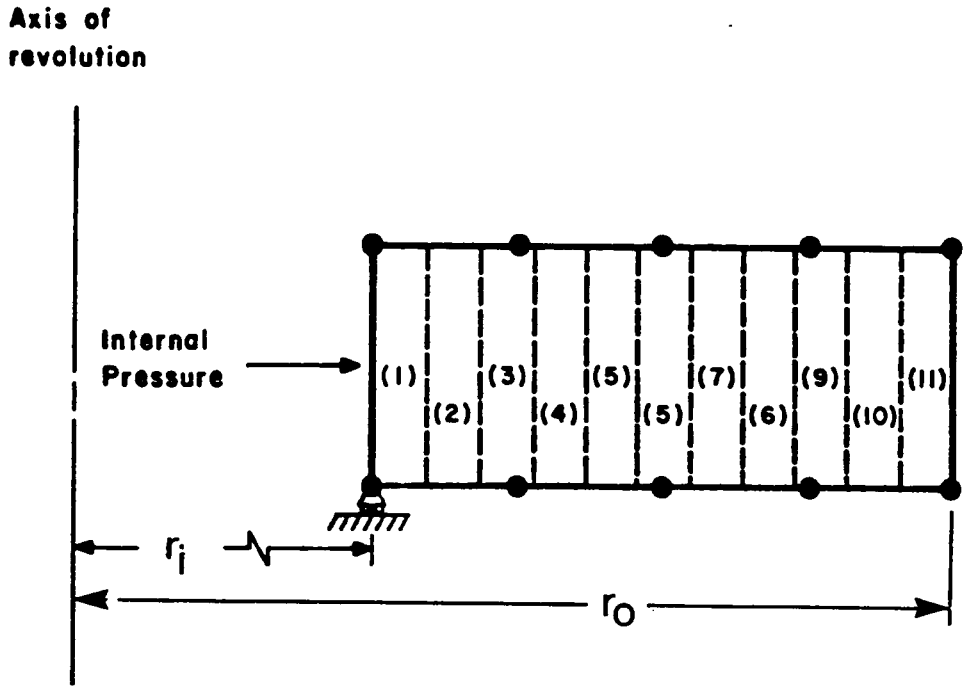

Figure 11. Computation Study Test Problem - Pressure Loaded Cylindrical Pressure Vessel

vessel models. This means that the nodes are numbered sequentially through the thickness of the cylinder as this will correspond to the 'short' side of a full generated mesh as shown in Fig. 10 on page 53. Numbering nodes across the 'short' side ('short' refers to the smallest number of nodes) is the 'rule of thumb' used to minimize the bandwidth [53]. This numbering scheme creates a significantly larger bandwidth for the conventional model of the cylinder than if the nodes were numbered across the 'short' side of the cylinder which would be its length, in this case. However, one of the objectives of this computational study is to determine how efficient the element will be in modeling the larger spherical pressure vessel. The numbering scheme employed in the models allows for this prediction to be made.

Only one set of results are presented which were generated for a 'generic' material. The model is not labeled as isotropic, orthotropic, or filament-wound as the solution method and computational effort is the same for all cases. Theoretically, transformations of material properties, stresses, and strains do not have to be performed for isotropic materials. Also, if the model contained elements which all contain the same fiber orientation, the material property transformation would only have to be carried out once. In the final 'design code', very few elements will contain the same fiber orientations and no isotropic materials will be modeled with the high-order elements, thus the finite element program transforms all material properties and also transforms the stresses and strains, orthotropic material or not. Therefore, the nature of the material is not important in terms of the number of computations or the CPU time.

Lastly, a few models that contain multiple high-order finite elements (and the equivalent conventional bi-linear element models) were used to determine the CPU time of models of the size expected for the spherical pressure vessels (see Fig. 10 on page 53) and the resulting efficiency. The high-order elements were stacked one on another so that the cylinder still contained a single high-order element through its thickness but now had several elements along its length. The node numbering of the models followed the same scheme used in the 'single element' models; numbering the nodes sequentially through the thickness of the cylinder. Therefore, the bandwidth for the 'single element' models was the same as in the 'multiple element' models.

3.3.2 CPU Time Results

The CPU time for each finite element solution was determined for the four most significant phases of the finite element solution method which together comprise the entire solution technique. The first portion of the solution method considered is the input phase. This includes reading the input data, generating nodes and elements from the input data, creating the connectivity, boundary condition, load, and material property arrays. The generation of the structure stiffness matrix is the second phase for which CPU time accounting is available. The third phase is the solution of the system equations for the nodal displacements. This includes the triangularization of the structure stiffness matrix and the actual evaluation of the nodal point displacements. The last phase is the calculation of the stresses at each integration point. This study will be used to demonstrate the relative importance of the order of the high-order element, the number of integration points used within each element, and the size of the model used (number of elements).

The most important quantity in this study is the total CPU time of the high-order solution compared to the conventional solution method. The total CPU time for the high-order elements ranging in degree of displacement field from third through sixth, versus the number of integration points is shown in Fig. 12. Recall that 44 integration points in the high-order element corresponds to the number of integration points used in the model of conventional elements (4 integration points per element × 11 elements). The horizontal line labeled bi-linear represents the total CPU time of the conventional method and is include in the figure as a reference to compare the CPU times of the various high-order elements (note that the number of integration points in the conventional elements are set to four). When eleven bi-linear elements are replaced with with a single bi-linear element (recall that the bi-linear elements were numbered for a bandwidth that corresponds to its use in the filament-wound sphere that is considerably larger than would be generated if the nodes were numbered efficiently), the elements of order three through six will reduce the computational time if one integration point per layer is used. If two integration points per layer are used, only the third- and fourth-order elements will reduce the overall computation time. When

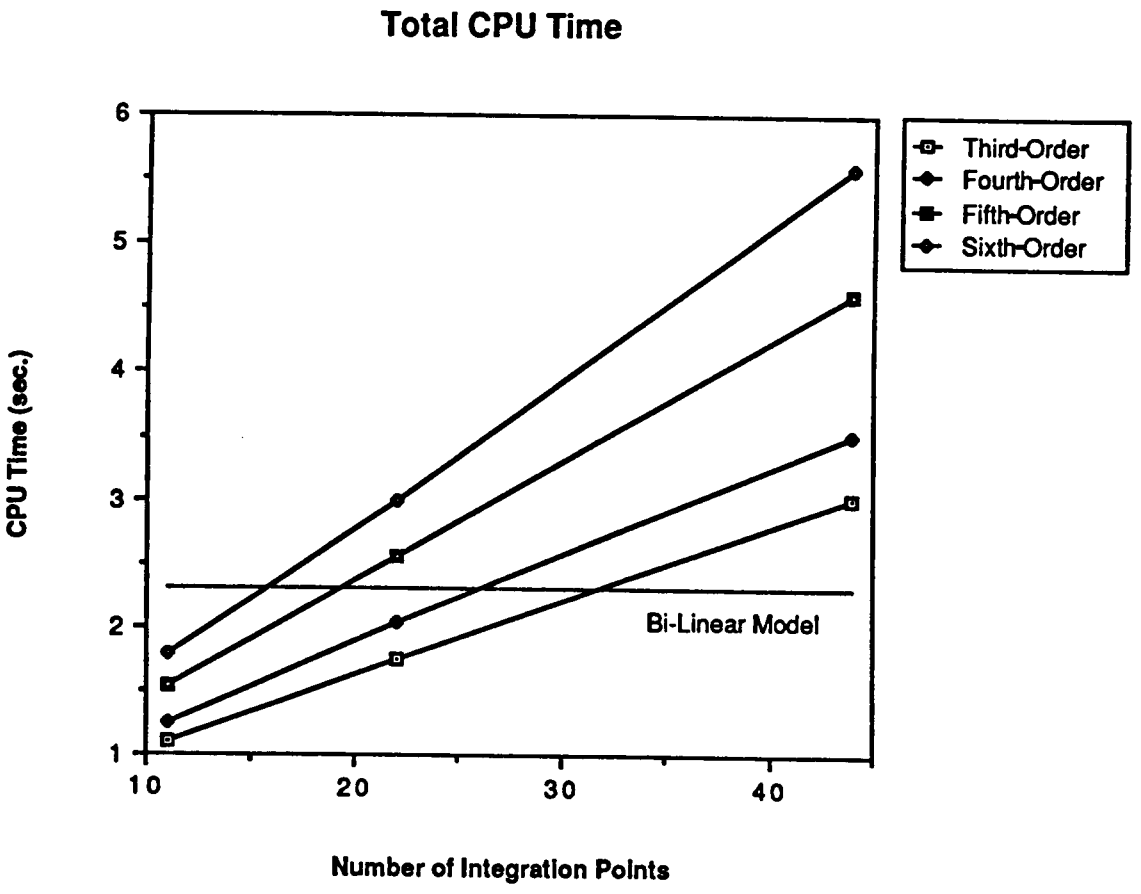

Figure 12. Total CPU Time for the Finite Element Solution

more than two integration points per layer are used, the high-order elements require more CPU time for a solution than the bi-linear model that actually contains four integration points per layer.

In the introduction, it was stated that one of the preliminary expectations was that the high-order elements would use less computational time in the input phase than the conventional finite element solution method. Figure 13 shows that this is in fact the case. It is also clearly shown that the CPU time is relatively constant for each order element and is not dependent on the number of integration points. There is, however an increase in the CPU time for higher order elements. The increase in CPU time is quantified by the efficiency (ratio of time savings to the CPU time for the bi-linear model) of high-order elements with respect to the conventional model, decreasing from 42 percent to 34 percent for the third- through sixth-order elements. The increase in the CPU time for the higher order elements is explained by the need to read and generate more nodal information. The increase of nodal information is created by the additional node definitions and larger connectivity, boundary condition, and related arrays.

One of the two phases of the finite element solution method that was evaluated in the theoretical study (section 3.2) was the generation of the structure stiffness matrix (section 3.2.2). This phase shows a strong dependence on the number of integration points used in the high-order elements. This dependence of the CPU time on the number of integration points is also shown in Eq. 3.9 which indicates the dependence is linear. The actual CPU times with the bi-linear element solution depicted as a horizontal line for comparison purposes are shown in Fig. 14. All but the third-order element are less efficient than the conventional method in this phase of the solution and for this particular model.

The potential efficiency of the high-order element during the solution of the nodal point displacements phase has been presented in section 2.2.1. As was expected based on those results, this phase of the solution method displayed the greatest efficiency for the composite element. However, as is shown in Fig. 15, the magnitude of the CPU time is relatively small and therefore its influence is consequently small also. The results presented in Figure 15 indicate that like the input phase, the CPU time is independent of the number of integration points and is highly dependent on the order of the element, as expected. Equations 3.7 and 3.8 (section 3.2.1) indicate that

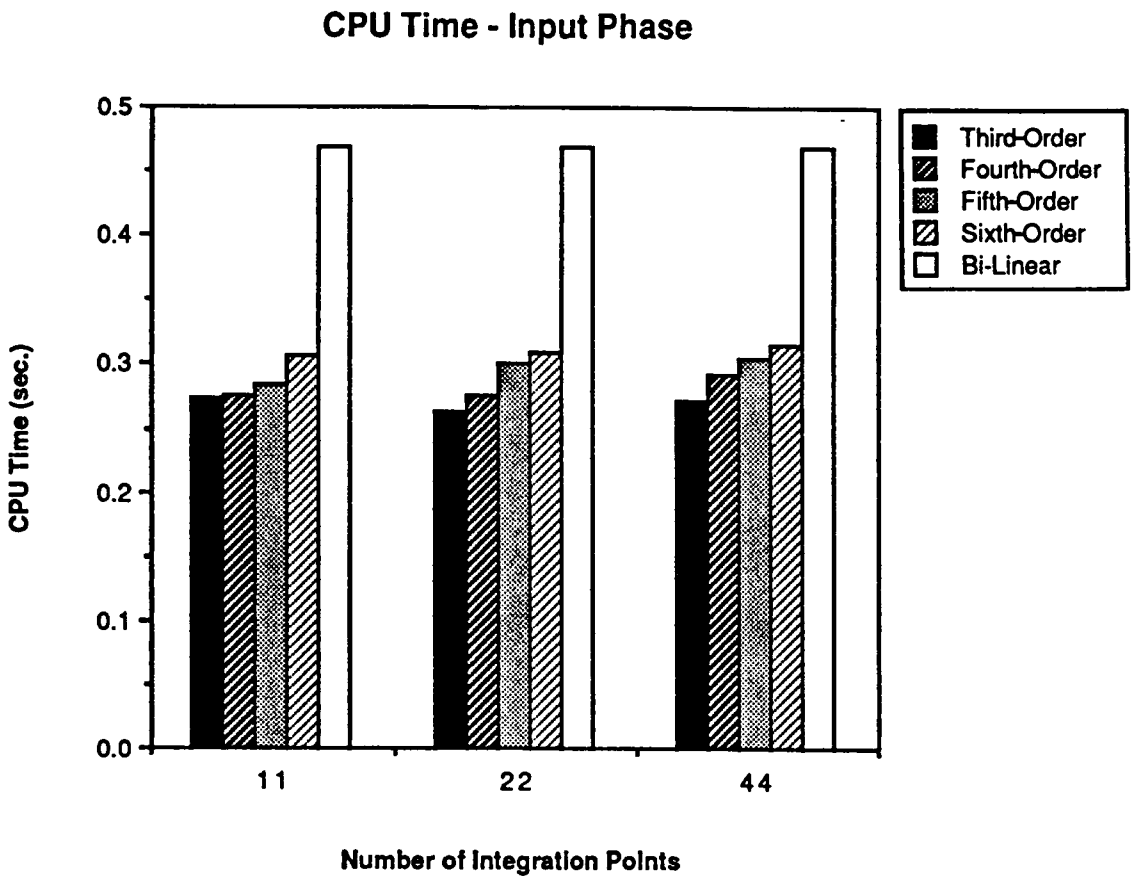

Figure 13. CPU Time for Input Phase of the Finite Element Solution

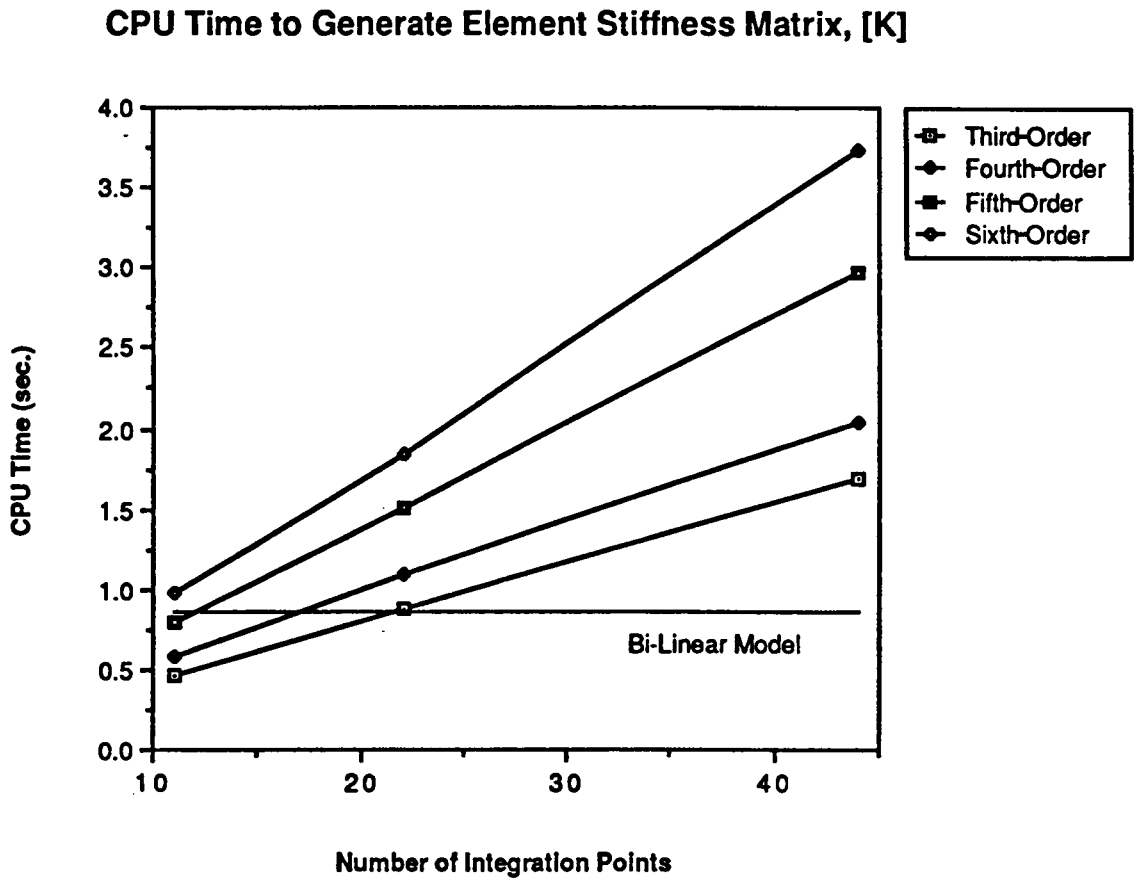

Figure 14. CPU Time for Generating the Structure Stiffness Matrix

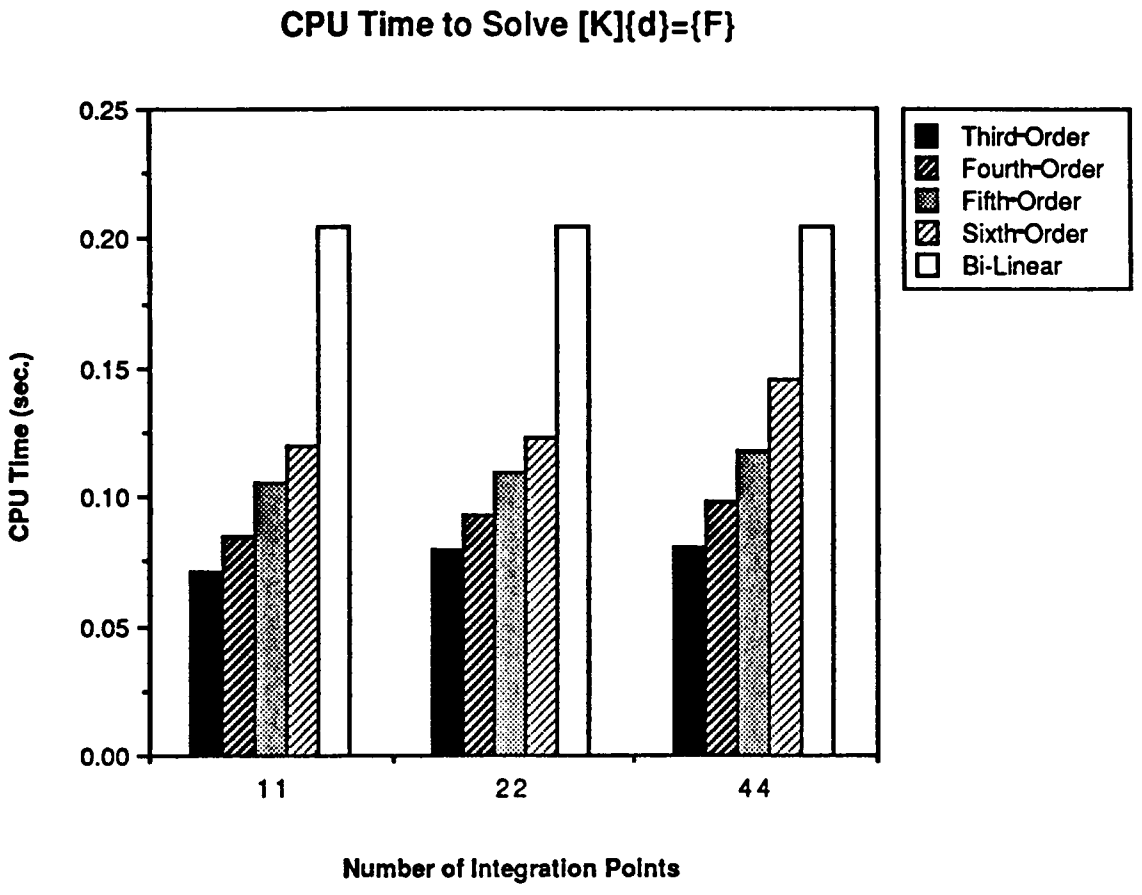

Figure 15. CPU Time to Solve the System Equations

the CPU time of the solution of the system equations is linear with respect to the number of equations and is quadratic with respect to the bandwidth. The actual CPU time appears to be linear with respect to the number of equations (nodes) as was the input phase as expected. The efficiencies range from 62 percent for the third-order element to approximately 40 percent for the sixth-order element.

The last phase of the solution method is calculation of the stresses and writing the results to the output file. The CPU times for this phase of the solution using high-order finite elements are presented in Fig. 16. Again, the influence of the number of integration points on the CPU time can be seen in Fig. 16, with the order of the assumed displacement field having a smaller influence. This phase of the solution method is also the second most CPU intensive process and therefore the time savings achieved with the option to reduce the number of integration points is significant when attempting to maximize the efficiency of the entire solution.

The relative importance of each phase of the solution method is more easily seen in Fig. 17, showing the portion of the total CPU time used by each of the four phases and illustrating the dominance of the structure stiffness matrix generation portion of the solution. It is important to note that the two most CPU intensive phases, creation of the structure stiffness matrix and calculation of the stresses, are both highly dependent on the number of integration points. The calculation of the stresses, once the nodal point displacements are calculated, is basically independent of order, which means that increasing the degree of the assumed displacement field is virtually 'free' for this portion of the solution.

The portion of the total CPU time used by the four phases for a fourth-order element with 11, 22, and 44 integration points is given in Table 3. It is clear that any significant improvements in the efficiency of this element will have to address the structure stiffness matrix generation phase. The primary motivation for initiating this research program was the belief that by reducing the number of nodes (system equations) with the use of the high-order elements that the overall solution time could be reduced. The percentage of the total CPU time is redistributed with an increase in the degree of the assumed displacement field and is shown in Table 4. Again, the importance of the structure stiffness matrix formulation phase is highlighted with the input phase and calcu-

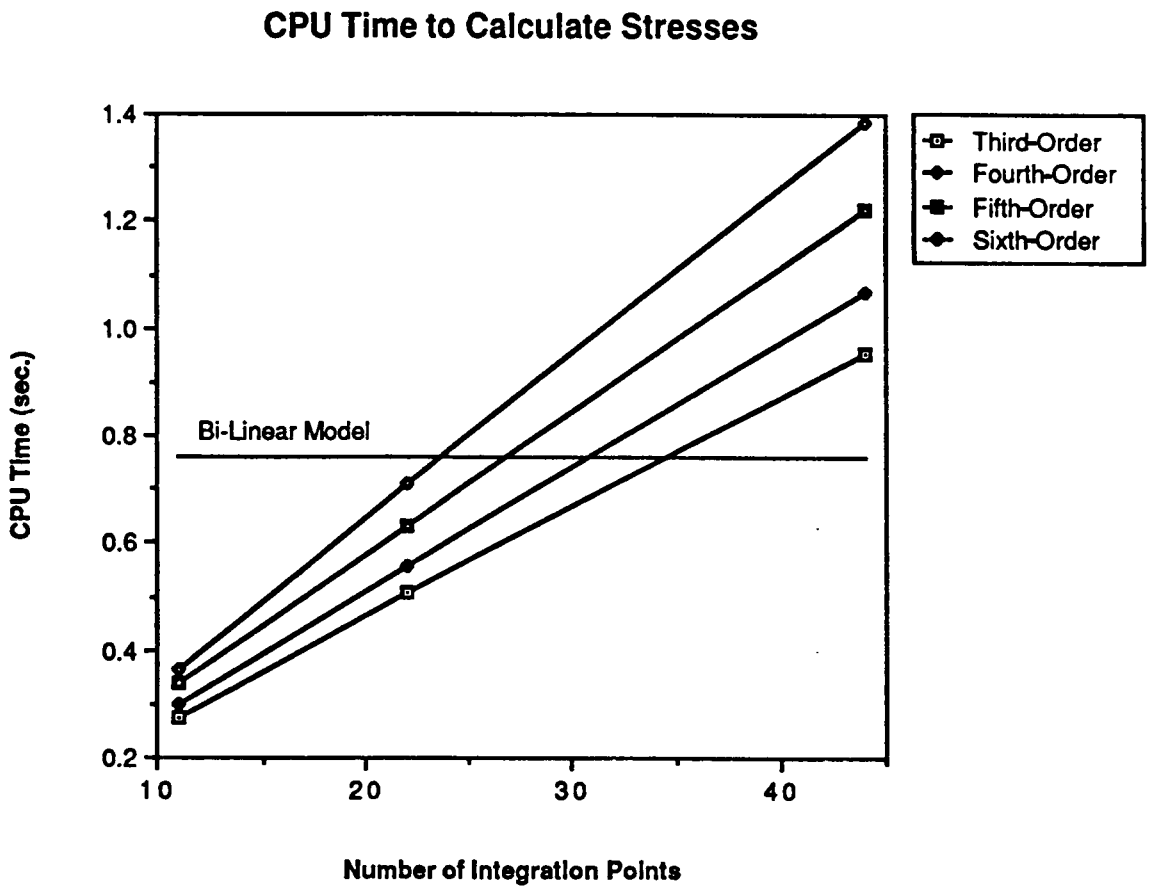

Figure 16. CPU Time to Calculate Stresses

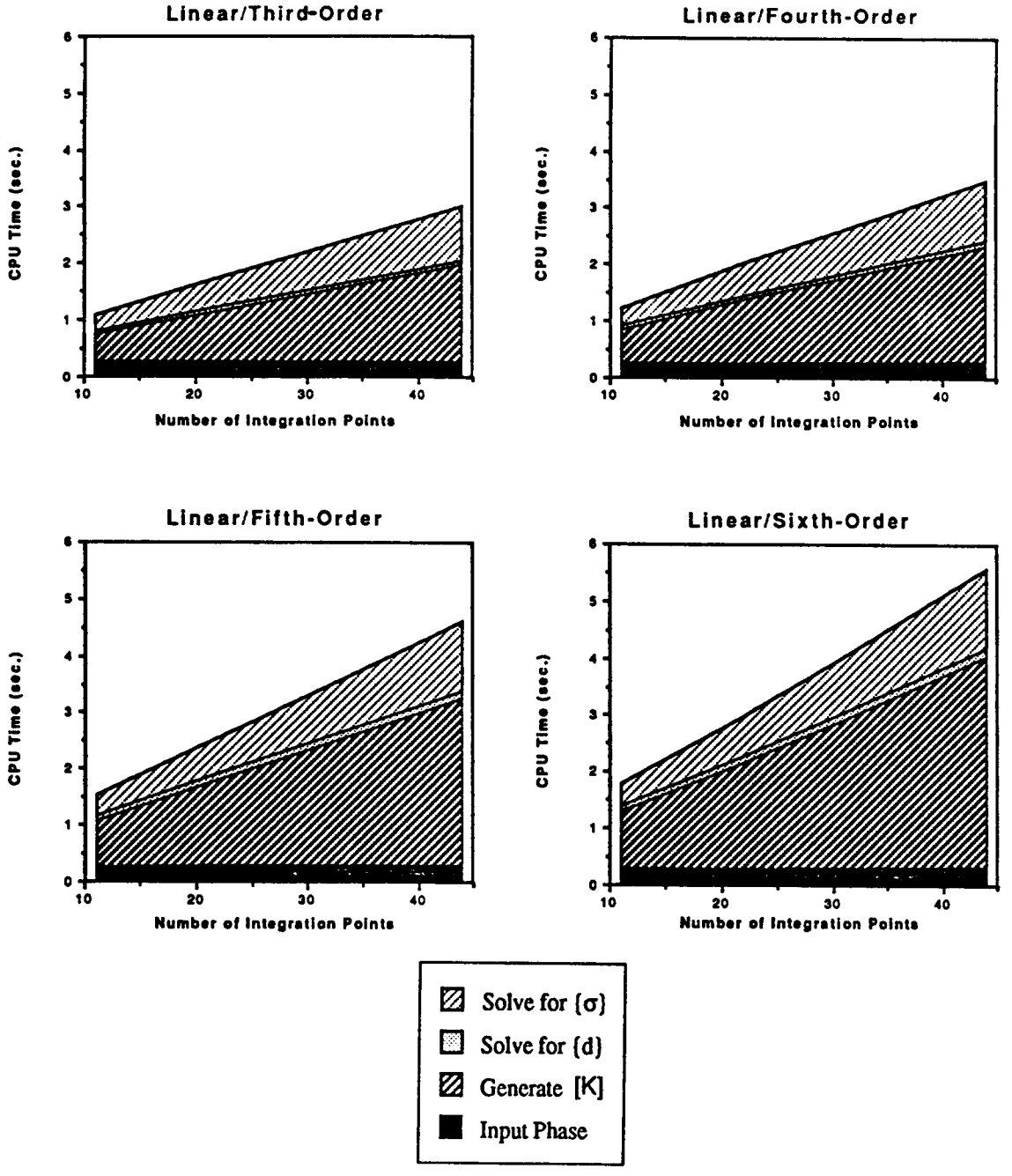

Figure 17. Portion of Total CPU Time for Each Phase of the Solution

Table 3. Percent of Total CPU Time - Fourth-Order Element

1 Element Model - 11 Integration Pts./Element				
Phase of Solution	Order of Element			
	3	4	5	6
Input	25%	22%	19%	17%
Generate [K]	43%	47%	52%	55%
Solve for {d}	7%	7%	7%	7%
Solve for {σ}	25%	24%	22%	21%
	100%	100%	100%	100%
Total CPU Time	1.094 sec.	1.243 sec.	1.533 sec.	1.784 sec.

Table 4. Percent of Total CPU Time - 11 Integration Points/Element

Phase of Solution	Number of Integration Points		
	11	22	44
Input	22%	13%	8%
Generate [K]	47%	54%	58%
Solve for {d}	7%	5%	3%
Solve for {σ}	24%	28%	31%
	100%	100%	100%
Total CPU Time	1.243 sec.	2.030 sec.	3.505 sec.

lation of the stresses having approximately equal weight when the number of integration points are fixed. It is also important to note that the some of the proportions shown in Table 4 are not linear with respect to the number of nodes in the model. As an example, the percentage of the total CPU time dedicated to solving the system equations for the eleven element model is only nine percent, as will be shown in Chapter 6 when approximately 1200 elements are used to model a filament-wound pressure vessel, the proportion raises to 32 percent and becomes the most CPU intensive operation.

4.0 Accuracy Study

The primary objective of this work was to develop a design-oriented code for filament-wound spherical pressure vessels that would decrease the computation time required when conventional linear elements are used. Generally, accuracy is sacrificed to some degree when computation time-saving options are exercised in the formulation of numerical techniques. In order for this element to be useful in design applications, where very little may be known about the resulting stress levels, an accuracy study was performed to generate results to problems for which exact solutions exist to determine the accuracy level of this novel formulation. Based on these results, the design engineer should more fully appreciate the advantages and limitations of the chosen high-order element and number of integration points within the element.

The finite element solution method is used for the analysis and design of filament-wound spherical pressure vessels because the geometry is so complex that exact solutions are not available. In order to test the accuracy of this element, a geometry that was simple enough to obtain the exact solution was necessary. The selected geometry was a cylindrical pressure vessel with various material properties, i.e., homogeneous isotropic, homogeneous orthotropic, nonhomogeneous orthotropic (filament-wound), and nonhomogeneous isotropic (steel-copper). The theoretical elasticity solution with which the finite element results are compared is presented in Appendix A.

4.1 High-Order Finite Element Results

4.1.1 Test Model

In order to evaluate the composite element, several simple material models were employed from which the results of the various high-order elements could be compared with theoretical solutions. The model used in this study is an internal pressure loaded thick wall cylinder with free ends as shown in Fig. 18. The high-order finite element model consists of a single axisymmetric element. The single element is subdivided into eleven layers, each of equal thickness. For 'single layer' models, all eleven layers of the finite element are given the same material property. The average stresses and strains in each layer of the element are generated by the finite element code, providing enough resolution to compare with the theoretical cylinder solutions discussed and presented in the previous section.

Three basic material-model types were studied; isotropic cylinders, homogeneous orthotropic cylinders and non-homogeneous orthotropic cylinders (filament-wound). The isotropic and orthotropic cylinders are characterized as 'single layer models'. That is, all eleven layers of the high-order element have the same material property. The material properties used in the models are shown in Table 5. Steel was the material chosen for the isotropic model and Kevlar 49-Epoxy for the orthotropic models. Kevlar 49-Epoxy was also used for the filament-wound models. Three filament wound cylinder models are presented. In the first model the fiber or winding angle changes incrementally from 0° on the inside to 90° on the outside of the cylinder. The second model is similar to the first, however, the fiber angle changes from 90° on the inside of the cylinder to 0° on the outside of the vessel. Eleven layers were used in both models, which means that the fiber angle was incremented 9° for each layer. The last model presented is one in which the fiber angle changes from 0° to 90° at the center of the cylinder wall, and back to 0°, which necessitates an 18° increment of the fiber angle per layer.

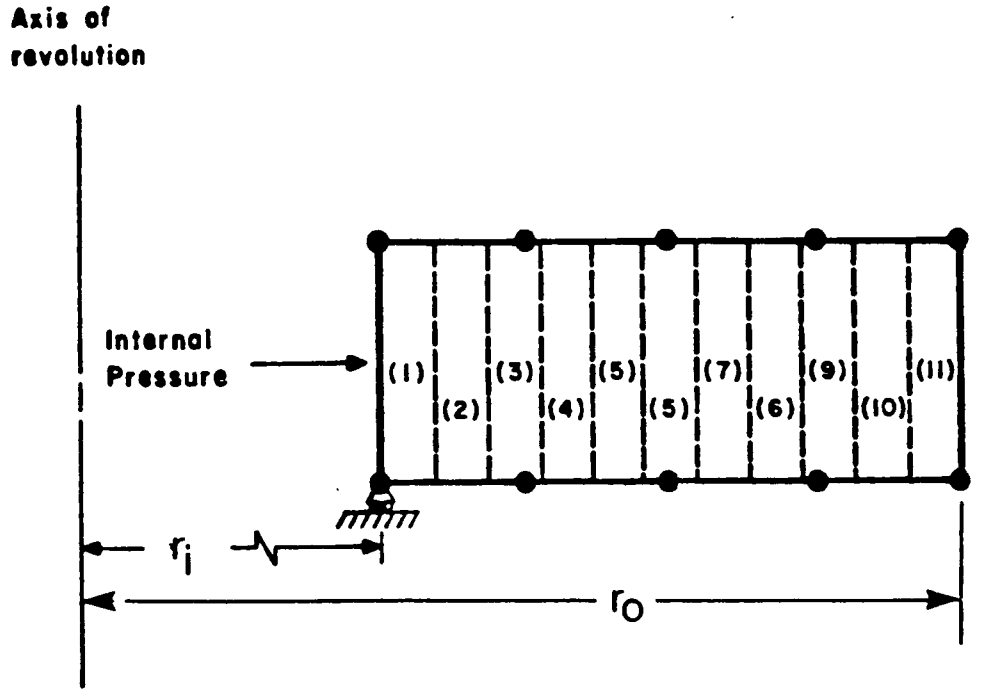

Figure 18. Finite Element Model of the Test Problem

Table 5. Material Properties of Test Models

Model #1 : Material - Steel
E = 207 GPa (30 Mpsi)
v = 0.3

Model #2, #3, #4, #5 : Material - Fiber-Epoxy	
E_t = 82.7 GPa (12 Mpsi)	ν_{zr} = 0.3
E_z = 6.9 Gpa (1 Mpsi)	ν_{tr} = 0.3
E_r = 6.9 Gpa (1 Mpsi)	ν_{tz} = 0.3

Fiber Angles (degrees from hoop direction)				
Layer No.	Model 2	Model 3	Model 4	Model 5
1	0	0	90	0
2	0	9	81	18
3	0	18	72	36
4	0	27	63	54
5	0	36	54	72
6	0	45	45	90
7	0	54	36	72
8	0	63	27	54
9	0	72	18	36
10	0	81	9	18
11	0	90	0	0

In the current finite element code, a single material is specified for each element and the fiber angle for each of the eleven layers of the laminate is also specified. The finite element program then performs the necessary transformations (material, stress, and strain) on each internal layer of the element. However, the material transformations from the principal material directions to the global, *r-z-t*, coordinate system have also been carried out externally for the filament-wound models, and the results are listed in Table 6 in order to clearly demonstrate the variation of material properties that the single finite element is attempting to model.

4.1.2 Isotropic Material Results

Before complicated filament-wound composite structures were analyzed with the high-order elements, the element's validity was first tested using the isotropic thick-wall cylinder. The values of radial and hoop stress for high-order elements with second- through fifth-order displacement field orders along with the theoretical values are listed in Tables 7 and 8. The theoretical value is calculated at the center of each layer and is not necessarily the average value for the layer because of the nonlinear nature of the profiles. However, the theoretical stress profiles may be closely approximated by a linear function within each layer, as can be seen in many of the figures to follow such as Fig. 19. The mid-layer stresses correspond to the average with a high degree of accuracy. Tables 7 and 8 show that the third-order element models the response of the thick-wall cylinder very well with very little being gained by increasing the order of the element to fourth- and fifth-order. The theoretical stress fields with the average layer stresses calculated by the finite element program superimposed on the graph are shown in Figs. 19 and 20. Both figures show excellent correlation of results. A more quantitative analysis is shown in Fig. 21 which plots the percent error for each calculated radial stress value. The percent error is defined as

$$\text{Percent Error}(i) = \frac{\text{calculated}(i) - \text{theoretical}(i)}{\text{theoretical}(1)} \times 100 \quad ; \quad i = 1,2,3,\ldots,11 \qquad [4.24]$$

Table 6. Transformed Material Properties of Filament Wound Test Models

Model : Filament Wound - 0° to 90°
Material : Fiber-Epoxy

Layer	E_t GPa (Mpsi)	E_z GPa (Mpsi)	E_r GPa (Mpsi)	ν_{zr}	ν_{tr}	ν_{tz}
1	82.7	6.89	6.89	0.300	0.300	0.300
	(12.0)	(1.00)	(1.00)			
2	77.4	6.82	6.89	0.293	0.218	0.554
	(11.2)	(.989)	(1.00)			
3	59.9	6.65	6.89	0.270	0.031	1.115
	(8.69)	(.965)	(1.00)			
4	35.0	6.56	6.89	0.229	-0.081	1.397
	(5.09)	(.952)	(1.00)			
5	17.3	7.05	6.89	0.164	-0.035	1.178
	(2.51)	(1.02)	(1.00)			
6	9.53	9.53	6.89	0.071	0.071	0.798
	(1.38)	(1.38)	(1.00)			
7	7.05	17.3	6.89	-0.035	0.164	0.481
	(1.02)	(2.51)	(1.00)			
8	6.56	35.0	6.89	-0.081	0.229	0.261
	(.951)	(5.09)	(1.00)			
9	6.65	59.9	6.89	0.031	0.270	0.124
	(.965)	(8.69)	(1.00)			
10	6.82	77.4	6.89	0.218	0.293	0.049
	(.989)	(11.2)	(1.00)			
11	6.89	82.7	6.89	0.300	0.300	0.025
	(1.00)	(12.0)	(1.00)			

Table 7. Comparison of Radial Stress for an Isotropic Cylinder Normalized by the Internal Pressure

Layer	Theoretical	Second-Order	Third-Order	Fourth-Order	Fifth-Order
1	-0.941	-0.880	-0.941	-0.950	-0.956
2	-0.828	-0.805	-0.832	-0.830	-0.824
3	-0.721	-0.727	-0.726	-0.719	-0.713
4	-0.620	-0.644	-0.624	-0.616	-0.615
5	-0.523	-0.559	-0.525	-0.520	-0.524
6	-0.432	-0.470	-0.431	-0.431	-0.436
7	-0.343	-0.378	-0.342	-0.346	-0.350
8	-0.262	-0.283	-0.258	-0.264	-0.264
9	-0.183	-0.185	-0.180	-0.186	-0.180
10	-0.107	-0.085	-0.106	-0.108	-0.102
11	-0.035	+0.018	-0.039	-0.031	-0.036

Table 8. Comparison of Hoop Stress for an Isotropic Cylinder Normalized by the Internal Pressure

Layer	Theoretical	Second-Order	Third-Order	Fourth-Order	Fifth-Order
1	5.487	5.512	5.488	5.484	5.481
2	5.374	5.385	5.373	5.374	5.376
3	5.267	5.266	5.266	5.268	5.271
4	5.165	5.157	5.165	5.168	5.168
5	5.069	5.055	5.069	5.071	5.069
6	4.977	4.962	4.979	4.978	4.976
7	4.891	4.876	4.892	4.890	4.888
8	4.807	4.798	4.810	4.806	4.806
9	4.728	4.726	4.730	4.727	4.729
10	4.652	4.661	4.653	4.652	4.654
11	4.580	4.601	4.579	4.582	4.580

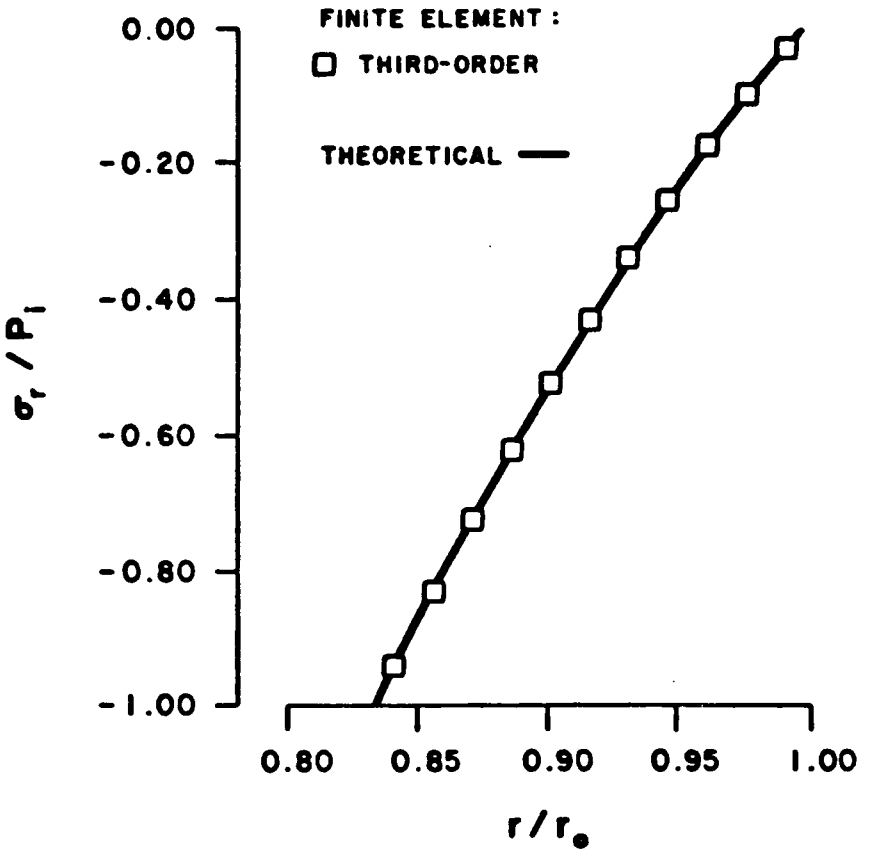

Figure 19. Radial Stress Profile in an Isotropic Cylinder Normalized by the Internal Pressure Load

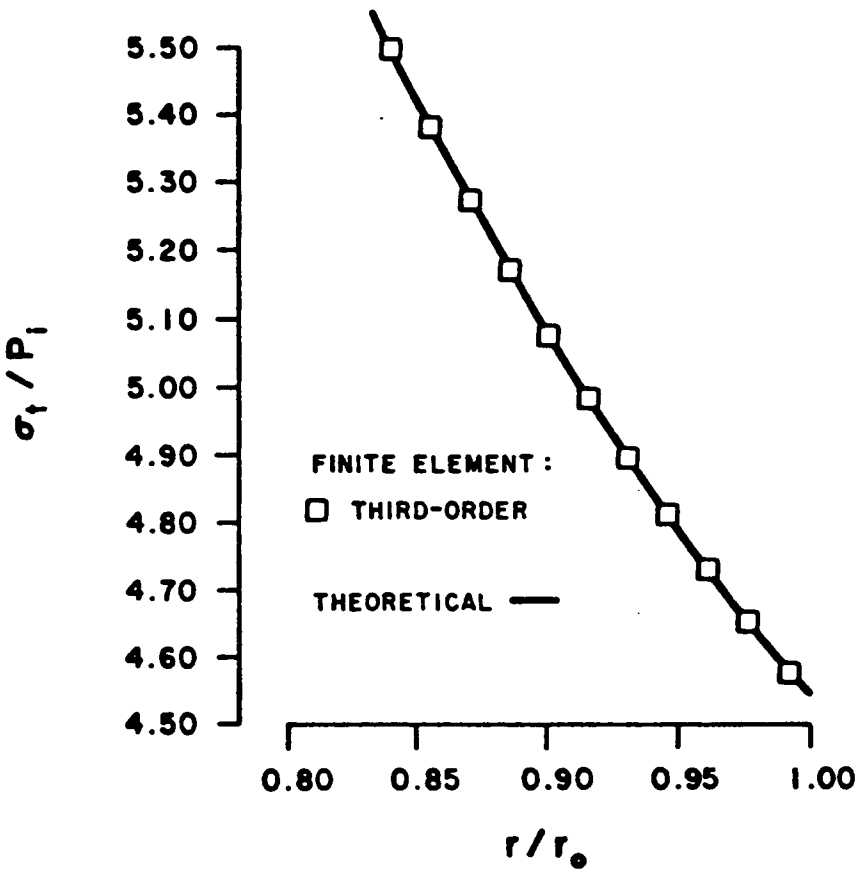

Figure 20. Hoop Stress Profile in an Isotropic Cylinder Normalized by the Internal Pressure Load

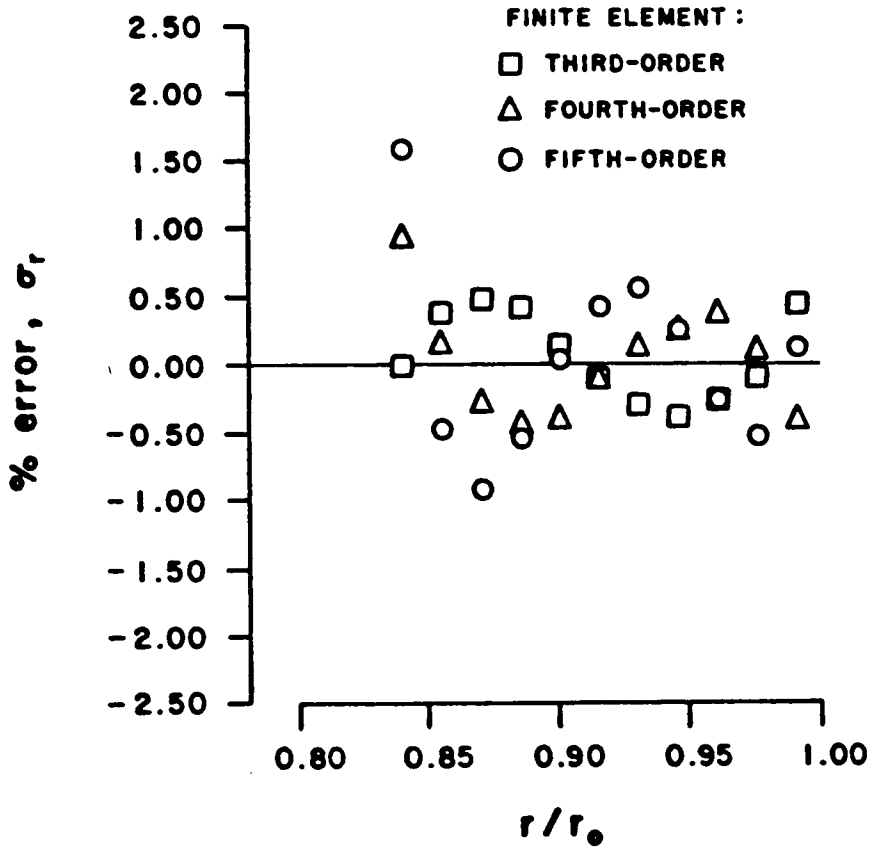

Figure 21. Radial Stress Error in an Isotropic Cylinder for a Third- through Fifth-Order Element

Where calculated(i) refers to the average layer value calculated by the finite element program, theoretical(i) refers to the theoretical value at the center of layer i, and theoretical(1) is the base.

Again, these results can be used to show excellent correlation between the calculated and theoretical results, however, increasing the order of the element beyond cubic generates slightly greater errors, particularly on the inside edge of the pressure vessel. The percent error in the radial stress for the third- through fourth-order elements is shown in Fig. 21 Again, the figure shows close agreement between theory and the calculated values from the finite element program. The error in the hoop stress is less than $\pm$ 0.1 percent.

4.1.3 Homogeneous Orthotropic Material Results

The second set of results to be presented is for the 'single-layer' orthotropic cylinder. As in the previous case, convergence to the theoretical values occurs in a relatively low-order element. The theoretical and finite element results for radial and hoop stress for the fourth-order element are presented in Figs. 23 and 24. The percent error for the radial and hoop stress are shown in Figs. 25 and 26, indicating that the percent error is typically less than 0.4% except for the radial stress in the first layer which is in error by approximately 1.0%.

4.1.4 Nonhomogeneous Orthotropic Material Results

The filament-wound composite cylinder presents a more difficult problem as the finite element must try to model a system that has a discontinuous radial-strain profile. The first of the filament-wound composite cylinders to be analyzed consists of Kevlar 49-Epoxy material that is oriented from 0° to 90° at 9° increments, as described in Tables 5 and 6. Because the model consists of eleven layers with significantly different elastic moduli in the global coordinate system (see Table 6) and the radial stress profile must be continuous, therefore, the radial-strain is discontinuous at

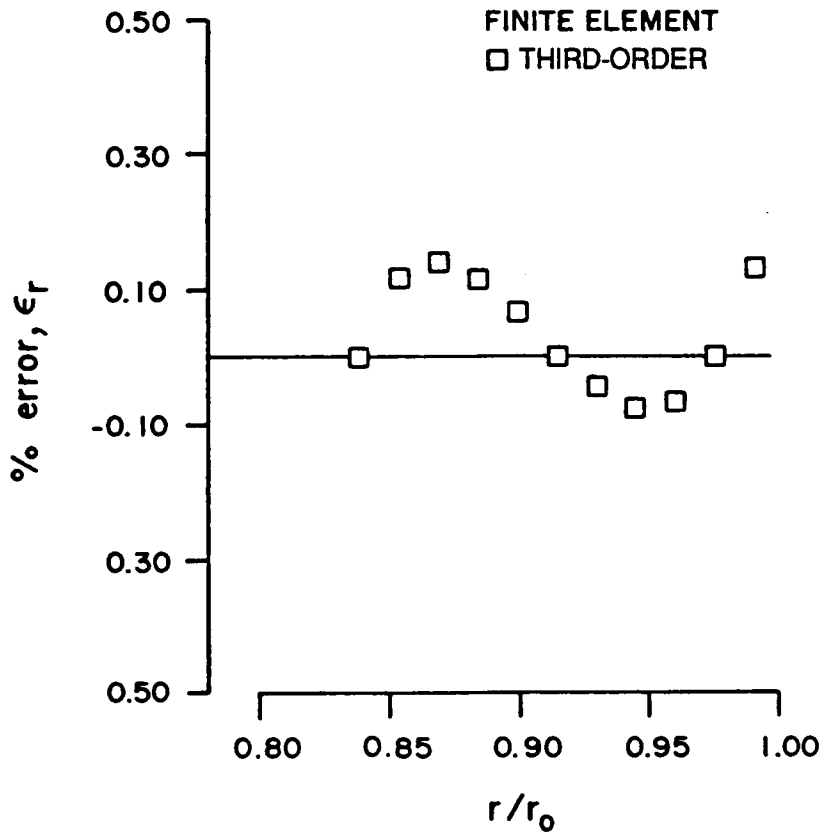

Figure 22. Radial Strain Error in an Isotropic Cylinder for a Third-Order Element

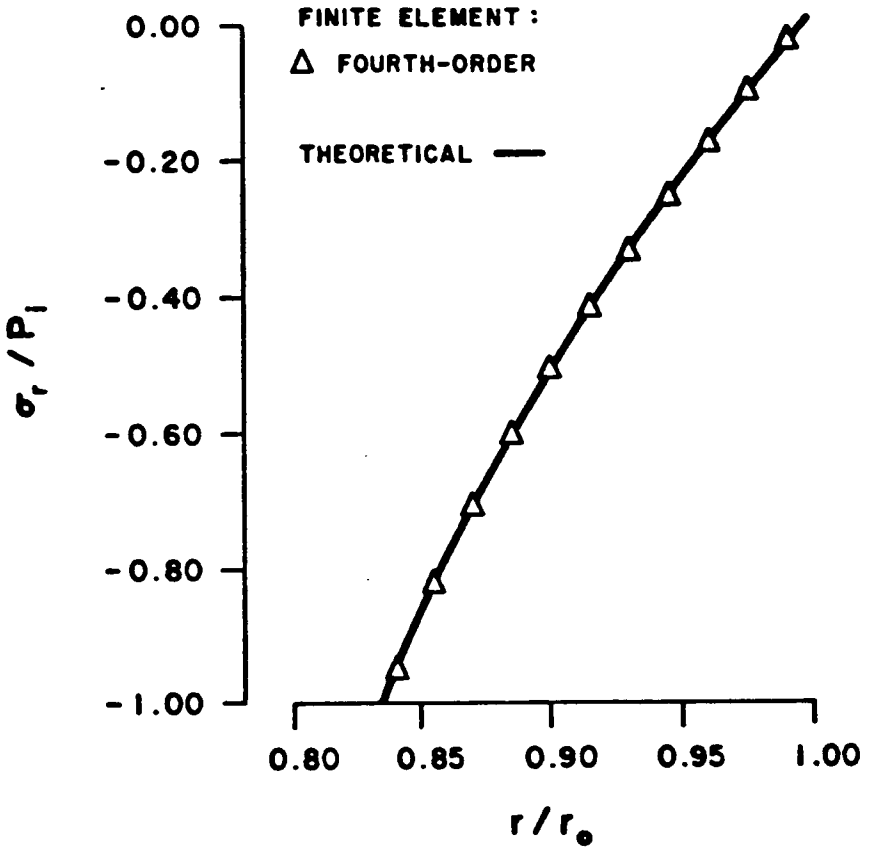

Figure 23. Radial Stress Profile in an Orthotropic Cylinder Normalized by the Internal Pressure Load

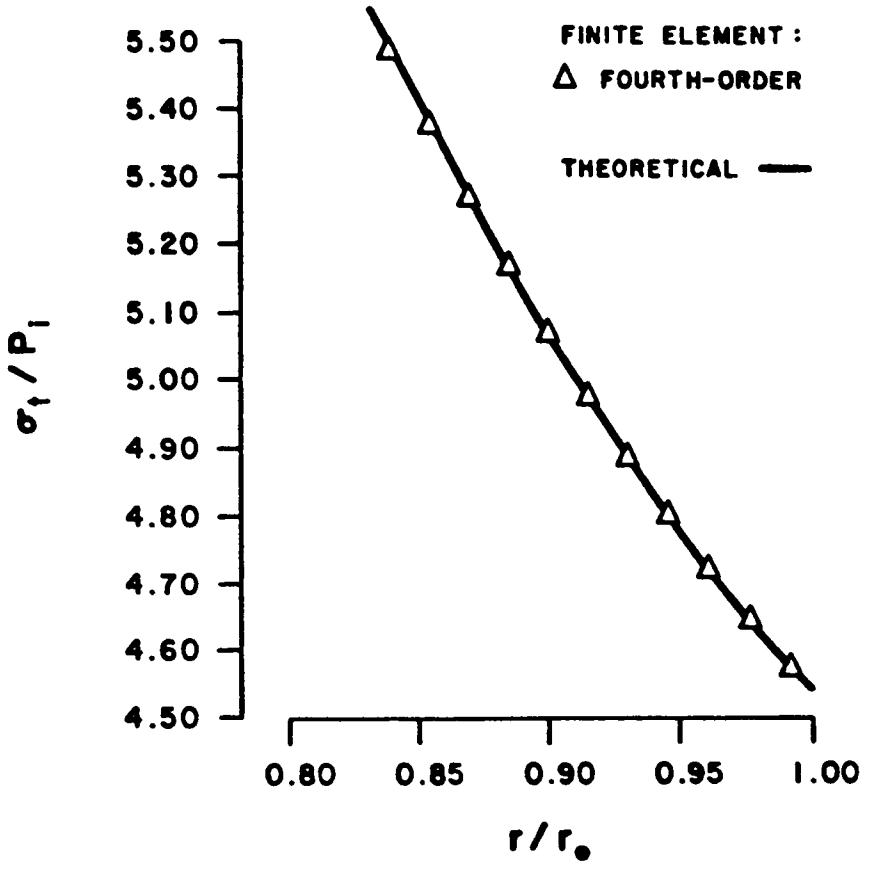

Figure 24. Hoop Stress Profile in an Orthotropic Cylinder Normalized by the Internal Pressure Load

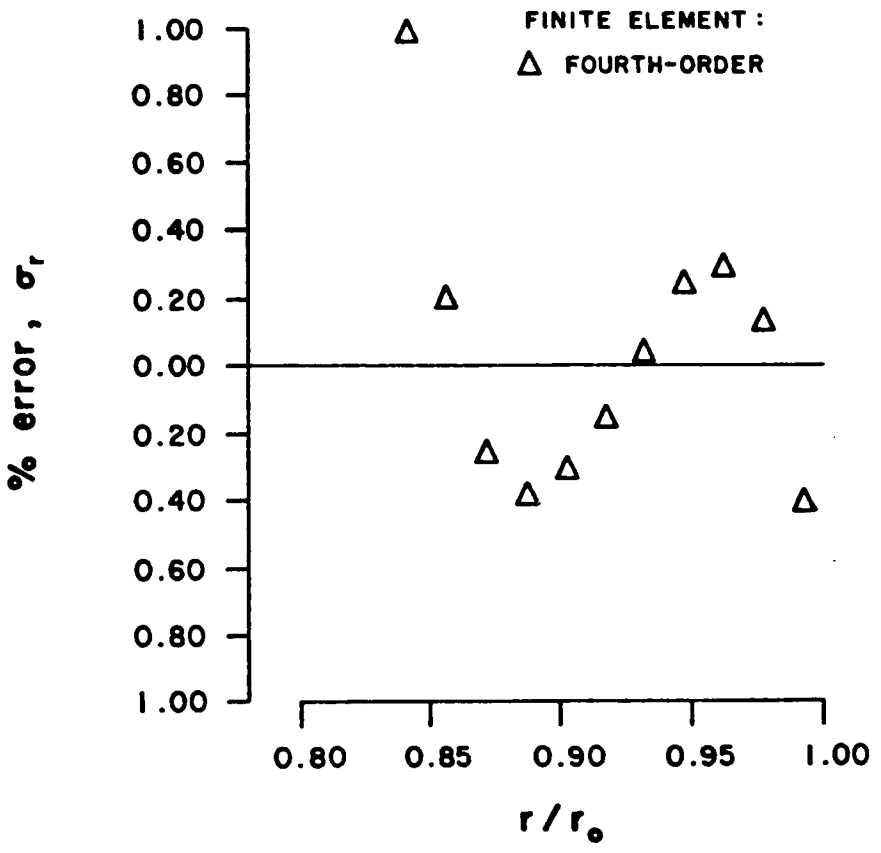

Figure 25. Radial Stress Error in an Orthotropic Cylinder for a Fourth-Order Element

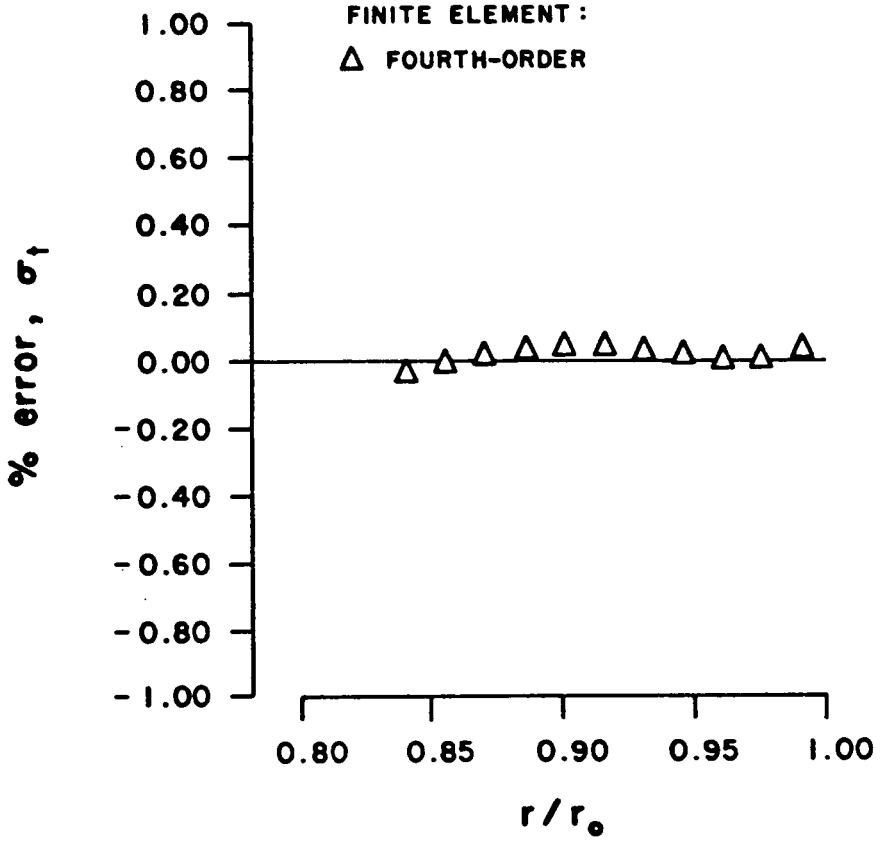

Figure 26. Hoop Stress Error in an Orthotropic Cylinder for a Fourth-Order Element

the interface of each layer. The theoretical radial and hoop stress profiles with the finite element results from a fourth-order element superimposed are presented in Figs. 27 and 28. A quantitative analysis of the previous two figures is given in Figs. 29 and 30 by showing the percent error, which remains below 3 percent, for both radial and hoop stress. The complexity of this problem can be appreciated by showing the discontinuous radial strain profile (Fig. 31) which the finite element is trying to duplicate with a continuous function.

Model #4 is similar to the previous model just described. This model simply reverses the order of the layers in model #3. Rather than the orientation of the fiber direction of the composite layers being from 0° to 90°, model #4 has layers with orientations varying from 90° to 0°. The theoretical and finite element results from the fourth-order element are presented in Figs. 32 and 33 showing the radial and hoop stress profiles.

The most complex model that has been evaluated by the high-order finite element and for which an elasticity solution has also been generated, thus far, is a filament-wound cylinder with the fibers oriented at 0° on the inside edge, changing to 90° in the center of the cylinder wall and rotating back to 0° on the outside edge of the pressure vessel. The radial stress profiles for the third- thru sixth-order elements are shown in Fig. 34, showing the accuracy is increased with the higher order elements but that there is very little change between the fifth- and sixth-order elements. This fact is shown more clearly in Fig. 35 which shows the fourth-, fifth- and sixth-order error in the radial stress. The excellent correlation between the theoretical hoop stress and the sixth-order finite element results can be seen in Fig. 36.

4.2 Discussion of Results

All of the theoretical results that have been presented have used a plane-stress assumption. The plane stress assumption, by definition, yields longitudinal stresses that are zero as the cylinder height approaches zero. In a cylinder of finite height the average longitudinal stress in an uncon-

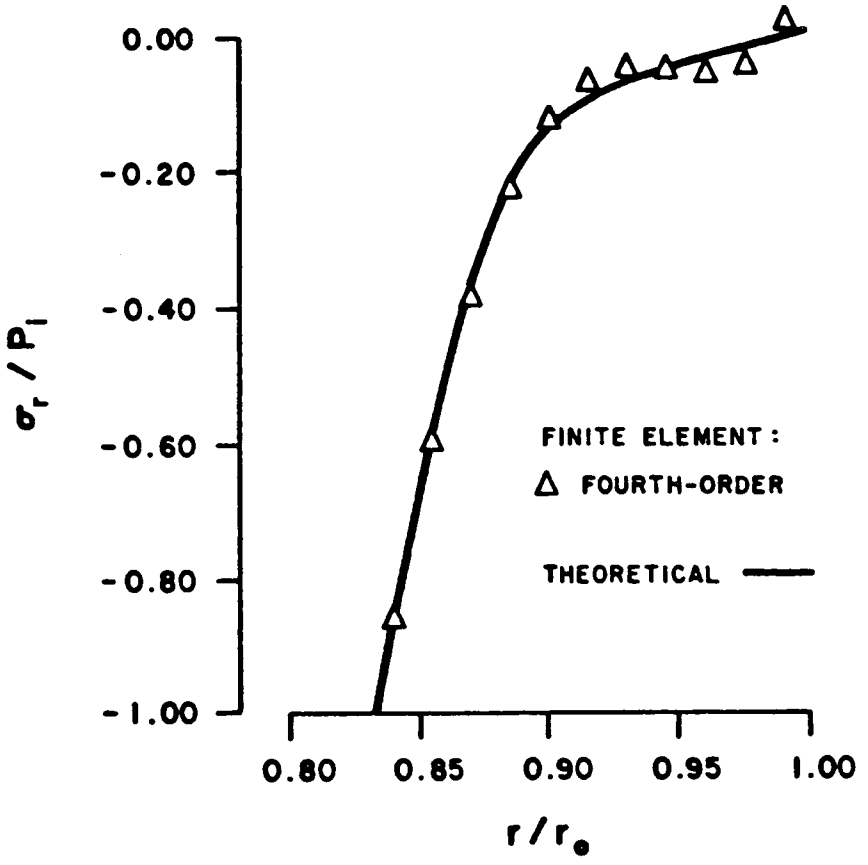

Figure 27. Radial Stress Profile in an 11 Layer Orthotropic Cylinder , Fiber Angles 0-90 degrees, for a Fourth-Order Element

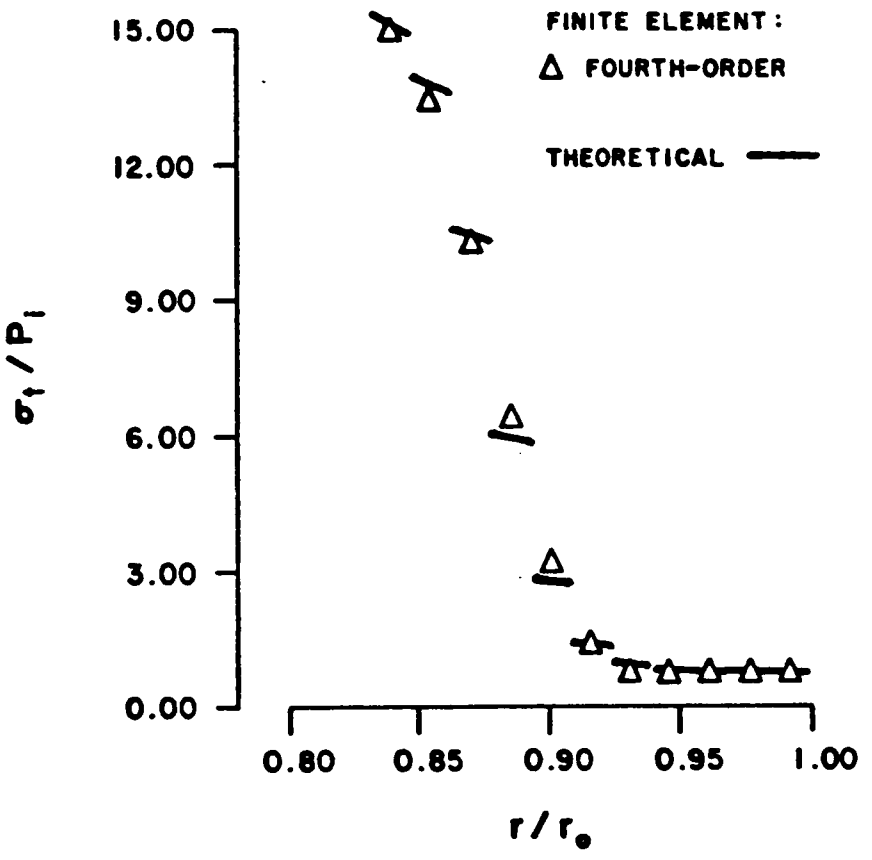

Figure 28. Hoop Stress Profile in an 11 Layer Orthotropic Cylinder , Fiber Angles 0-90 degrees, for a Fourth-Order Element

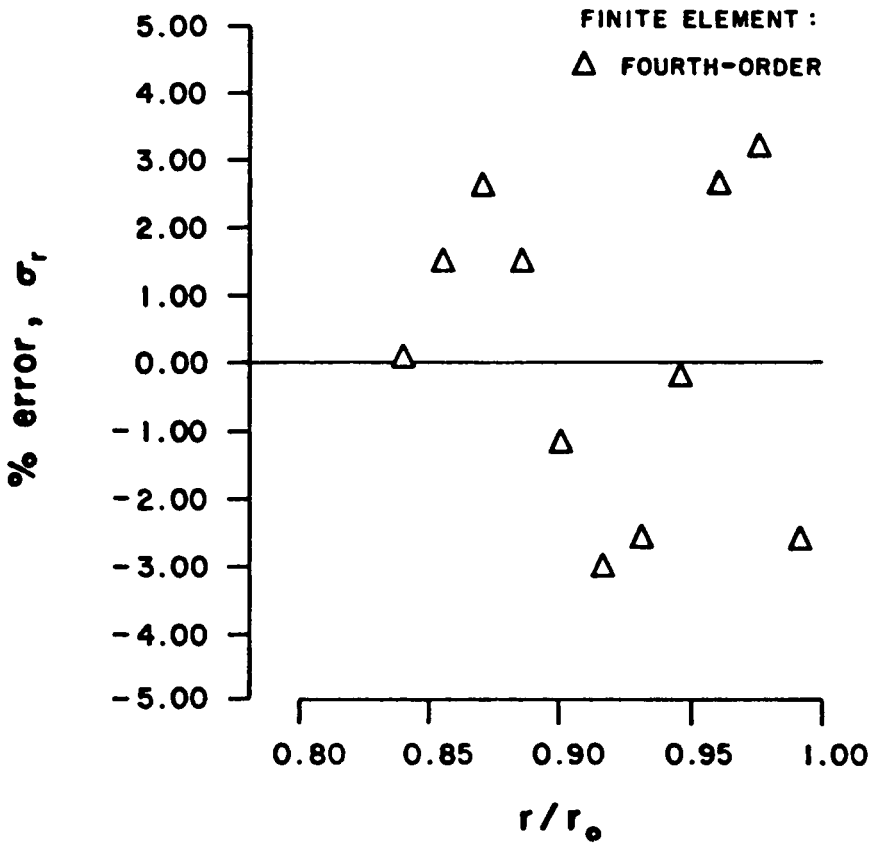

Figure 29. Radial Stress Error in an 11 Layer Orthotropic Cylinder , Fiber Angles 0-90 degrees, for a Fourth-Order Element

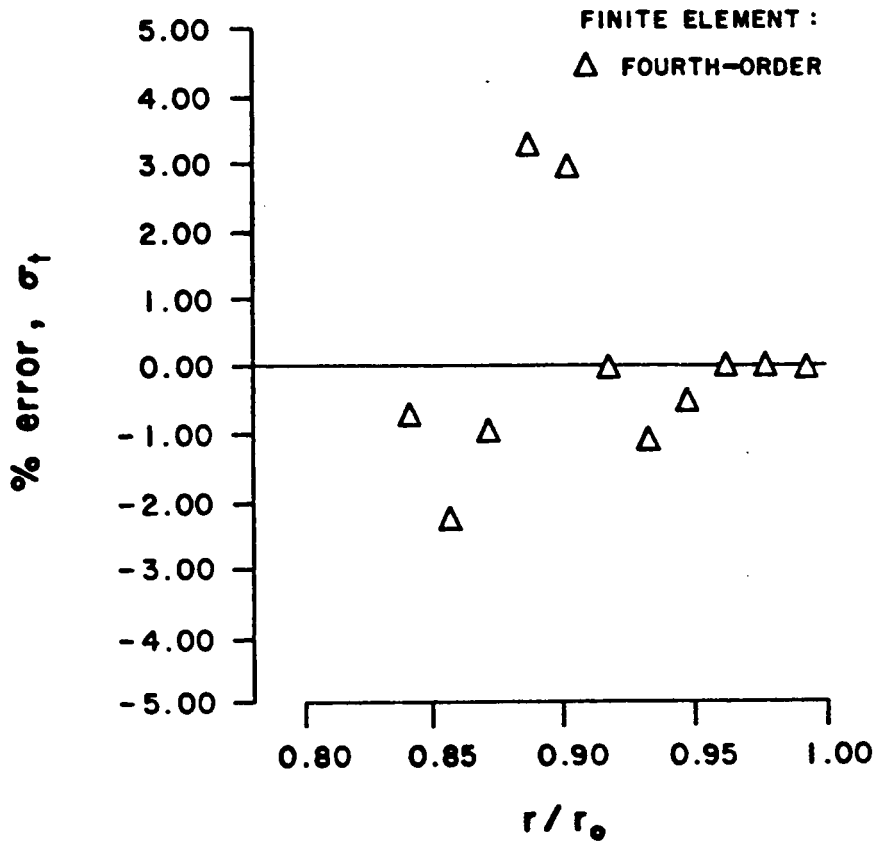

Figure 30. Hoop Stress Error in an 11 Layer Orthotropic Cylinder , Fiber Angles 0-90 degrees, for a Fourth-Order Element

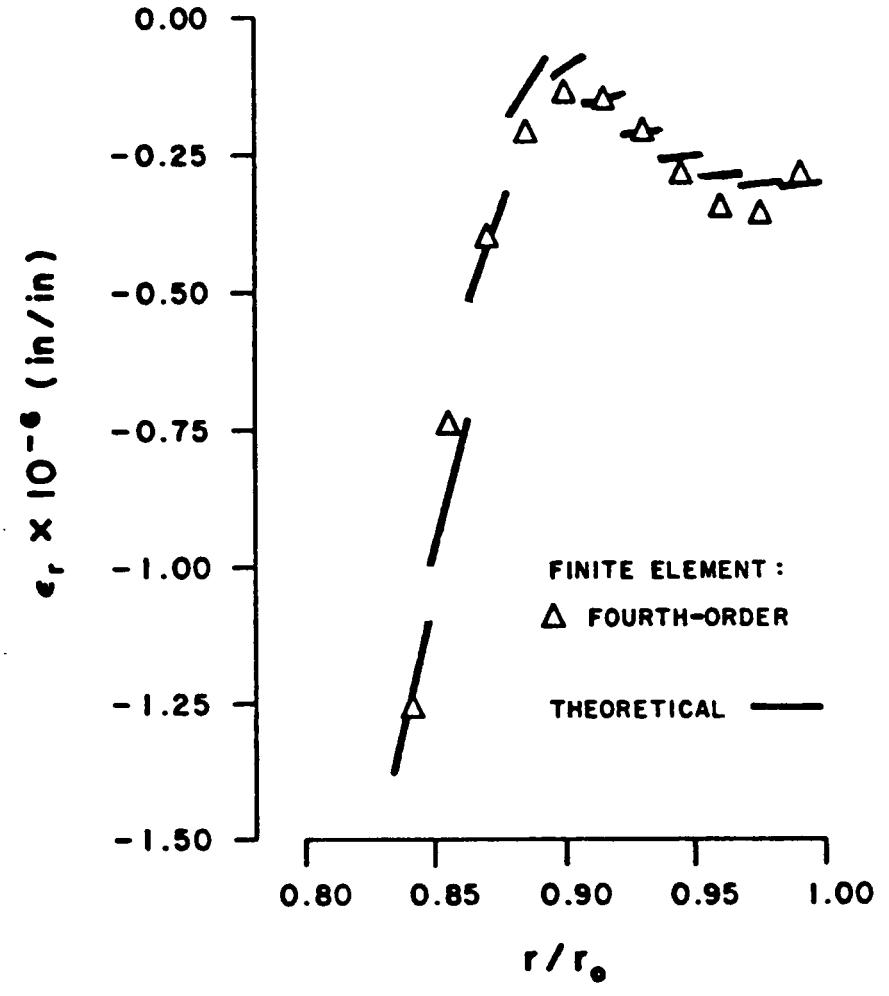

Figure 31. Radial Strain Profile in an 11 Layer Orthotropic Cylinder , Fiber Angles 0-90 degrees, for a Fourth-Order Element

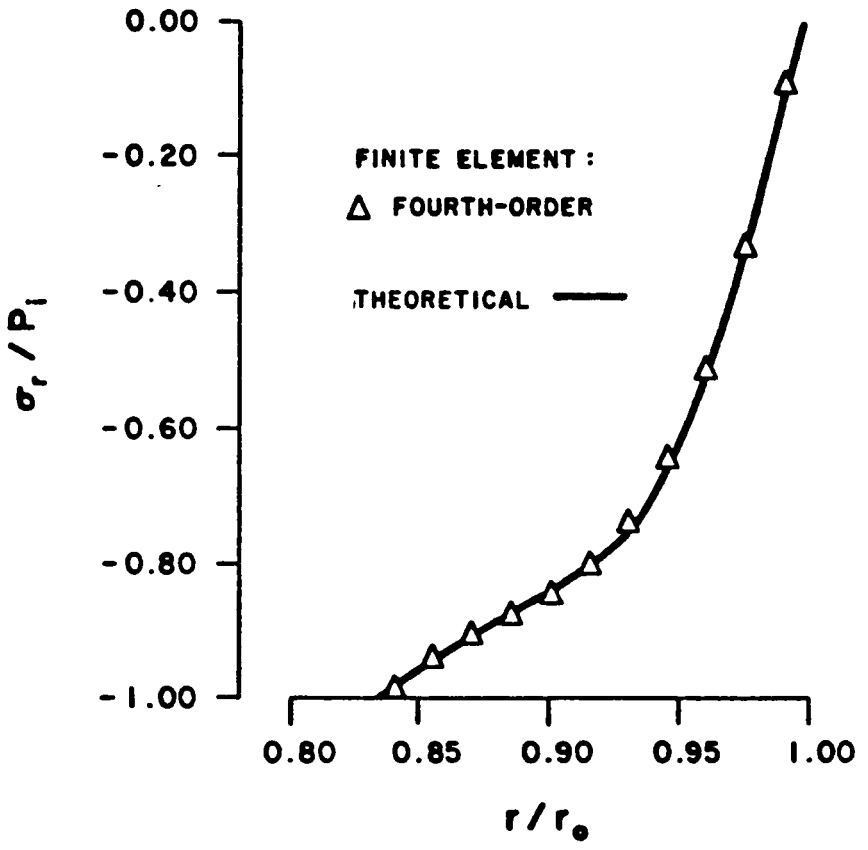

Figure 32. Radial Stress Profile in an 11 Layer Orthotropic Cylinder , Fiber Angles 90-0 degrees, for a Fourth-Order Element

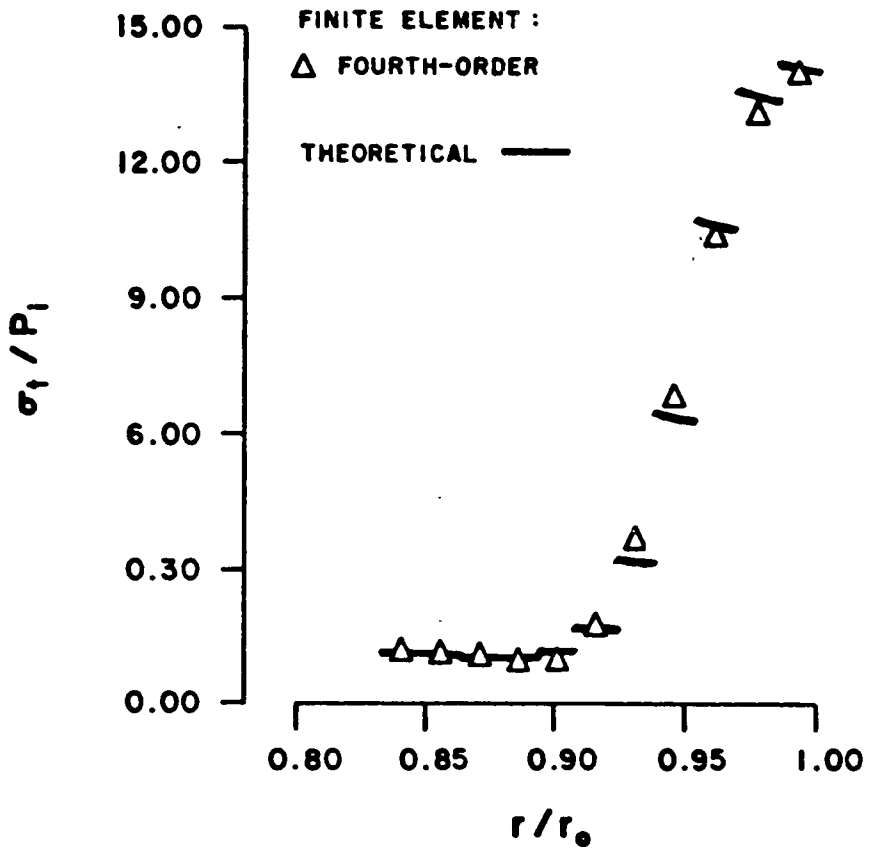

Figure 33. Hoop Stress Profile in an 11 Layer Orthotropic Cylinder , Fiber Angles 90-0 degrees, for a Fourth-Order Element

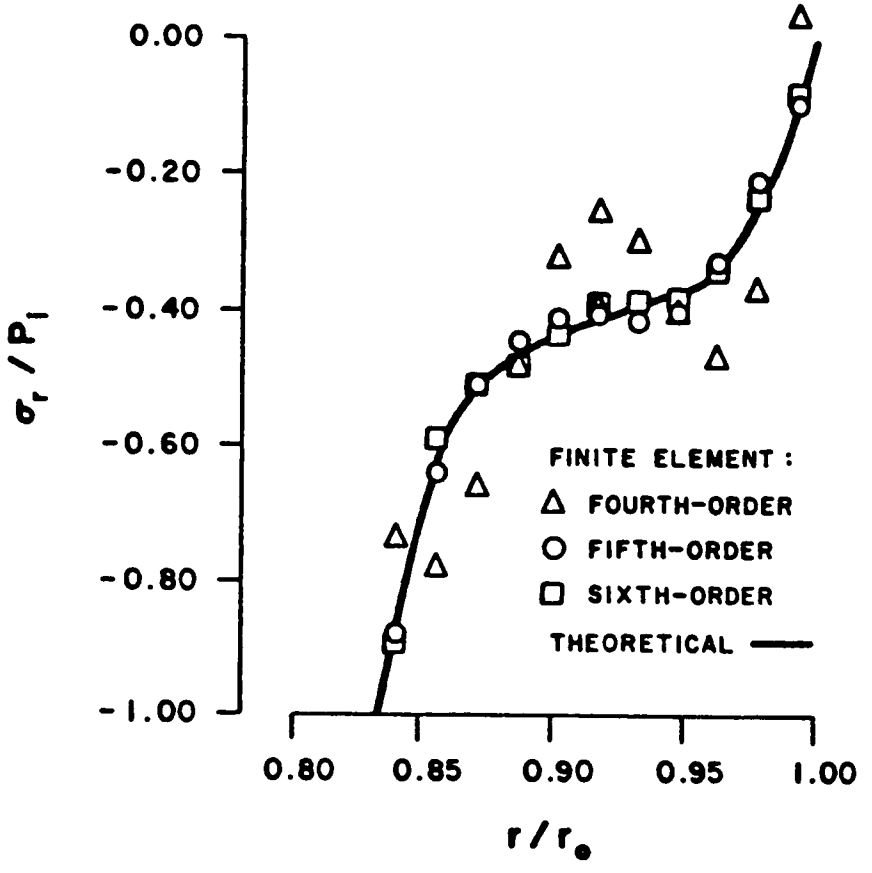

Figure 34. Radial Stress Profile in an 11 Layer Orthotropic Cylinder , Fiber Angles 0-90-0 degrees, for Fourth- thru Sixth-Order Element

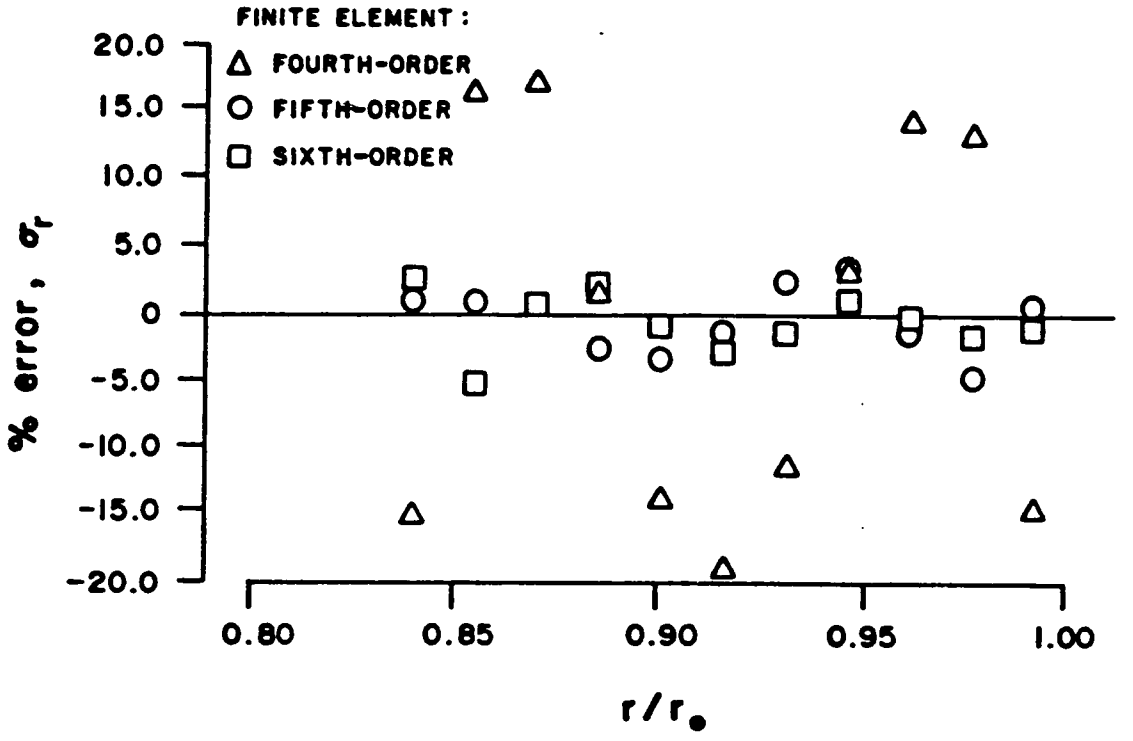

Figure 35. Radial Stress Error in an 11 Layer Orthotropic Cylinder , Fiber Angles 0-90-0 degrees, for Fourth- thru Sixth-Order Element

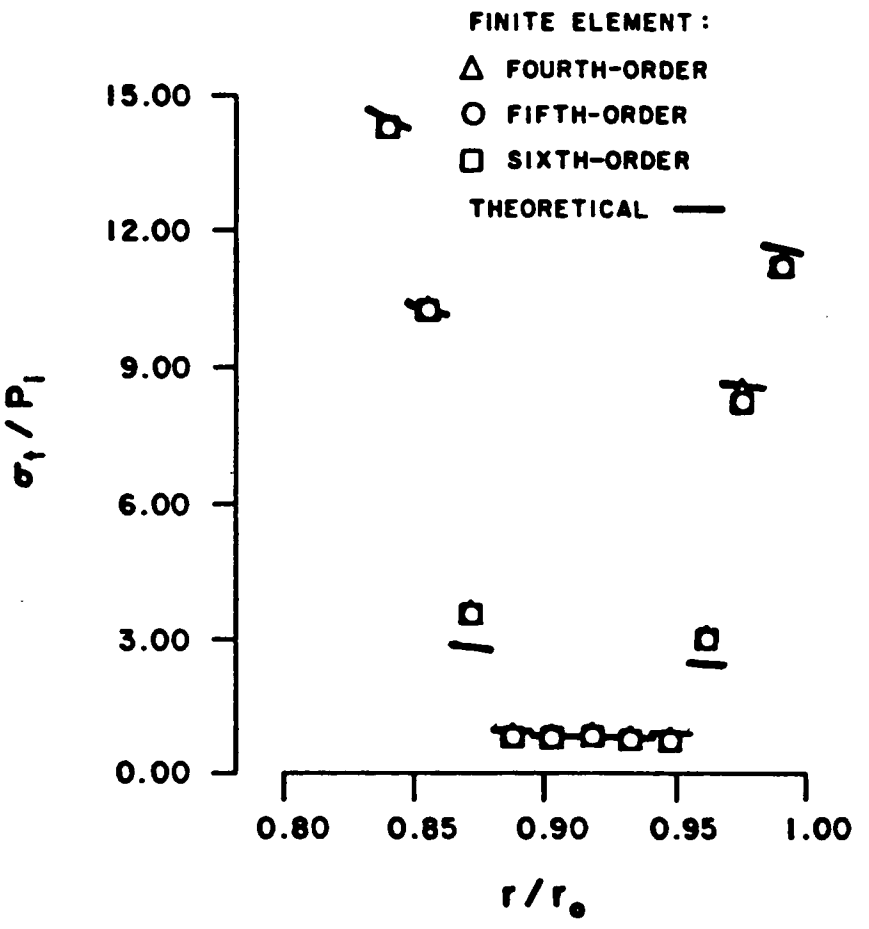

Figure 36. Hoop Stress Profile in an 11 Layer Orthotropic Cylinder , Fiber Angles 0-90-0 degrees, for Fourth- thru Sixth-Order Element

strained cylinder must be zero if there is no longitudinal load. The finite element formulation used to create the new high-order element is based on continuum mechanics and is a three-dimensional element as no assumption of plane-stress nor plane-strain has been made. However, the element is trying to model a nonhomogenous medium. The standard approach to modeling composite laminates is to assume that each layer is a linear-elastic orthotropic continuum. The finite element formulation also requires that compatibility and force equilibrium be satisfied on the entire structure, therefore, each element may have its own set of material properties and the solution carried out as if the structure is in fact a continuum. The finite element formulation does require that equilibrium and compatibility be satisfied for each element (as a whole) as equilibrium is established from the nodal point forces. Compatibility is satisfied from using the same interpolation function on the mating boundaries of connected elements. Compatibility and equilibrium are not evaluated inside the element.

The element that has been used to generate the results that have been presented uses the standard displacement-based finite element formulation to calculate the nodal forces and the strains and stresses at the integration points. However, in the high-order element, the formulation allows for a medium to be described that is not a continuum. The new element may have several different materials 'stacked' inside one element which will not necessarily yield a continuous function of elastic moduli, therefore, not a continuum. The element will still maintain equilibrium and compatibility on the whole. This means that the average longitudinal stress throughout the element will equal zero. There may be a longitudinal stress distribution through the element, however.

The three-dimension continuum mechanics formulation of the element can be illustrated by comparing results from models with various heights of elements used to model an unconstrained cylindrical pressure vessel. The longitudinal strains and stresses for three different elements, all modeling the 'single' layer orthotropic cylinder (model #2), are shown in Tables 9 and 10. The heights of the three elements are 2.54 mm (0.100 in.), 25.4 mm (1.00 in.), and 254 mm (10.0 in.). It can be seen that the longitudinal strains vary considerably with the height of the element. The plane stress condition is created when the height of a free-end cylinder approaches zero, whereas plane strain is created when the height of the cylinder approaches infinity. The finite element results

Table 9. Longitudinal Strains for an Orthotropic Cylinder Using a Free-End Model

Layer	Theoretical	2.54 mm (0.1 in) High Element	25.4 mm (1.0 in) High Element	254 mm (10 in) High Element
	(mm/mm)x10^{-6}	(mm/mm)x10^{-6}	(mm/mm)x10^{-6}	(mm/mm)x10^{-6}
1	129.9	131.5	94.8	8.3
2	100.9	101.4	83.1	7.9
3	73.9	73.5	66.4	7.1
4	48.4	47.6	46.4	6.2
5	24.3	23.6	24.8	5.1
6	1.7	1.2	3.0	4.0
7	-19.9	-20.0	-17.8	2.9
8	-40.6	-40.1	-36.6	1.9
9	-60.5	-59.7	-52.5	1.0
10	-79.6	-79.0	-64.8	0.4
11	-98.0	-98.6	-73.1	0.1

Table 10. Longitudinal Stresses of an Orthotropic Cylinder of Various Heights Using a Free-End Model Normalized by the Internal Press

Layer	2.54 mm (0.10 in) High Element	25.4 mm (1.0 in) High Element	254 mm (10 in) High Element
1	-0.001	-0.038	-0.126
2	0.000	0.019	0.095
3	0.000	0.007	0.067
4	0.000	0.001	0.042
5	0.000	0.001	0.019
6	0.000	0.002	0.003
7	0.000	0.002	0.023
8	0.000	0.003	0.042
9	0.000	0.007	0.061
10	0.000	0.014	0.080
11	+0.001	+0.026	+0.100

presented in Tables 9 and 10 demonstrate that the high-order element formulation does in fact perform as expected and predicted by continuum mechanics theory.

The discontinuous radial-strain approximation error mentioned earlier becomes more apparent when trying to model a multi-layer, multi-material isotropic cylinder. The isotropic cylinder is more severe than the orthotropic cylinders because the radial elastic modulus change is usually much greater in an isotropic multi-layered, multi-material cylinder than in filament-wound composite cylinders. In all of the models presented thus far, the radial moduli have remained relatively constant (see Table 6). In theory, the radial stress must be a continuous function, i.e., the radial stresses on either side of the layer boundaries must be equal for equilibrium to be satisfied. This condition means that there are discontinuities in the radial strain profile at the interface boundaries because of the change in the elastic moduli. The radial elastic modulus variation has the strongest influence, but the tangential modulus variation also causes a discontinuity.

In a finite element, the nodal point displacements are first calculated by satisfying force equilibrium for the structure. Once the nodal displacements have been found, the strains are calculated by a technique that involves differentiating the assumed displacement function. The conventional modeling approach uses several linear elements to approximate the non-linear displacements that generally occur. When a high-order element is used, the order of element is chosen to closely approximate the actual displacement field thereby replacing the numerous linear elements with a single high-order element. However, the linear elements can generate a piecewise continuous displacement function as only continuity needs to be maintained at the intra-element boundaries. In the high-order elements, the assumed displacement field is continuous and smooth. When the displacement field is differentiated, the high-order elements yield another smooth and continuous function; the strain field within the element. The numerous linear elements that are replaced with a single high-order element can generate a discontinuous strain field as the displacements need only to be piecewise continuous at the element boundaries. When a high-order element is used to model a multi-layer, multi-material cylinder in which the radial moduli are different, the element assumes a smooth, continuous displacement function which in turn yields a continuous and smooth radial strain field. Because the radial moduli change between layers, when evaluating

the stresses which are functions of the partial derivatives of the strains, the stresses are discountinous at points where the material properties change. In continuum theory, the displacements need only to be continuous which allow for piecewise continuous functions. When the piecewise continuous functions are differentiated to derive the strains, discontinuities will occur at points where the radial displacements are not smooth (but continuous). The piecewise continuous displacement functions and the resulting discontinuous strain fields are caused by the change in the material properties from layer-to-layer. However, the discontinuities in the radial strain and the change in the material properties are related by the need for equilibrium to be satisfied at the layer boundaries. In summary, continuum theory states that the radial stress profile in a multi-layer isotropic cylinder must be continuous and the radial strain profile will be discontinuous at the layer boundaries. A finite element model using numerous linear elements in the radial direction will closely approximate the continuum theory showing a relatively continuous and smooth stress profile within each layer and discontinuities at layer boundaries. The high-order element will approximate the the radial displacement field with a smooth, continuous function which will yield a smooth and continuous strain field and therefore, discontinuities in the radial stress at points where the radial moduli change.

A two-layer cylinder made of steel on the inside and copper on the outside of the pressure vessel was used to investigate the relative importance of this problem. The model consisted of steel for the inside six layers and copper for the outside five layers. As expected, discontinuity in the radial stress profile was created by the high-order finite element formulation. It is important to note that the discontinuity in the radial stress field is an error of the high-order element approximation as a result of the formulation in which a non-continuum medium is being analyzed as a continuum. However, the apparent error is expected from the continuum approach being applied in the high-order finite element formulation and only represents a limitation of the element. The finite element's predicted stress field is shown in Fig. 37. Realizing that the difference in the radial elastic moduli between the two layers is a factor of two, the element is still able to simulate the response of the system relatively well.

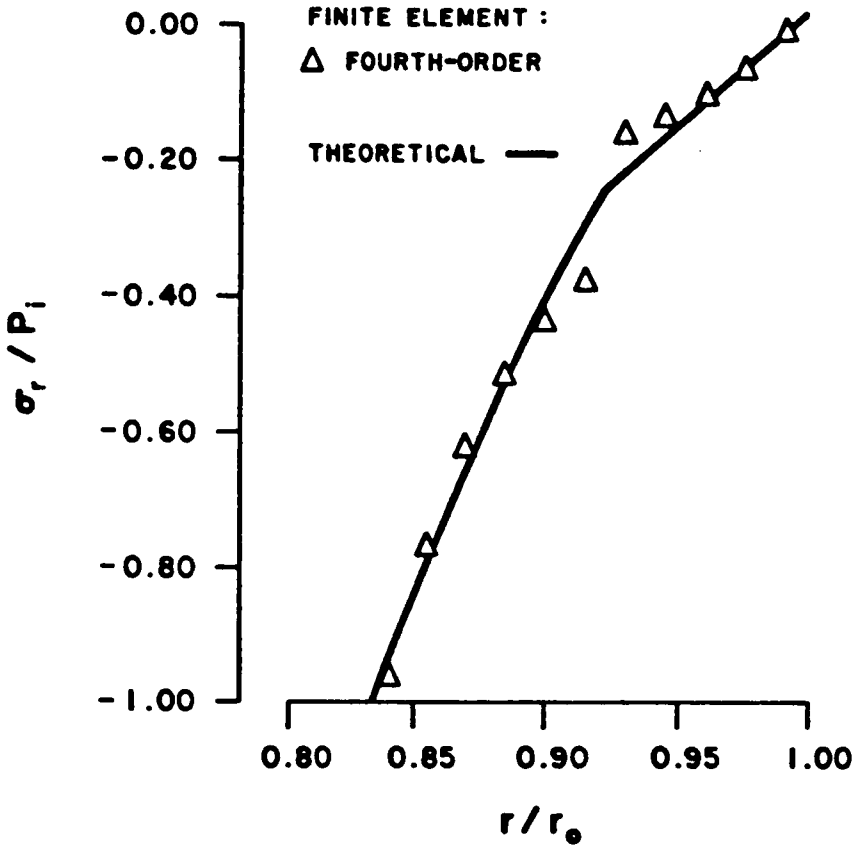

Figure 37. Radial Stress Profile in a Two-Layer Isotropic Cylinder Normalized by the Internal Pressure

4.3 *High-Order Element vs. Bi-Linear Accuracy*

Naturally the most important consideration with respect to the accuracy of the high-order element is how it compares to theory. However, because the newly developed element is to replace the conventional four-noded elements in the design-analysis code, comparing the accuracies of the two finite element solutions is also appropriate. Comparing the high-order element to the conventional bi-linear element solution will enable an experienced user of conventional elements to model filament-wound structures and make reasonable decisions concerning the mesh size, order of the assumed displacement field, number of integration points, etc..

The test cases for this accuracy study are the same as presented in the preceding section; pressure-loaded cylinders of varying material properties and construction. The results will be presented as percent error (see Eq. 4.24). The actual stress profiles can be found in section 4.2. Only the 'best' high-order results are presented. The 'best' element was chosen based on my own sense of the utility of the elements, meaning that the lowest-order element was selected that did not degrade the accuracy significantly. The lowest-order element was chosen because of the economy that it posseses and so that this accuracy study would model the actual philosophy that will be used by the design engineer.

4.3.1 Results and Discussion

All of the test models used in section 4.2 have also been evaluated for inclusion in this comparison study. The first model, a homogeneous isotropic cylinder, was analyzed by the bi-linear elements model to within three significant figures. The stress levels in all eleven layers of the bi-linear element model were those predicted by elasticity theory. The cubic model had an accuracy of ± 0.5 percent for the radial stress and ± 0.15 percent (round-off error is becoming significant at this level of accuracy) for the hoop stress.

The homogeneous orthotropic model had a similar behavior. The percent error for the bi-linear element was ± 0.2 percent. The percent error in the radial stress for the fourth-order element was approximately ± 0.5 percent. The percent error for both modeling techniques was an order of magnitude smaller for the hoop stress predictions than for the radial stress predictions.

The nonhomogeneous orthotropic material (filament-wound) test cases displayed greater differences in the relative accuracy of the two modeling techniques. The bi-linear element model produced an insignificant amount of error, + 0.2 percent, whereas the fourth-order element model manifested an error of ± 3 percent (see Fig. 38). The hoop stress error is basically within the same ranges for both modeling techniques as shown in Fig. 39

Similar behavior is noted for the 90°-0° filament wound cylinders. The percent radial stress error, shown in Fig. 40, is half that produced by the fourth order-element for the 0°-90° cylinder model. However, the percent hoop stress error, Fig. 41, remained relatively unchanged from the previous model. Again, the conventional bi-linear elements predicted the state of stress to within ± 1.5 percent for both the 0°-90° and 90°-0° cylinders.

The last filament-wound cylinder used in this study, 0°-90°-0° , shows the largest error created for both modeling schemes. The percent radial stress error for the bi-linear element model is shown in Fig. 42 and is approximately ± 0.25 percent while the fourth-order element produces an error of ± 4 percent. The percent hoop stress error for the fourth-order element is about the same as for the radial stress, ± 4.5 percent. However, the percent hoop stress error for the bi-linear model, Fig. 43, is significantly greater than for the radial stress. The bi-linear element models are still significantly better than the high-order elements, however for most design applications, these results indicate that the high-order element models are still very acceptable. As expected, there is a cost associated with the increased efficiency of the high-order elements.

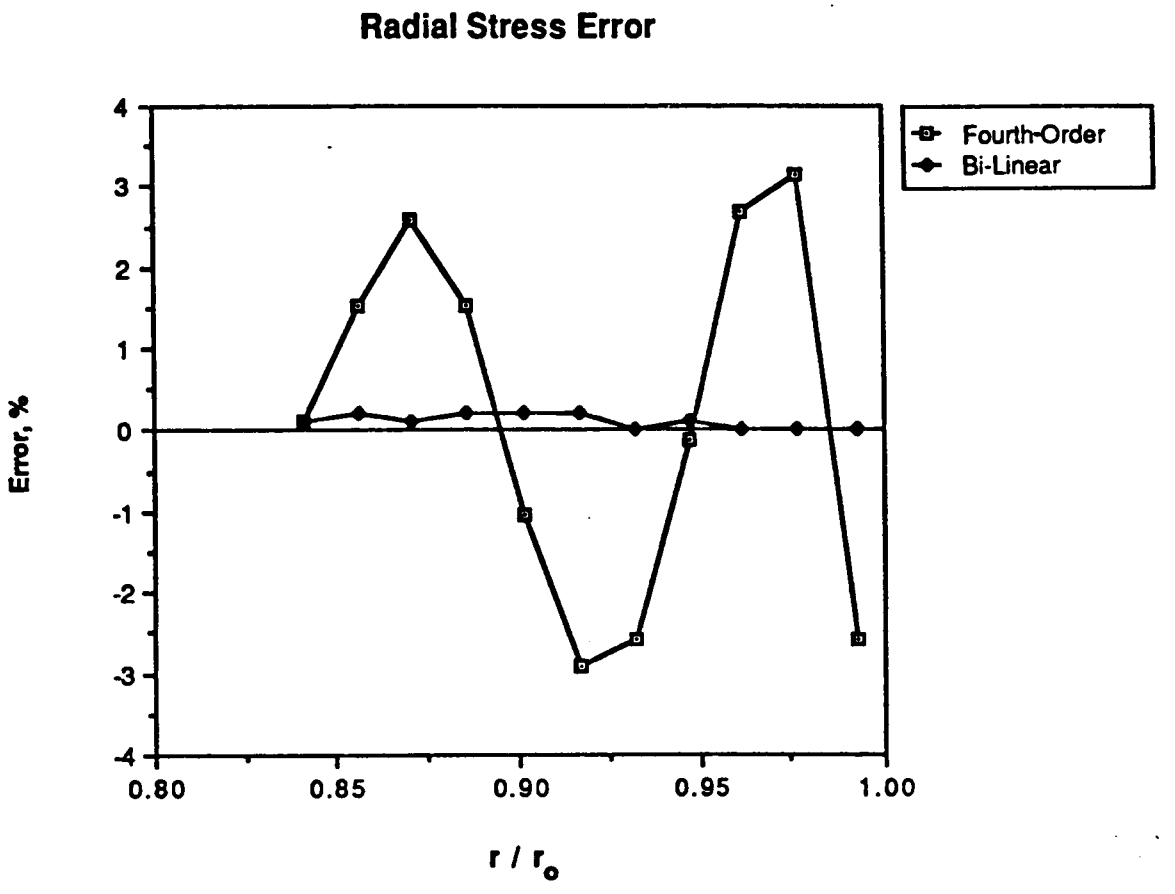

Figure 38. Radial Stress Error in a Nonhomogeneous Orthotropic Cylinder : 0°-90°

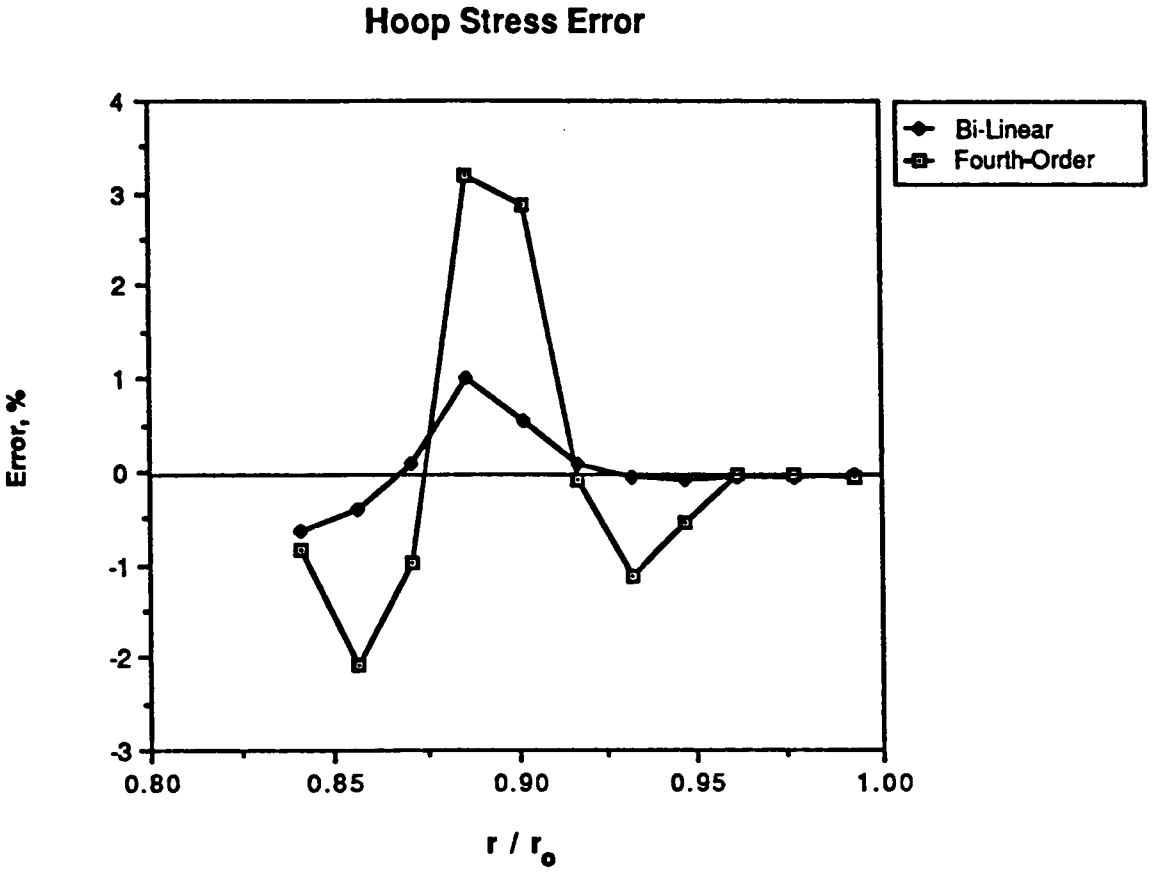

Figure 39. Hoop Stress Error in Nonhomogeneous Orthotropic Cylinder : 0°-90°

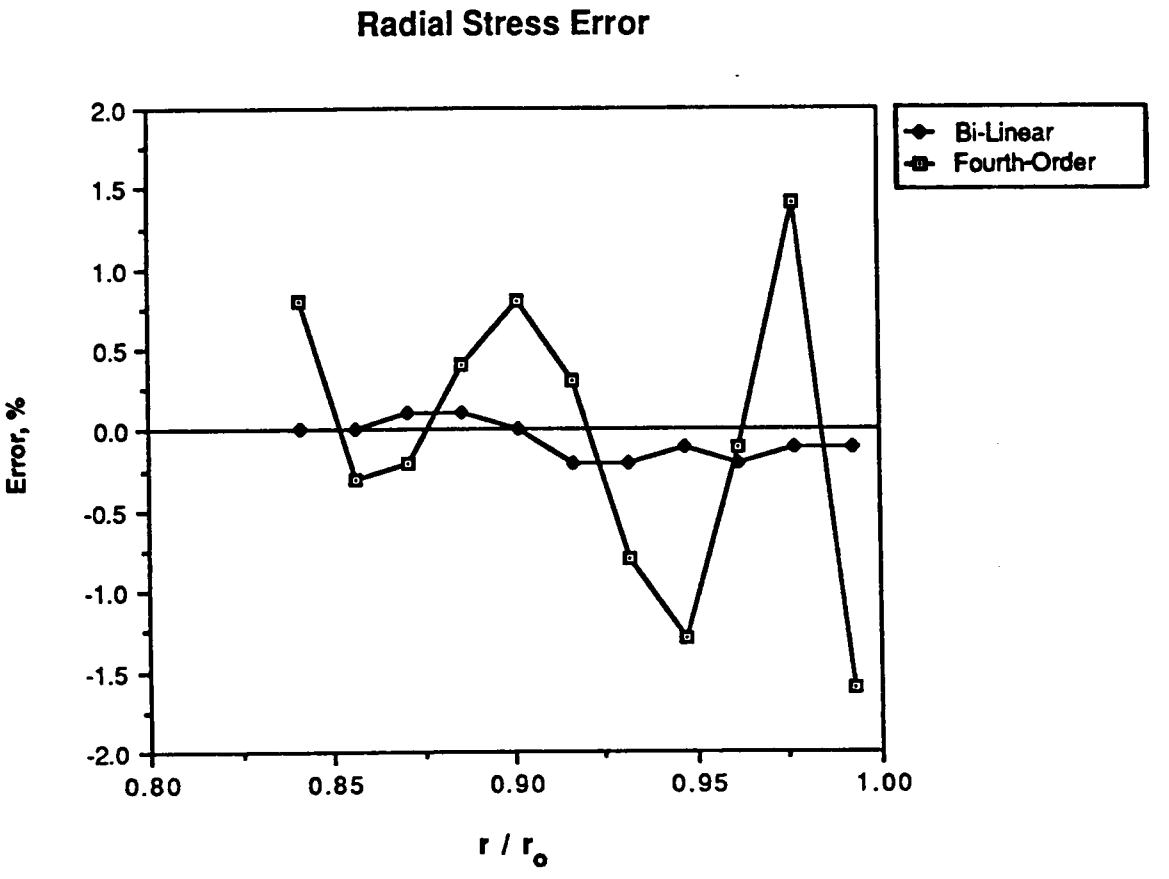

Figure 40. Radial Stress Error in a Nonhomogeneous Orthotropic Cylinder : 90°-0°

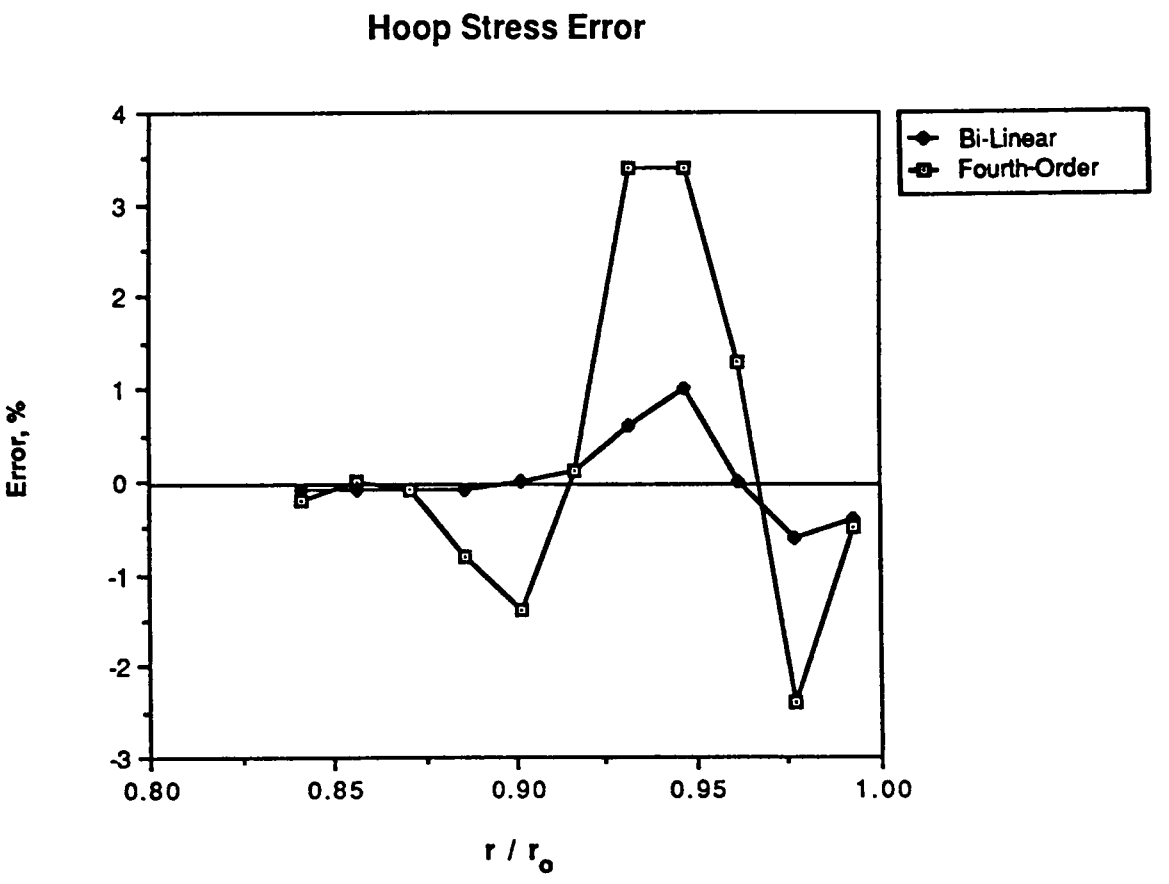

Figure 41. Hoop Stress Error in Nonhomogeneous Orthotropic Cylinder : 90°-0°

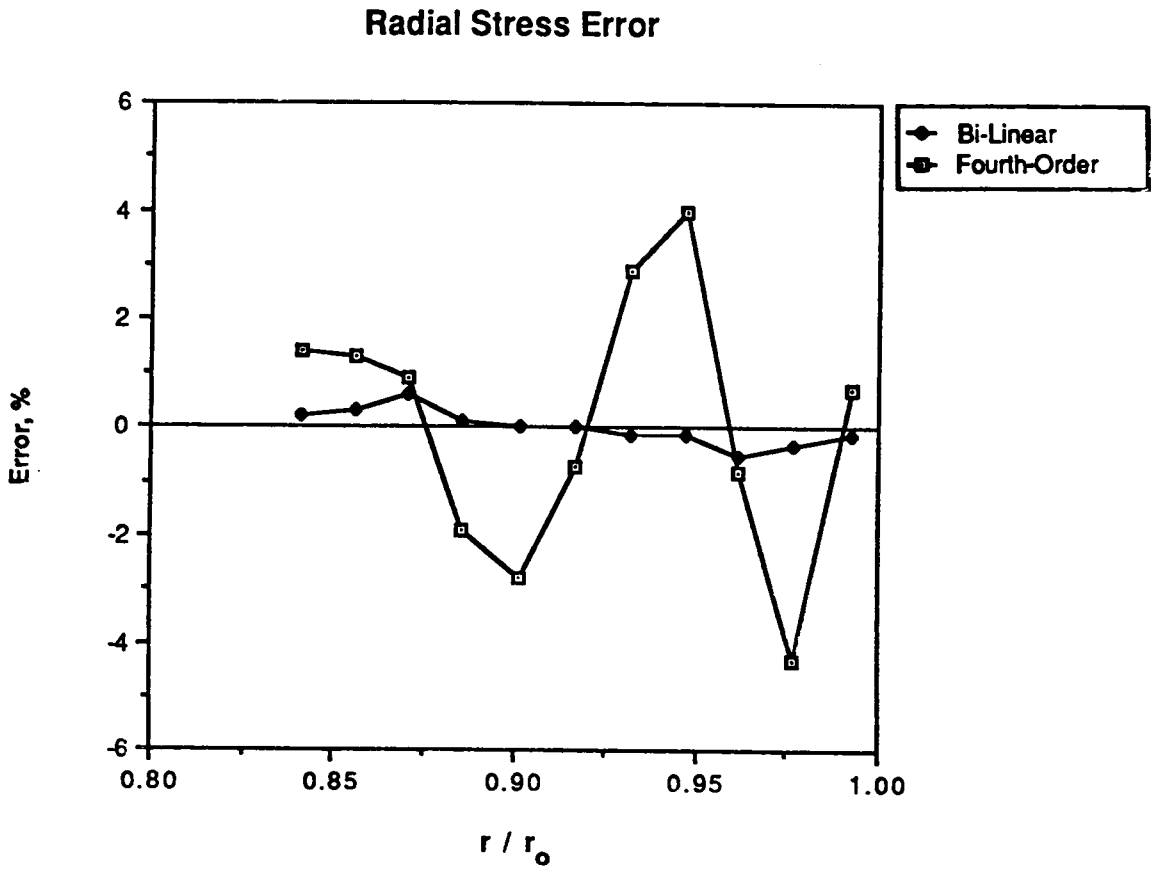

Figure 42. Radial Stress Error in a Nonhomogeneous Orthotropic Cylinder : 0°-90°-0°

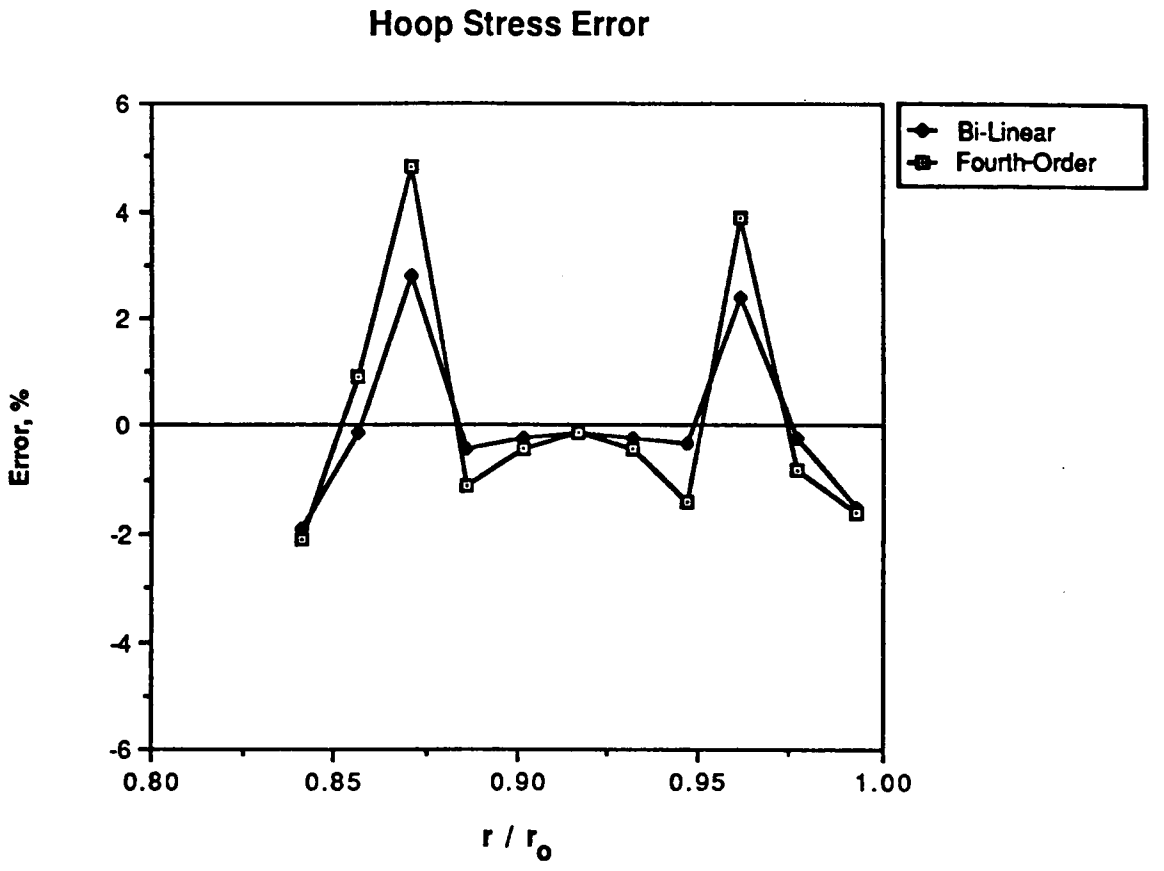

Figure 43. Hoop Stress Error in Nonhomogeneous Orthotropic Cylinder : 0°-90°-0°

5.0 Design Code Development

5.1 Introduction

Once the element formulation was verified for significant accuracy while still maintaining an efficient computational time advantage over the conventional approach, the element was then incorporated in a specialized design-analysis code for filament wound spherical pressure vessels (see Fig. 9 on page 52). The high-order composite element was first incorporated in a skeleton finite element program so that it could be evaluated on a set of relatively simple test cases of composite laminates. These results were presented and discussed in Chapter 4. The framework of the finite element code is actually a simple finite element program known as STAP (STatic Analysis Program), which is given in references [54,55] and initially contained only a truss element. STAP has been formulated to easily accept one- , two- , and three-dimensional elements and perform the associated analysis. In the following sections, each phase of the total design package will be explained. More complete information such as the actual program listing, examples of input files and the resulting output files, and detailed descriptions of the flow of the most significant programs, is available in the User's Guide [59]. Because STAP represents the foundation with which the high-order

element was built upon, a brief introduction and description of the flow and storage scheme of STAP will be presented in section 5.1.1.

A design code based on the finite element method should consist of three parts; i) the pre-processor, ii) the finite element code, and iii) the post-processor. The existing pre-processor consists of three programs; i) NTHICK, a program to calculate the layer thicknesses for a delta-axisymmetric winding pattern, ii) SPHMESH, a mesh generator specifically for filament-wound spherical pressure vessels, and iii) COUPLE, an interfacing program that reads the output data file from SPHMESH, as well as a user-generated input file. The existing pre-processor formed the basic foundation from which the new pre-processor was created, so each of the three original programs will be described along with a description of the modifications and additions.

A careful evaluation of options and implementation schemes had to be completed before proceeding with the development and implementation of the design code. There are basically three options that could be considered for implementation. The first was to use the original pre-processor that was used for creating a model of four-noded quadrilaterals and write a program that would take the output from the mesh generator to create a new mesh utilizing the high-order elements. The second option was to create an entirely new pre-processor tailored specifically for the high-order composite element. The third option was to utilize the existing pre-processing and simply add capabilities to generate a model with the high-order elements as well as a 'conventional' model.

The third scenario was eventually accepted. The reasons for implementing this scheme were basically twofold. First, simply adding high-order element capabilities to the existing mesh generator was the easiest and most straightforward technique from a programming standpoint. Secondly, it has an important benefit that was not possible with the other two scenarios; two finite element meshes are created simultaneously, one utilizing the high-order composite element and the other utilizing the four-noded quadrilaterals. Having the ability to view both meshes, the user can verify that the mesh using the high-order elements was properly defined and created while viewing the other mesh gives the user a graphical representation of the structure in a form that should be familiar. The high-order element model does not show any definition of the structure within each element, i.e., number of fiber layers or locations of integration points. Each quadrilateral within

the filament-wound section of the sphere (mandrel excluded) represents an intra-element layer within the high-order element. Each of the quadrilaterals contains a single integration point for which the stress state will be calculated. Therefore, the resolution of the finite element solution is best visualized with the mesh of quadrilaterals. Lastly, the accuracy of a finite element solution is primarily dependent on the users ability to model the structure and interpret the results. Giving the user a model and results that can be easily compared to a conventional model will create a sense of familiarity with this new element.

5.1.1 Description of STAP

The STatic Analysis Program (STAP) presented in references [54,55] is an in-memory solution algorithm for linear elastic static analysis. Like virtually all finite element programs, it can be divided into four basic sections.

1. Input phase

2. Calculation of the stiffness matrix.

3. Solution of the equilibrium equations.

4. Evaluation of the element stresses.

Basically, the structure stiffness matrix is evaluated by the following steps

1. The nodal point and element information are read and/or generated.

2. The element stiffness matrices and the equivalent nodal loads are calculated.

3. The structure stiffness matrix is assembled from the individual element stiffness matrices.

In step 1, the nodal point and element information is read from an input file which consists of; the type of element to be used, number of nodes in the model, number of elements, location of nodes in the global coordinate system and the connectivity of the nodes to form elements, and lastly, information relating to the allowed degrees of freedom of each node. The exact input data required for an element depends on the specific element type. Certainly the information to be required for the high-order composite element will be unique. In general, the information required for each element is the element's node numbers (connectivity) corresponding to the nodal point numbers of the complete assembly, the element's material properties, and the forces applied to the element (actually to the nodes).

The procedure to calculate the element stiffness matrices was presented in section 2.1 and the numerical integration technique used to evaluate the element stiffness matrix in section 2.2.2. However, once the element stiffness matrices have been determined, they must be assembled to generate the structure stiffness matrix

$$[K] = \sum_{i} [K^e]_i \qquad [5.1]$$

where the matrix K_i^e is the stiffness matrix of the i^{th} element and the summation includes all elements in the structure model. Therefore, the element stiffness matrix for each element must be of the same order as the structure stiffness matrix. This results in each of the element stiffness matrices containing an extremely large number of zero coefficients representing unused degrees-of-freedom. In order to avoid performing a large number of operations on zero terms and requiring a large amount of storage to be allocated for storing the zero coefficients, STAP uses a compacted element stiffness matrix. Meaning that only the rows and columns of the element stiffness matrix that contain nonzero coefficients are stored and an array is created that relates each element degree of freedom to the corresponding structure degree of freedom. This array acts like a road map to locate specific terms in the stiffness matrices for mathematical operations to be performed on the matrix. The compacted element stiffness matrix approach is fully explained in references [54,55] which also contains numerical examples showing precisely how the system operates.

The solution of the equilibrium equations was discussed in section 3.1 and suffice to say here that the program STAP uses the LDL^T decomposition method to solve the system equations [54].

Once the nodal point displacements have been calculated, the element stresses are calculated in the final phase of the program. The theoretical method of determining the element stresses is presented in section 2.2.4. However, as is the case with the structure stiffness matrix, the strain-displacement matrix, [*B*], matrix may be a sparse matrix, containing a large number of zero coefficients. Therefore, a similar procedure is used to operate only on the compacted form of the strain-displacement matrix, again using the array of the degree-of-freedom identifiers as a map to locate the nonzero terms. This method is also completely described in references [54,55].

In the sections to follow, descriptions of the program development will be presented. Brief descriptions of the programs and the algorithms that have been developed specifically for solving problems associated with filament-wound spherical pressure vessels will be included. The three programs that comprise the existing preprocessing code will be described even though no changes were made to two of the three programs. This is necessary because a clear understanding of the first two programs (to which no changes were made) is needed to understand the creation of the interface program. The actual finite element program, the high-order element subroutine, and associated algorithms will be presented in detail.

5.2 *Pre-Processing Code*

The actual mesh used in the analysis of a filament-wound spherical pressure vessel with the conventional bi-linear quadrilateral elements is shown in Fig. 10 on page 53. One of the most difficult tasks involved with implementing the high-order composite element in a design code is the generation of the input data file that must include the order of the displacement field for each element, the number of layers to be contained within each element, the material properties of each

layer within the element, the fiber angles for each layer along with the details of the winding pattern. Most finite element programs designed to solve specific problems contain some sort of a pre-processor or mesh generation program to aid in creating the full detailed mesh and also create the necessary input data files for the finite element analysis program. There are numerous automatic mesh generation schemes presented in the literature, which cover the structure from boundary to boundary with uniform or linearly varying density meshes. When modeling the filament-wound sphere with the conventional quadrilateral element, it was important for the mesh generator to recognize internal winding layer boundaries and to then create elements that would not cross any of these boundaries. P. J. Leavesly [27] created such a mesh-generator based on a concept presented by Kalkani for creating finite element meshes of earthen dams. The pre-processing portion of the design code that was developed for the high-order composite element was created by using a pattern simulation program written by C. E. Knight which describes the basic geometry of the structure and how the fibers are wrapped onto the vessel. The mesh-generator used was developed by P. J. Leavesly to model the structure with four-noded quadrilaterals. A complete description of the pattern simulation program can be found in reference [27] along with a detailed description of the mesh generating program. A rather complete description of both of these programs will be presented here so that the tasks involved in converting the 'conventional input data' to the form necessary for the high-order element may be better illustrated. Some details of the winding pattern will be presented, before presenting a description of the actual code.

5.2.1 Winding Pattern Definition

The delta-axisymmetric pattern can be designed to yield a uniform distribution of fiber orientations and uniform total thickness over most of the surface of the sphere. The delta-axisymmetric pattern on a sphere is shown in Fig. 3 on page 36, illustrating that the fibers being wound around the sphere are actually bands of fibers and they are placed equally around the polar axis. The spherical coordinate system used to describe the geometry is shown in Fig. 44.

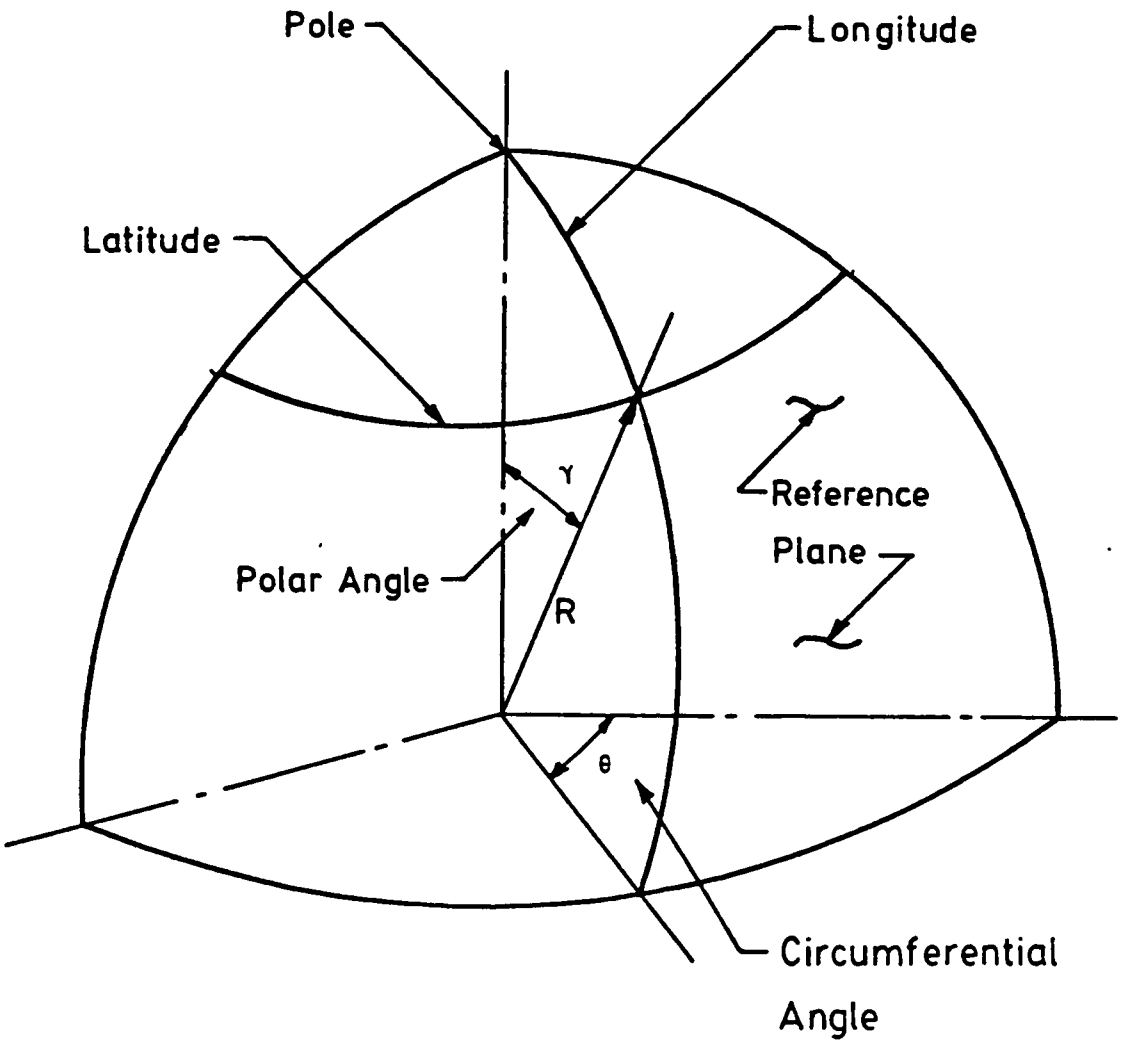

Figure 44. Spherical Coordinate System; after Leavesley [27]

Using the spherical coordinate system to define a point in the structure involves specifying a polar angle, γ, a circumferential angle, θ, and a radius, r. The polar angle is the angle between the polar axis (the top of the vessel) and the radius to the point of interest measured along a longitudinal axis. The circumferential angle is the angle measured between the reference plane to the longitudinal plane that passes through the point of interest.

Total coverage of the spherical structure with the specified design thickness is used to define the basic winding pattern. The number of band sets needed to completely cover the sphere is found by dividing the design thickness by two times the thickness of a single band as each band set gives two layers of coverage, one at a positive fiber angle and the other at a negative winding angle. The band sets are applied equally from the pole to the equator along a longitudinal axis. The number of bands in each set that are require to completely cover the equator is related to the band set's longitudinal position. As an example, consider the sphere with a fill tube as shown in Fig. 45. The winding pattern must be slightly altered in order to accommodate the fill tube but will not be discussed here, but a more complete discussion of the winding pattern can be found in reference [27]. The first set of bands are placed with the inner edge tangent to the polar axis. The position of the band is defined by two angles, γ_1 and γ_3 , which define the polar angle to the inner edge of the band in one hemisphere and the polar angle to the outer edge of the band in the opposite hemisphere, respectively.

A band is formed by starting at a one edge of the band location and circumferentially winding the fiber along a helical path at the correct lead angle until the specified band width is reached. The number of bands in this set must then be the circumference of the sphere divided by the coverage accomplished by one band width.

The second set of bands is applied in like fashion but their inner edge must be tangent to the latitude circle created by the outer edge of the first set. This set of bands will naturally require slightly fewer bands than the first set to provide complete coverage of the equator as the band set angle, γ_2 is greater. Similarly, the other sets are applied progressively along a longitudinal axis to the equator.

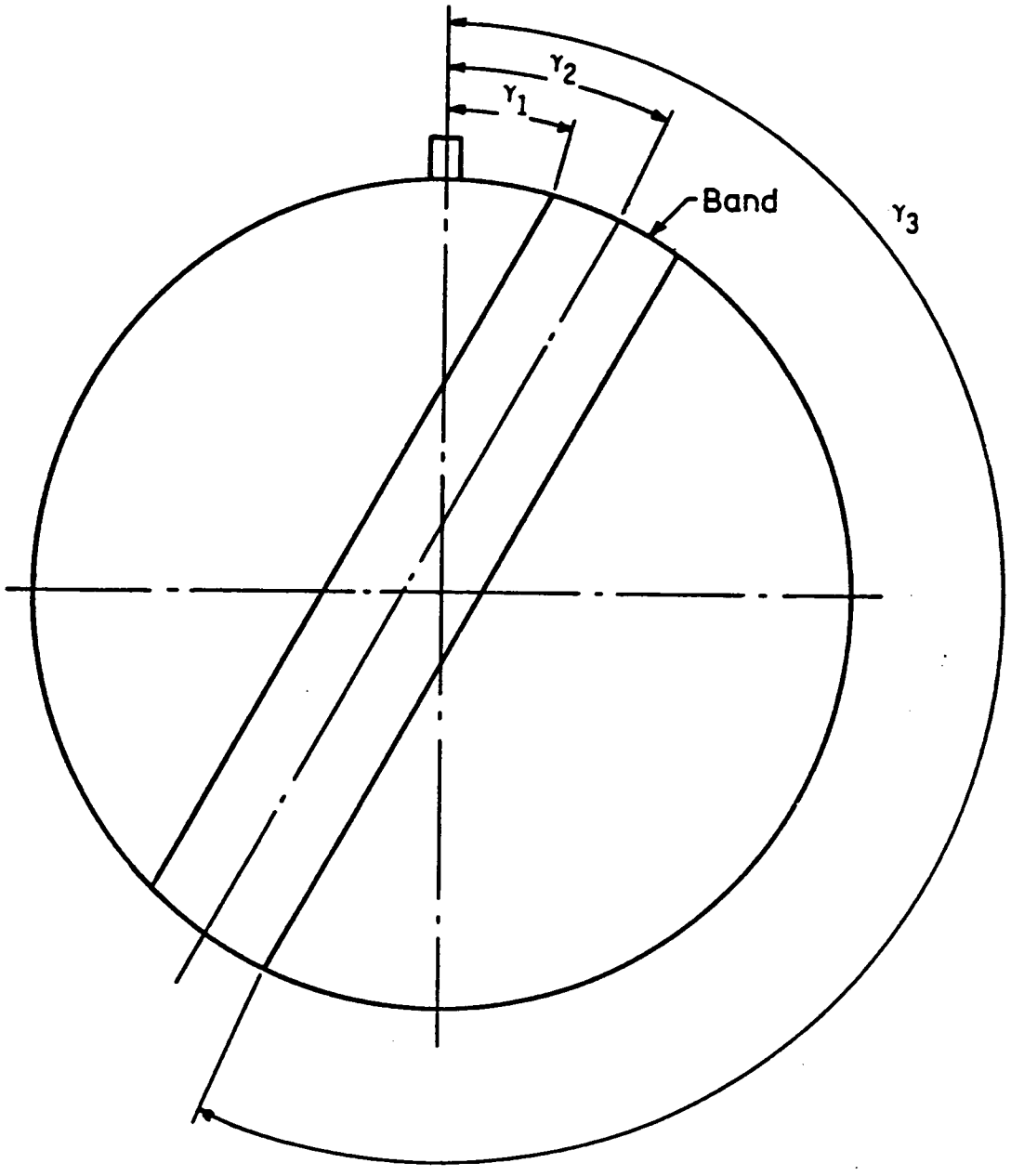

Figure 45. Band Location Specifications; after Leavesley [27]

There are basically two variations of delta-axisymmetric winding patterns. The first is called a downwind and is created precisely as described above. Namely the band sets are applied from the pole to the equator. The other winding variation is an upwind which is simply the inverse of that described above. The band sets are applied from the equator up to the pole. Normally a sphere will have a downwind followed by an upwind to produce a balanced sphere. Both the downwind and upwind are complete patterns and are also refered to as 'shells'.

5.2.2 Description of NTHICK [27]

The program NTHICK is a pattern simulation program that was first written by C. E. Knight and modified by P. J. Leavesley. Leavesley's version of the program created the output for a mesh-generating program that he created and included the layer thicknesses and the fiber orientation angles at all polar angles where nodes and elements are to be generated for his linear quadrilateral elements.

To accommodate the high-order finite element, the output produced by the program NTHICK must again be modified. The information generated from Leavesley's modification is used by the mesh-generator program, SPHMESH, to define the inter-element material boundaries and specify the fiber angles for each inter-element layer. The layer thickness build-up is determined by considering the geometry shown in Fig. 46. The concentric circles represent latitudes on the sphere and the straight lines represent the coverage of a single band. The arc length along the latitude that is covered by a band, known as the 'band arc coverage', is then calculated. The thickness build-up for a band at a given latitude is given by the band arc coverage times the band thickness times the number of bands in the set divided by the circumference of the latitude. The fiber orientation angle, BETA, is the angle between the fiber direction and the latitude line. The fiber angle is calculated at ten locations across the band as the angle changes across the band and then averaged to specify the fiber angle, BETA, for that particular latitude and for that particular inter-element layer within the composite element. The thickness build-up is calculated for each band set and is

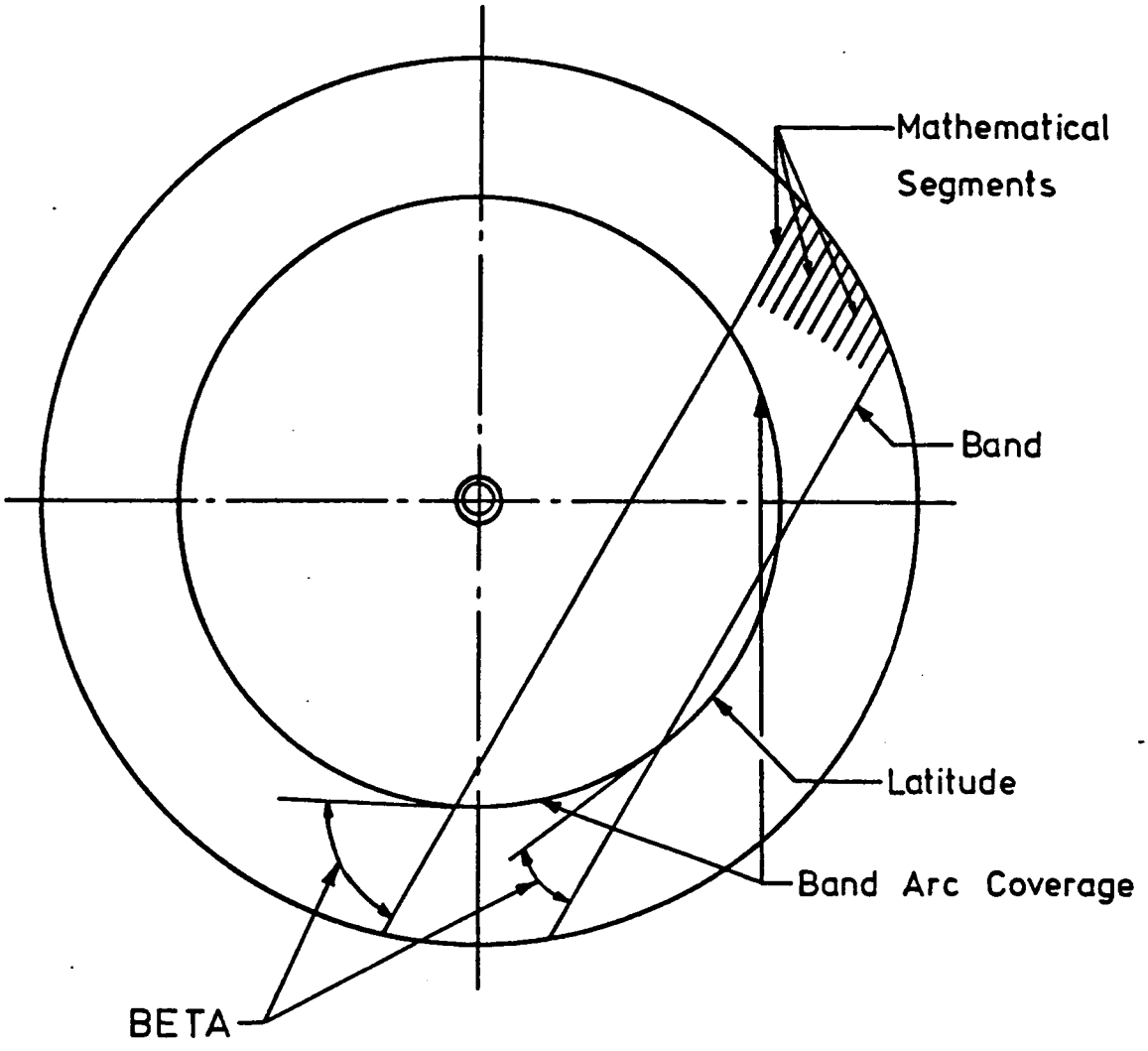

Figure 46. Thickness Calculation Method; after Leavesley [27]

summed to obtain the total thickness profile. The output from the program NTHICK is a set of data which specifies completely the fiber angles for all regions of the structure and the total thickness profile for the given pattern. The output from the program is a data file which includes the material type (which is the fiber angle for the composite structure) for each layer and a set of nodal-point cards for the nodes of linear quadrilateral elements that must be transformed to the proper set of data needed by the finite element program containing the high-order composite elements.

5.2.3 Description of SPHMESH [27]

The program SPHMESH is a mesh-generator program that was written by P. J. Leavesley specifically for the analysis of a filament-wound sphere. Because the output of this program, which was written for four-noded quadrilateral elements, is to be modified to create the input data file for the finite element program containing the high-order element, this program will be described in some detail.

In the introduction to this chapter, the philosophy behind the architecture of the design code was explained. There is another reason for creating a new version of the original mesh-generator that contains the capability to model the sphere with four-noded quadrilaterals. Figure 47 is a fully generated mesh that was created with the original program SPHMESH which actually utilized the conventional linear elements. Figure 47b shows a mesh of the same structure that utilizes the high-order composite finite elements. The mesh which uses the composite element losses all definition of the detail within the structure. In Fig. 47a, each element represents an individual layer or a portion of the layer. By looking at this model, an engineer with a reasonable amount of practical experience modeling these structures can generally derive a qualitative assessment of the accuracy to be expected from the analysis. However, referring to Fig. 47b, there are too many unknowns that directly affect the accuracy and quality of the model, such as the number of layers

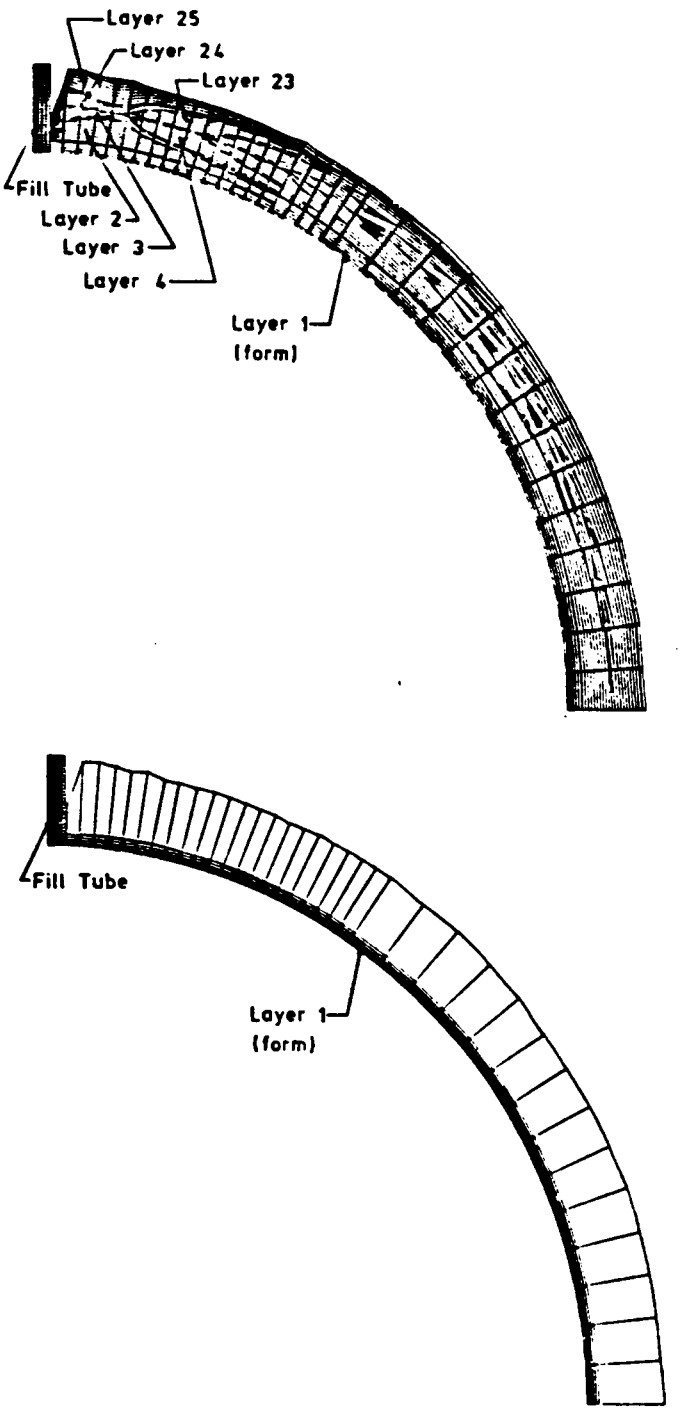

Figure 47. Generated Mesh of a Filament Wound Spherical Pressure Vessel: a) Conventional Elements, b) High-Order Elements

within each element, the number of integration points that are used in the radial and meridian directions, and the variation of the material properties from layer to layer.

Another important reason for not developing a new mesh-generator for the new composite element specifically is based on one of the main objectives of this work; to develop a design-oriented code that would significantly reduce the computation time of the conventional analysis method. In a design scenario, several modifications and iterations are generally required to be made to the initial model before accurate results are produced and convergence of the solution assured. When using four-noded quadrilaterals, the modifications to the model can only consist of regenerating the model and refining the mesh in areas of high stress gradients. One of the features of the high-order element is the ability to specify any order displacement field in the radial direction along with the number of integration points to be used in the radial directions. These two options have the potential to increase the accuracy of the finite element program results. The accuracy of the results will also be dependent on the mesh-generated by the original portion of SPHMESH that models the sphere with quadrilaterals. If changing the number of integration points and/or the order of the displacement field does not increase the accuracy of the results to within acceptable limits, the mesh of quadrilaterals itself may then also be refined which increases the number of integration points within each high-order element.

The program, SPHMESH, creates a model of the filament wound spherical pressure vessel such that no quadrilateral element will cross a band set layer boundary. The layer boundaries are defined and calculated by the program NTHICK and are a part of the input information used by the mesh-generator. The mesh generator performs two main functions as related to the conventional analysis program, it generates the nodes and linear elements with the constraint that no element cross a layer boundary. The mesh-generator also determines the average fiber angles within each quadrilateral element (BETA and SETA).

One of the primary functions of a mesh-generator, is to provide the engineer/designer with some sort of verification that the structure has been modeled properly. This is normally accomplished with a graphical representation of the structure showing nodes and/or the elements. The program SPHMESH has graphical capabilities that draws the mesh of the structure which may

include only nodes or only elements. Options are also available to plot only selected portions of the model as will be shown in the figures below. There are also two choices of output format; i) a file may be created for user inspection, and ii) an output file which serves as the input file for the interface program, COUPLE. Both versions of the model may be displayed. The four-noded quadrilateral model will better indicate the filament-wound structure showing the fiber layer boundaries and each element within the filament-wound portion of the structure which is represented by at least one integration point in the corresponding high-order composite element. The mesh of the structure utilizing the high-order elements will indicate if the mesh has been properly defined, constructed, and output properly for use by the finite element processor.

The two main features of the mesh-generating program will be explained because of the importance of these results in converting this information to a form that is useful to the high-order composite element.

5.2.3.1 Node Point Generation [27]

In the discussion to follow, the presentation will be directed to applications in which conventional four-noded quadrilateral elements are to be used as this is the original purpose for which the program SPHMESH was created. In section 5.2.3.2 the manner in which the information supplied by the four-node quadrilateral portion of the mesh-generator, SPHMESH, is used to create the high-order element mesh and material definition will be detailed.

The node point generation algorithms locate the position of the nodes so that the nodes fall on the boundaries of each layer in the composite structure and so that there are a fixed number of nodes along each radial line. Maintaining a constant number of nodes in the radial direction and numbering the nodes sequentially along these radial lines keeps the bandwidth of the structural stiffness matrix a minimum. As was explained in Chapter 3, minimizing the bandwidth greatly enhances the computational efficiency of the LDL^T decomposition solution method. The actual

node placement or generation is separated into two parts; i) the fill tube generation and ii) the metal mandrel and filament-wound structure.

Nodes are created throughout the fill tube by starting on the base and on the inside edge as shown in Fig. 48. The base of the fill tube is assumed to be flat and joins the spherical form at the first polar position as indicated in Fig. 48. The nodes are then generated by moving up the inner surface of the fill tube. The node numbers are assigned in sequential order during this process. When the top of the fill tube is reached, another line of nodes is created which is parallel to the first and is separated from the first line an amount that will allow for a 'user specified' number of elements through the fill tube wall. The other nodes in the fill tube are generated in a similar fashion. Flags are set which will identify the intersection of the outside diameter of the fill tube and the first polar position, and the inner node on the first polar position (nodes 31 and 35 in Fig. 48). These flagged positions will be used as starting points in the next phase of the node generation.

The generation of nodes throughout the rest of the model treats the spherical form or mandrel as one of the composite laminate layers in almost all aspects except in the input of layer thickness and fiber angles. The thickness of the mandrel or spherical form is input to the mesh-generator program and not read from the input file created by NTHICK. The fiber angles at all nodes within the mandrel are set to zero as the fiber angle has no significance for an isotropic material.

The user must specify the number of elements to be generated through all the fiber layers (which includes the mandrel) and the number of polar positions to be used. The program then loops through each polar position and spaces nodes along the radial such that a node is placed at least on each layer boundary. The number of nodes placed within any one layer (as there may be more than one element per layer) is dependent upon the thickness fraction of each layer with respect to the total thickness. The 'start' and 'finish' nodes at each polar position that identify a layer boundary are flagged for use in the element generation phase of the program.

All layers must have at least one node space or there will be no element generated in that layer. There is one exception, occuring at the leading edge of a layer's spherical coverage. It is unlikely that the leading edge of a band set will start exactly on a polar position line as shown in

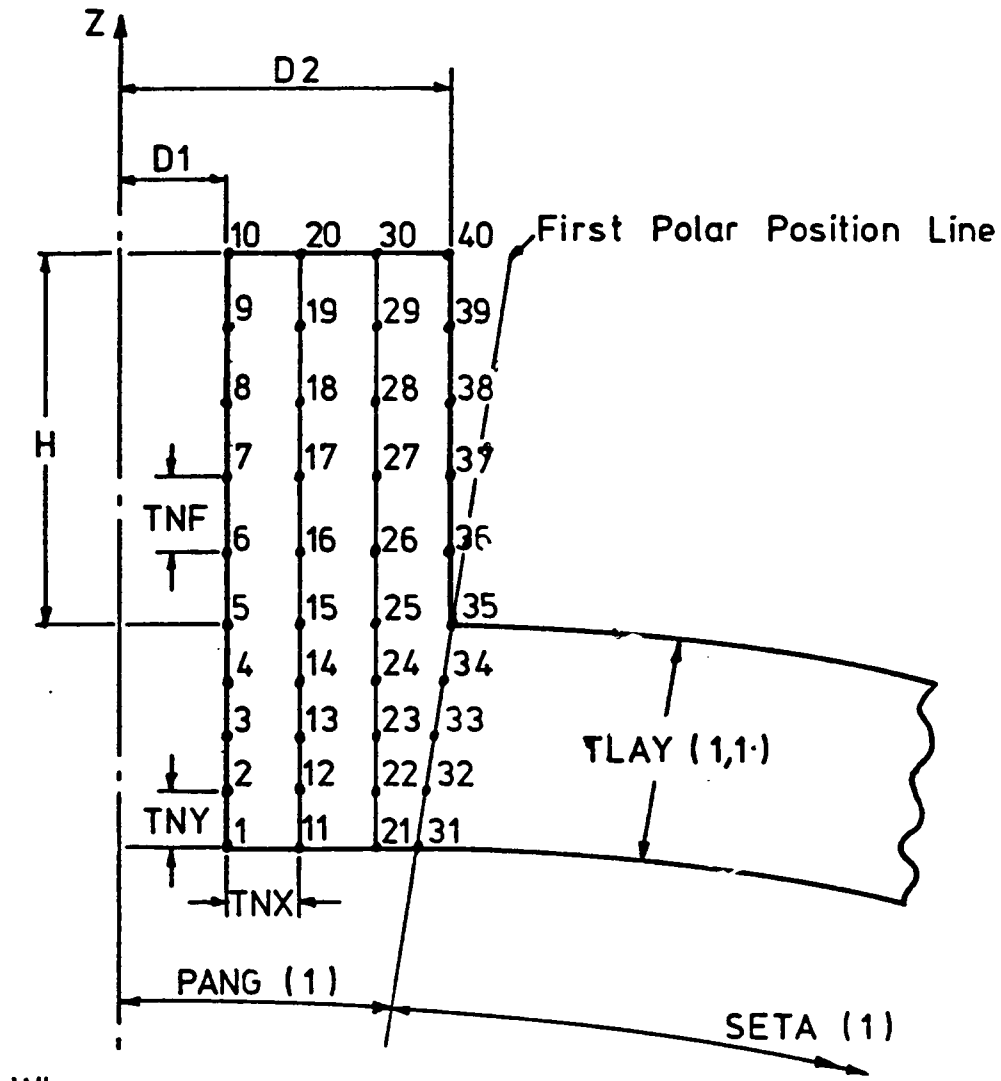

Where

TNY = TLAY(1,1) × cos[PANG(1)] / NF

TNX = (D2 - D1) / (2 × NH)

TNF = H / NV

NF = Number of elements through spherical form

NV = Number of elements up fill tube

NH = Number of elements across fill tube

Figure 48. An Example of the Node Point Placement for the Fill Tube; after Leavesley [27]

Fig. 49. The program decides whether to create a node space or not by the actual thickness of the specified polar line.

The nodes are numbered starting on the first polar position line in the first layer. The numbering then moves radially outwards along the polar line until the outer surface is reached. The next node to be numbered is on the second polar line on the inner surface of the spherical form. The nodes are again numbered radially. This procedure is repeated as shown in Fig. 50.

Each node placed within the spherical structure (composed of the mandrel and the composite) is assigned a fiber angle, BETA. The fiber angle of the inner and outer surfaces of a layer are known from the thickness calculation program, NTHICK. The nodes on layer boundaries are assigned two fiber angles, one for each of the two layers meeting at that boundary. The nodes between layer boundaries are assigned fiber angles using a linear distribution from layer boundary to layer boundary. The nodes within the fill tube and the spherical form are assigned zero fiber angles.

5.2.3.2 High-Order Composite Node Generation

The mesh of the filament-wound sphere using the high-order elements contains linear elements which are used to model the metal liner or mandrel, as in the conventional model. The high-order elements are used to model only the filament-wound portion of the structure. Therefore, the generation of the nodal points for the metal fill tube and metal liner are identical to the conventional method described above.

The generation of the nodes through the filament-wound structure is a much simpler process than that needed with four-noded quadrilaterals. The entire thickness is modeled with a single high-order composite element. Therefore, the nodes of each high-order element are generated on polar position lines as described above and are equally spaced from the metal linear to the outside surface of the structure. The total thickness of the structure at any polar position is determined from the pattern simulation program and this information is read by the mesh-generator. A separate input file used by the high-order element portion of the mesh-generator is created by the user

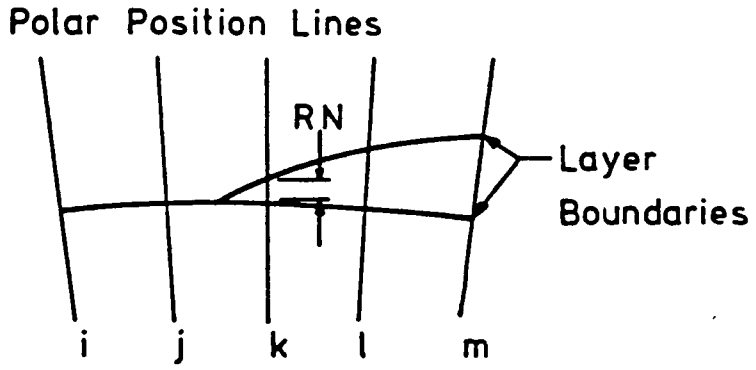

a) Actual relationship between polar position lines and layer boundaries.

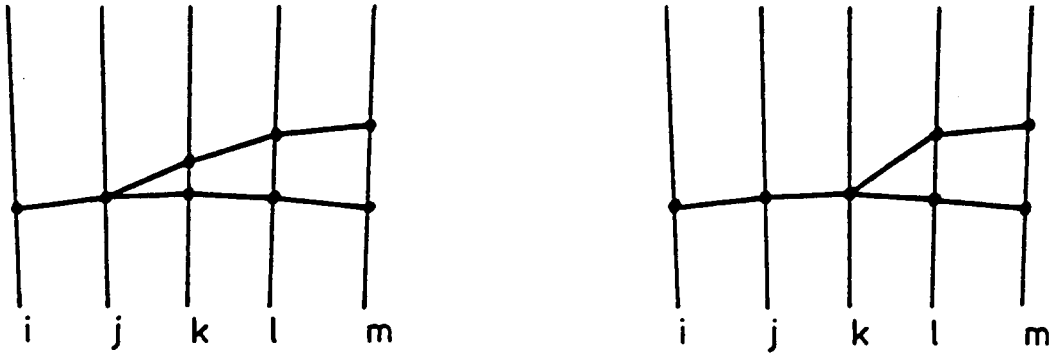

If RN > NT/4

If RN < NT/4

Where NT - Total composite thickness divided by the number of elements through the composite.

b) Two possible modeling solutions to a layer starting.

Figure 49. Creation of Elements to Model the Beginning of Layer Boundaries; after Leavesley [27]

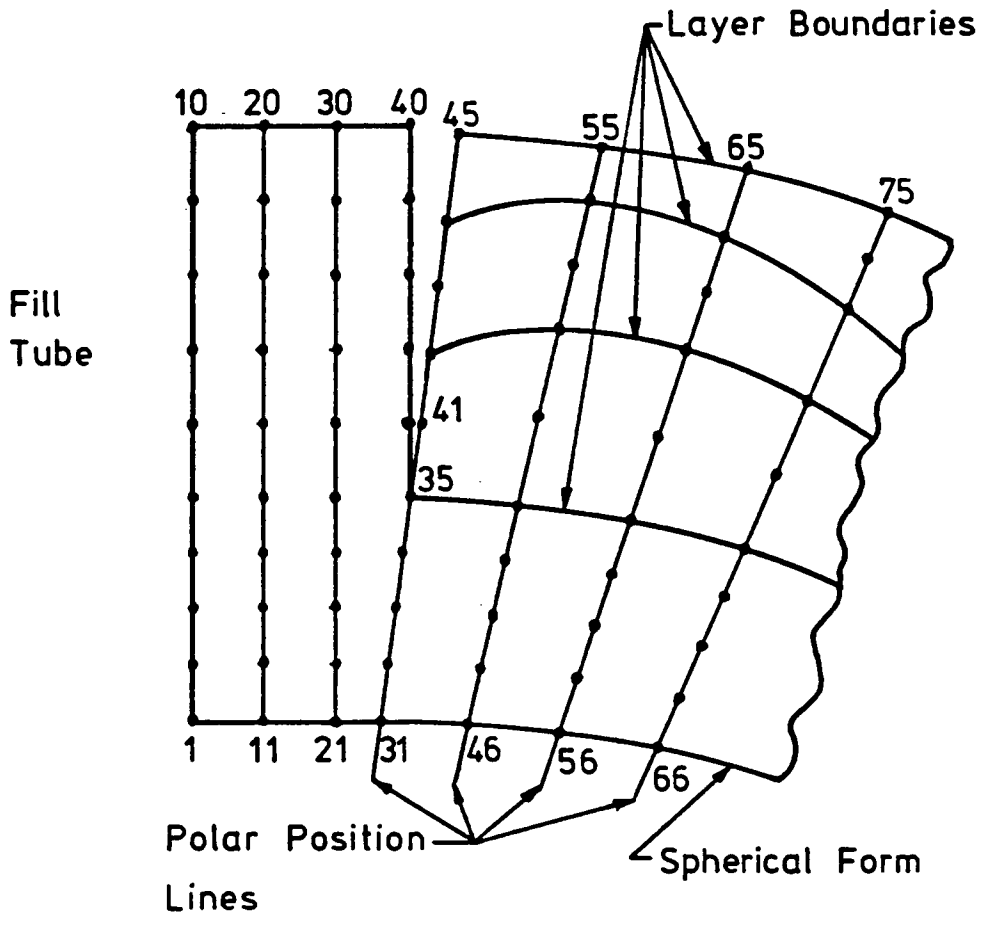

Figure 50. Nodal Point Placement and Node Numbering of the Spherical Pressure Vessel; after Leavesley [27]

which includes the order of the element and the internal pressure. The number of nodes corresponding to the order of the radial displacement field are then generated equally spaced from the outside surface of the mandrel to the outside surface of the filament-wound sphere. As before, the nodes are numbered radially outwards and sequentially along the polar positions to minimize the bandwidth of the structure stiffness matrix.

5.2.3.3 Four-Noded Quadrilateral Element Generation [27]

The element generation portion of the program SPHMESH has one constraint; no four-noded quadrilateral element may cross a band-set layer boundary. The element generator creates two type of elements by connecting the nodes that have been previously positioned by the node generator. The two types of elements are four-noded quadrilaterals and collapsed quadrilaterals to form triangles. Like the node generator, this routine is divided into two parts. The first portion of the code generates the elements in the fill tube and the second part generates the element in the spherical form of the structure.

The elements within the fill tube are created in columns parallel to the polar axis starting at the inner diameter of the fill tube. The element definition is illustrated in Fig. 51. The first element uses the first two nodes on the first two radial lines. Subsequent elements are formed outward to the top of the fill tube and this procedure repeated until all the nodes have been incorporated into elements. The elements are numbered as they are created outwards in columns. All the elements within the fill tube are assigned fiber angles, BETA, of 0° and polar position angles, SETA, of 90°. The angle SETA is defined as 90° minus the polar angle, PANG, as shown in Fig. 48.

The elements generated in the filament-wound composite portion of the structure will consist of four-noded quadrilaterals except where layers begin or end which often require triangular elements as shown in Fig. 49. The method used to position the nodes at these layer boundaries is shown in Fig. 49. These transition elements are actually 'collapsed' quadrilaterals which means that they are formed by specifying two of the four corners of the quadrilateral as the same node. Ele-

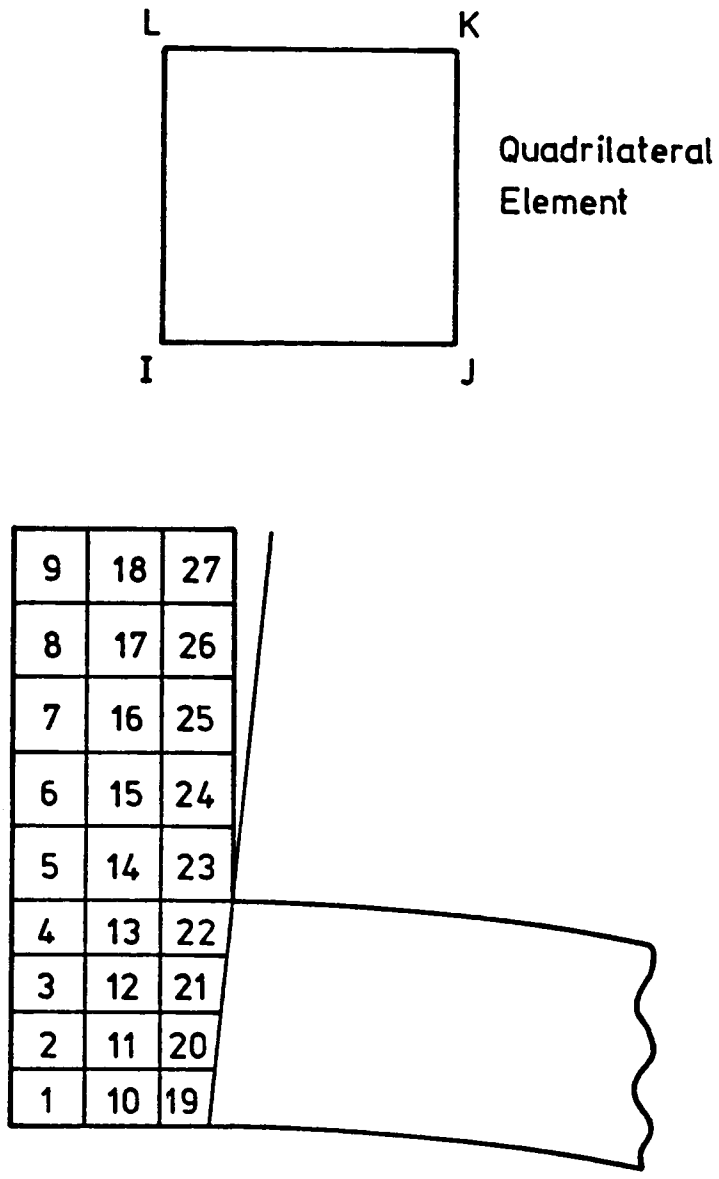

Figure 51. Element Numbering for the Fill Tube; after Leavesley [27]

ment generation is carried out layer by layer. The generation within a layer is by columns of elements along polar position lines moving from the fill tube to the equator.

The elements are created between two adjacent polar position lines of nodes as shown in Fig. 52. The program SPHMESH is used to check to see if any triangular transition elements are required in this column of elements of the current layer. The check for triangular elements is made by comparing the node number difference between the start and finish flags of the layer along the two adjacent polar lines. If the difference is zero, no triangular elements are necessary. A detailed description of the actual connectivity algorithm used in SPHMESH to assign node numbers to the elements is contained in reference [27].

Lastly, SPHMESH assigns both a fiber angle, BETA, and a polar angle, SETA, to each element. The fiber angle is the average of the fiber angles of its four-nodes and the polar angle is the average of the angles for the polar lines that form the element sides.

5.2.3.4 High-Order Composite Element Generation

The elements within the fill tube and metal spherical form are generated precisely as described above in the conventional technique. The isotropic mandrel and fill tube is modeled with bi-linear elements in both modeling techniques. The numbering of elements within the isotropic region of the structure is also performed using the technique described above.

The efficiency of the design code is achieved by replacing the numerous four-noded quadrilateral elements for the filament-wound composite with relatively few high-order composite elements. The use of two different elements in the same model is achieved by defining two 'element groups'. The finite element processor separates the element groups in both the computation phase and when creating the output of element stresses. Therefore, the elements within each element group are numbered begining with one. The high-order element nearest the fill tube is numbered one with the remaining elements numbered sequentially from the fill tube to equator.

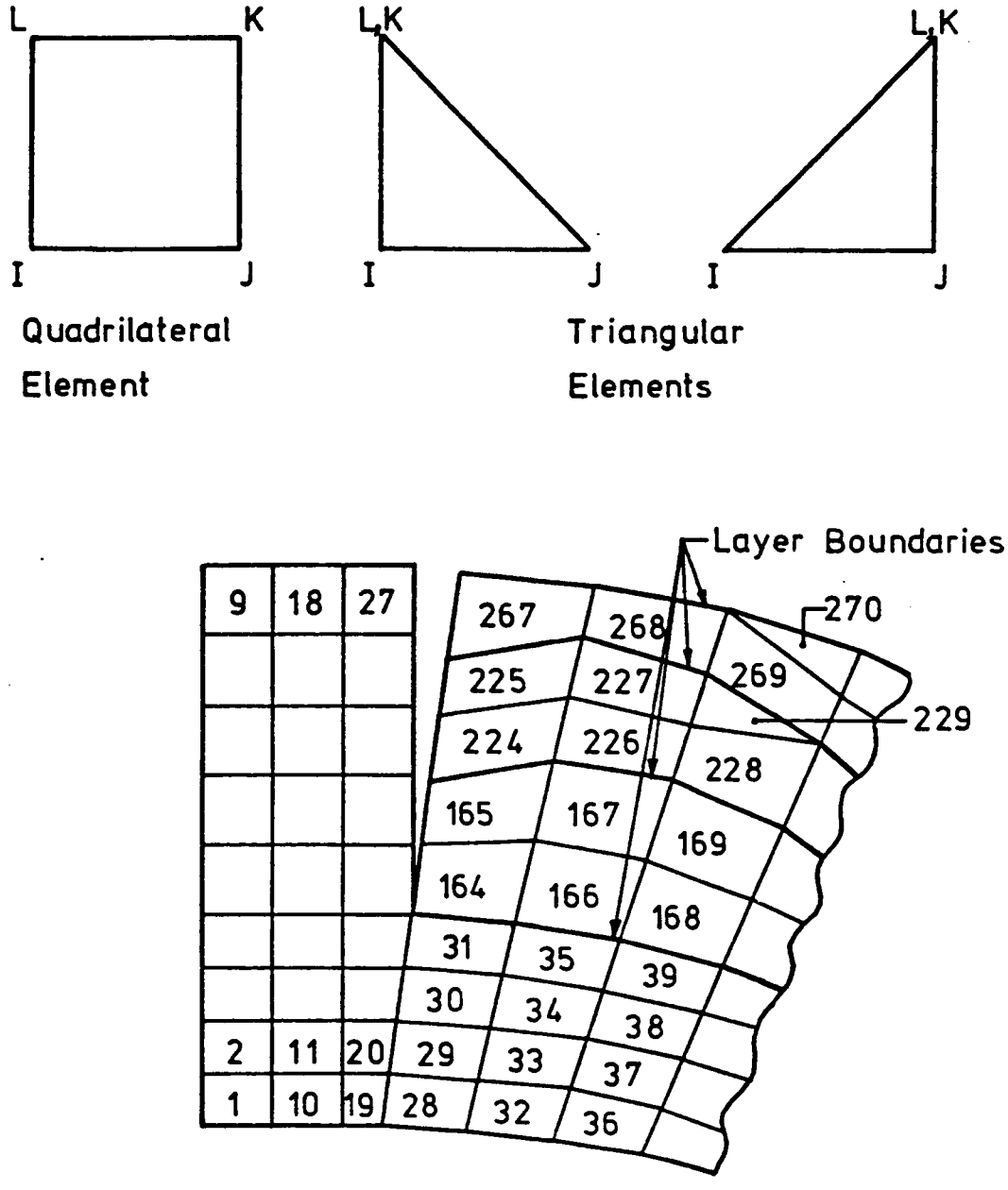

Figure 52. Element Numbering within the Spherical Form; after Leavesley [27]

The intra-element layers are defined based on the four-noded quadrilaterals generated for the 'conventional' model. The location of the integration points are calculated by using the centroid of the bi-linear elements that are replaced with the composite element. The weighting factors associated with each of the integration points is determined from the area ratio of the four-noded quadrilateral being replaced to the area of the high-order element. Material properties and fiber angles are defined as described in the section above.

5.2.4 Description of COUPLE

The program couple reads the output from the mesh-generator, SPHMESH, and then reformats it to create the input file for the finite element processor, HICOM. An additional input file is also read which contains all the control and option information that is needed by the finite element processor but that has no significance to the model generation or definition, i.e., titles, perform a data check or a full solution, etc.. The output file that is created by COUPLE is simply a reformatted version of the output file created by the mesh-generator with the additional control information read from the user created input file. The program COUPLE is a convenient means to tie the mesh-generator and the finite element program together as it is a simple piece of code that can be easily changed when refinements in the mesh-generator or finite element processor is made without having to change the more complex code of HICOM or SPHMESH.

5.3 Finite Element Code

It is this portion of the 'design code' that is of greatest interest in terms of the efficiency and utility of the newly formulated composite element. As has been explained, the primary area of the finite element method that was focused upon in trying to create an efficient solution scheme was

the reduction of the number of system equations. A result of using high-order elements with a user specified displacement field order, is that numerous other algorithms or sections of the conventional elements code needed to be modified, deleted or generalized to handle any order of element. Some additional algorithms were also needed to accommodate the unique characteristics of the high-order composite element. Presented below, is a description of the base finite element program along with the primary element subroutine of interest (COMPRING). The description of the base finite element code and the element subroutine will be of considerable detail as there are still areas in the actual computer implementation that may be candidates for further study to increase the efficiency of the program further. The recommendations will be presented in Chapter 7.

5.3.1 Description of HICOM

The program HICOM (HIgh order COMposite finite element program) is a modification of the program STAP (STatic Analysis Program) found in references [54,55] by Bathe which was written initially for static linear elastic finite element analysis. Rather than discuss in detail the specifics of the program itself, which have been mentioned in Chapter 3 and may be found in the references, the flow of this program will be presented. One of the basic objectives, as stated in section 5.1, was to create this design code to be as generic as possible. If the program could be written so that the high-order finite element could simply be included in the 'library' of element subroutines, the high-order subroutine would be more useful and widely accepted. Because of this design constraint and philosophy, very few changes in the base code were made. The basic flow of the program is identical to STAP and illustrated in Fig. 53. However, the following outline will more fully explain each part of the flow diagram (Fig. 53).

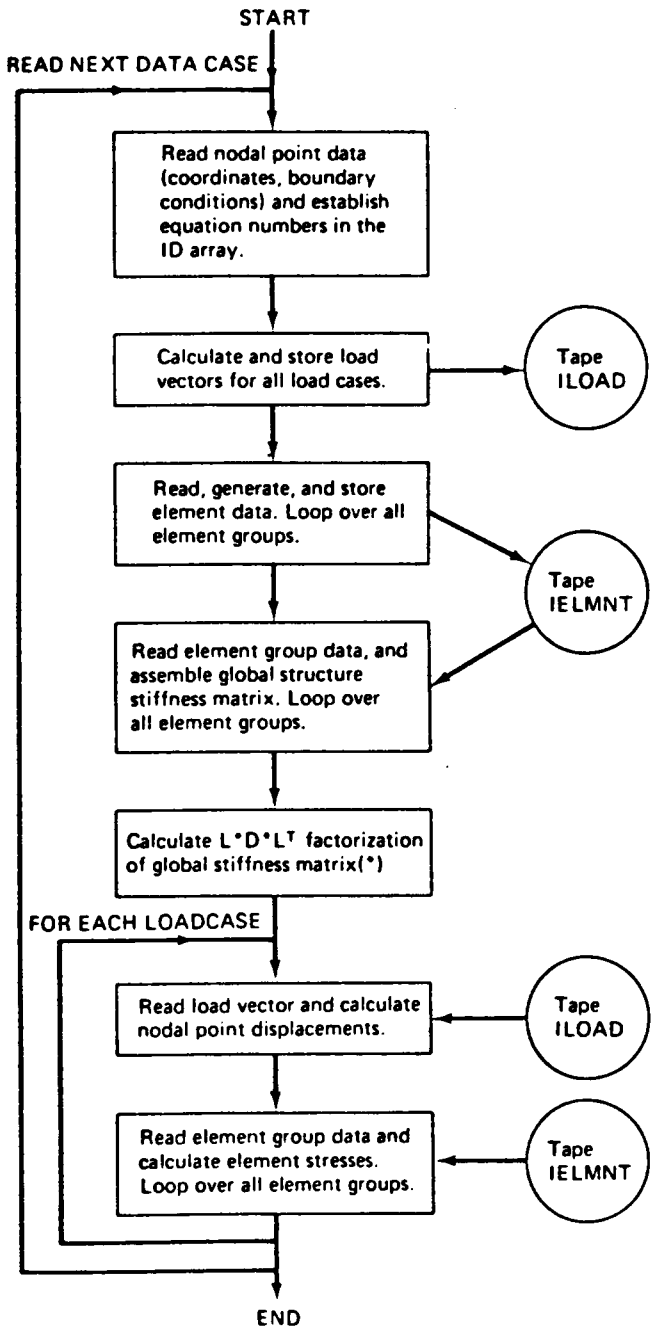

Figure 53. Basic Flow of the Program STAP; after Bathe [54]

5.3.2 Description of COMPRING

COMPRING is actually the collection of subroutines that comprise the high-order composite element portion of the finite element program. The subroutines in COMPRING are:

1. TRING : Allocates storage in the master 'A' array.

2. RING : Actual element subroutine.

3. SUM : Calculates the strain-displacement matrix.

4. MATSTF : Calculates the transformed material properties with the use of subroutine TRAN.

5. STRAN : Transforms the stresses from the *r-z-t* coordinate system to the 1-2-3 (principal material direction coordinate system).

The element subroutine is called three times by the main program, HICOM. The first time to simply read and store the element information from the input data file. The second time to form the element stiffness matrices, and the last time to calculate the stresses. The outline on the following pages gives a brief description of the features of each program and the flow of the element subroutines.

5.3.2.1 Stiffness Matrix Renumbering and Storage Algorithm

The program STAP is written in a form that allows for new elements to be added to its 'library' relatively easily. To do this, STAP uses a scheme where all element stiffness matrices are stored assuming that each node has three degrees of freedom. Each element subroutine handles the storage and retrieval of the stiffness matrix being certain that not only the active degrees of freedom

are accounted for but also the inactive degrees of freedom. The inactive degrees of freedom are not actually stored because of the compacted storage and solution method described in section 5.1.1. The standard procedure used in most element subroutines that have been incorporated in STAP, or a modification of STAP, is to manually identify the active and inactive degrees of freedom and then store the active degree of freedom stiffness coefficients in an array that can be stored or passed to the solution phase of the program. This method is described below followed by the description of the new algorithm used to perform this task automatically for any order element.

Consider a quadratic axisymmetric element that has six nodes, three on each side. These six nodes have two degrees of freedom per node. However, the finite element program assumes that all nodes have three degrees of freedom. Therefore, the stiffness matrix for this element contains six extra rows and columns than is necessary and they contain only zeros. To avoid storing an unnecessary large amount of zeros, the following scheme is employed. The stiffness matrix for the quadratic element is 18 × 18 (6 nodes × 3 d.o.f). Only the upper triangular portion of the matrix will be stored, as the matrix is symmetric. Each element of the stiffness matrix is then individually denoted sequentially as shown in Fig. 54. Now, the third degree of freedom of each node is deleted from the matrix shown in Fig. 54 to form a matrix containing only the 'active' degrees of freedom, resulting in a 12 × 12 stiffness matrix. Every third row and column is deleted and the resultant matrix collapsed to form the 'active' stiffness matrix (STF) shown in Fig. 55. The purpose of this active stiffness matrix is to identify the locations of the active degrees of freedom. For instance, notice that in Fig. 54 there are 171 locations in the upper triangular portion of the element stiffness matrix. However, many of those terms are zero, and in fact 92 of those coefficients are unconditionally zero because they represent inactive degrees of freedom, or degrees of freedom that simply are not present in the element, namely a displacement in the tangential direction. The solution phase of the program is expecting a structure stiffness matrix whose order is three times the number of nodes in the model. Therefore, the nonzero coefficients of the element stiffness matrix must be stored in a matrix that assumes the additional degree of freedom. The storage of the active stiffness matrix (STF) in the array (S) was initially performed by a series of equality statements. The technique of using equality statements to condense the stiffness matrix, which occurs twice in the code,

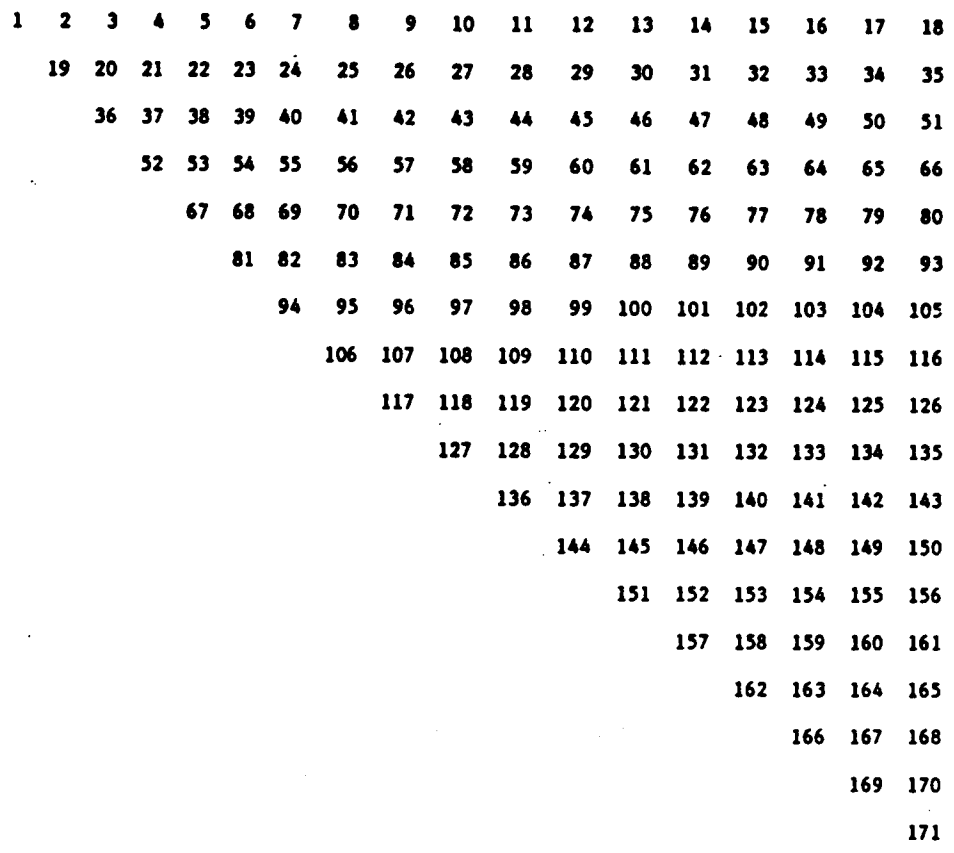

Figure 54. Coefficient Identifications for a Second-Order Element Stiffness Matrix

1	2	4	5	7	8	10	11	13	14	16	17
	19	21	22	24	25	27	28	30	31	33	34
		52	53	55	56	58	59	61	62	64	65
			67	69	70	72	73	75	76	78	79
				94	95	97	98	100	101	103	104
					106	108	109	111	112	114	115
						127	128	130	131	133	134
							136	138	139	141	142
								151	152	154	155
									157	159	160
										166	167
											169

Figure 55. Identification of Coefficients Representing the Active Degrees-of-Freedom of a Second-Order Element Stiffness Matrix

would require separate subroutines for each high-order element desired. A fifth-order element would require approximately 175 equalities specifying the exact locations of the stiffness matrix to be stored.

5.3.2.2 Lagrangian Shape Functions and Jacobian Algorithm

One of fundamental problems encountered in creating a single element subroutine that can generate the element stiffness matrices and then calculate the stress and strain field within a linear/high-order element is the capability to calculate the Lagrangian Shape functions and the Jacobian for any order element. The Lagrangian shape functions for several displacement orders could be contained in separate subroutines, but this would be a tremendously inefficient programming technique and would also place a constraint on the order of element possible.

The current linear/high-order element subroutine, COMPRING, is used to evaluate the element stiffness matrix of any order element and is only bounded by the array dimensions in the subroutine (currently set to allow up to a 25^{th} order element). The actual algorithm to calculate the Lagrangian Shape functions in the natural coordinates, ξ and η, can be found in the user's guide [59]. A description of the algorithm is given below.

The order of the element is passed to the Lagrangian shape function and partial derivative algorithm, from which the number of side nodes is calculated.

$$NSIDE = NORDER + 1 \qquad [5.2]$$

The local coordinate ξ is the linear direction and η is the high-order direction. The location of the nodes in the local coordinate system must be calculated. The nodes are equally spaced in the local coordinate system between -1.0 and + 1.0. Once the local coordinates of the nodes are determined, the shape functions and their derivatives in the η direction are calculated as follows.

First, the numerator of the Lagrangian shape function is calculated for each node (see Eq. 2.28).

$$ALETA(I) = \prod_{J=1}^{NSIDE} [\text{ETA} - NL(J)] \quad ; \quad I \neq J \qquad [5.3]$$

in which $ALETA(I)$ = Numerator of the Lagrangian shape function for node I

ETA = Local coordinate, η

$NL(J)$ = Location of node J in the η direction

The denominator of the shape function is found in a similar manner.

$$DEN = \prod_{J=1}^{NSIDE} [NL(I) - NL(J)] \quad ; \quad I \neq J \qquad [5.4]$$

in which $NL(I)$ = Location of node I in the η direction

$NL(J)$ = Location of all other side nodes in the η direction

The one-dimensional Lagrangian shape functions for each node, I, in the η direction are then calculated.

$$SHAPE(I) = \frac{ALETA(I)}{DEN} \qquad [5.5]$$

The two-dimensional Lagrangian shape function is then calculated by simply multipling the one-dimensional shape functions in the ξ and η directions together.

$$SF(I) = ALXI(I) \bullet SHAPE(I) \qquad [5.6]$$

in which $SF(I)$ = Two-dimensional Lagrangian shape function of node I

$ALXI(I)$ = Shape function in the ξ direction

$= \frac{(1.0 - \text{XI})}{2.0}$ for the bottom row of nodes

$= \frac{(1.0 + \text{XI})}{2.0}$ for the top row of nodes

XI = Local coordinate, ξ

The partial derivatives of the shape functions are calculated by first determining the numerator using the chain rule

$$DER(I) = \sum_{J=1}^{NSIDE} SHAPE\frac{(I)}{\text{ETA} - NL(J)} \quad ; \quad I \neq J \qquad [5.7]$$

The partial derivatives of the shape function with respect to η are then calculated.

$$TB(I) = ALXI(I) \bullet DER(I) \qquad [5.8]$$

The partial derivatives of the shape function with respect to ξ are calculated as follows:

$$TB(I + NUMNODE) = SHAPE(I) \bullet DLXI \qquad [5.9]$$

in which DLXI(I) = -0.5 for nodes on the bottom row of the element

= + 0.5 for nodes on the top row of the element

5.3.2.3 Integration Point Mapping Transformation Algorithm

One of the unique problems that has been created by the need for the element to account for the different layer thicknesses that can reside in each high-order element is the ability to transform coordinates from the global structure coordinate system, *r-z-t*, to the natural coordinate system, ξ, η. The typical numerical integration technique is to use a quadrature method as explained in section 2.2.2. However, being that conventional elements contain only one set of material properties, the integration points can be specified anywhere inside the element. The location of the integration points is specified based on various criteria, i.e., Gauss quadrature points are determined to minimize the integration error based on a Taylor series expansion of the Lagrangian interpolation polynomials. The formulation of the high-order composite element necessitates using an integration scheme that allows for unequally spaced integration points as well as spacing that is not preselected but that is specified by the user. Therefore, a zeroth-order integration method was selected.

The zeroth-order integration technique is by far the easiest numerical integration technique to incorporate as it reduces fundamentally to summing rectangles. The area of each rectangle is the functional value of the integration points times the weight factor which is equal to the thickness ratio of the layer attributed to each integration point.

A description of the purpose, utility, and implementation of the program COUPLE that converted the output from the mesh-generator to a form useable by the finite element program is given in section 5.2.4.. One of the important features of that program was to specify the locations of the integration points in the global coordinate system so that the effect of each layers stiffness could be accounted for and so that the stresses could be calculated in each layer at least once. The problem is simply to transform the global coordinates to natural coordinates for each element. This transformation is accomplished with Lagrangian interpolation polynomials. Generally, the transformations involving the Lagrangian polynomials is executed in the other direction.

The location of the integration points in the natural coordinate system are needed as well as the weight factors. The easiest technique to calculate the weight factors for a zeroth-order integration is to calculate the area ratio of each layer with respect to the entire element in the natural coordinate system. Using the natural coordinate system is convenient as all quadrilaterals in the global coordinate system are mapped as rectangles in the natural coordinate system. The transformation from the *r-z* coordinate system to the ξ-η coordinate system is done with a linear transformation in the radial direction. The transformation is identical for all order elements as the transformation is performed in the undeformed geometry to locate the centers of each layer in the natural coordinate system. Because the assumed displacement is a Lagrangian polynomial of an order greater than one and the transformation of the geometry within an element is performed with respect to the corner nodes using a linear Lagrangian polynomial, the element is termed 'subparametric'.

Linear interpolation using Lagrangian interpolation polynomials is expressed as

$$\begin{Bmatrix} x \\ y \end{Bmatrix} = [N]\{c\} \qquad [5.10]$$

where x and y = location of the integration points in the r-z coordinate system

$[N]$ = matrix of linear Lagrangian interpolation polynomials

$\{c\}$ = location of the corner nodes in the r-z coordinate system

The matrix of the linear interpolation polynomials has the form

$$[N] = \begin{bmatrix} N_1 & 0 & N_2 & 0 & N_3 & 0 & N_4 & 0 \\ 0 & N_1 & 0 & N_2 & 0 & N_3 & 0 & N_4 \end{bmatrix} \qquad [5.11]$$

where $N_1 = 1/4(1 - \xi)(1 - \eta)$

$N_2 = 1/4(1 + \xi)(1 - \eta)$

$N_3 = 1/4(1 + \xi)(1 + \eta)$

$N_4 = 1/4(1 - \xi)(1 + \eta)$

The natural coordinates in the equations above are the unknowns that must be determined. Therefore, rewriting the two equations shown in Eq. 5.10 results in

$$\begin{aligned} f_1(\xi, \eta) = 0 = (1 - \xi)(1 - \eta)c_1^r + (1 + \xi)(1 - \eta)c_2^r + \\ (1 + \xi)(1 + \eta)c_3^r + (1 - \xi)(1 + \eta)c_4^r - 4r \\ f_2(\xi, \eta) = 0 = (1 - \xi)(1 - \eta)c_1^z + (1 + \xi)(1 - \eta)c_2^z + \\ (1 + \xi)(1 + \eta)c_3^z + (1 - \xi)(1 + \eta)c_4^z - 4z \end{aligned} \qquad [5.12]$$

where c_i^r and c_i^z represent the global coordinate locations of corner node i in the r and z directions respectively. Refer to Fig. 1 on page 22 for the proper relative orientations of the corner nodes. Equations 5.24 and 5.25 are therefore two nonlinear equations of ξ and η. One method of solution selected to solve these equations is the Newton-Raphson technique which is explained in several references [58]. However, if the location of the integration points in one of the two natural coordinates can be assumed (or preset) then either function given in Eq. 5.12 can be reduced to an explicit function of a single unknown.

Because the efficiency of the high-order composite elements was of primary concern, the explicit technique of performing the coordinate transformation was selected. The disadvantage, of course, is that the location of each integration point must be set in the code and only one coordinate can be passed from the program COUPLE to the finite element processor.

Once the location of the integration points have been determined in the natural coordinate system, the weight factors must be determined. The method used to calculate the weight factors is based simply on determining the area ratio of each layer with respect to the total area of the high-order element. Using this technique allows each intra-element layer to be weighted according to its relative influence on the stiffness of the high-order element. The current integration scheme uses only one integration point within each intra-element layer which are usually unequally spaced in the η direction and sometimes in the ξ direction. Each of the integration points is located at the centroid of the layer in the *r-z-t* coordinate system. If two integration points per layer are desired, the weighting factors in the high-order direction, η, should be calculated based on the intra-element layer's thickness ratio along the specified ξ coordinate.

6.0 Design Code Test Case

6.1 Introduction

This research program was initiated to investigate the potential for developing a design code for filament-wound structures by incorporating an efficient and accurate high-order element. Based on the results of computation and efficiency studies, a design code specifically for filament-wound spherical pressure vessels was to be developed. Theoretical and actual finite element computation studies that demonstrated the efficiency of the composite element formulation were presented in Chapter 3. The accuracy of the newly developed element for carefully selected models and geometries was presented in Chapter 4. Based on the results that have been presented in Chapters 3 and 4, the design code discussed in Chapter 5 was developed. This chapter will present some sample results from a number of test cases that have been run. The design code, HICOM, has been tested with models and test cases that will be presented in this chapter to i) demonstrate that the design code works, ii) the show that the design code was more efficient than the conventional solution technique and model, and iii) to get some indication of the accuracy of the solution and approximately what order displacement field will be needed for practical problems.

6.2 *Description of the Test Model*

The filament-wound spherical pressure vessel that was used as the test case in this study was also used in the study presented in reference [27]. The spherical structure consisted of a copper mandrel and two composite shells. A shell is a complete set of bands that provide uniform thickness over the spherical form or mandrel. The vessel has a 101.6 mm (4.000 in.) inside diameter and the mandrel has a thickness of 1.02 mm (0.040 in.). The fill tube height is 7.11 mm (0.280 in.) which allows the fill tube to become basically flush with the wound shells. The winding pattern used was the delta-axisymmetric pattern, described in section 5.2.1., and the material is Kevlar 49-Epoxy. The average thickness of the two shells is 6.07 mm (0.239 in.).

The delta-axisymmetric pattern was created with a nominal band width of 7.5 degrees of arc coverage and a band thickness of 0.135 mm (0.0053 in.). The first polar position angle is 2.647 degrees as shown in Fig. 48 on page 132. The pattern is constructed with a downwind followed by an upwind and each of these shells are formed with twelve band sets.

The finite element model, shown in Fig 56, was created by specifying the following quantities within the mesh generator (see section 5.2.3).

1. Number of elements up fill tube = 24
2. Number of elements across fill tube = 4
3. Number of elements through the spherical form = 4
4. Number of elements through the fibers = 24

A corresponding model consisting entirely of linear orthotropic elements was also created so that the high-order element model could be compared to a 'conventional' model. The bi-linear element model is created by using a single element for each band of fibers which means that it contains 24 elements radially from the spherical form at each polar position. The high-order element models use bi-linear elements to model the metal mandrel.

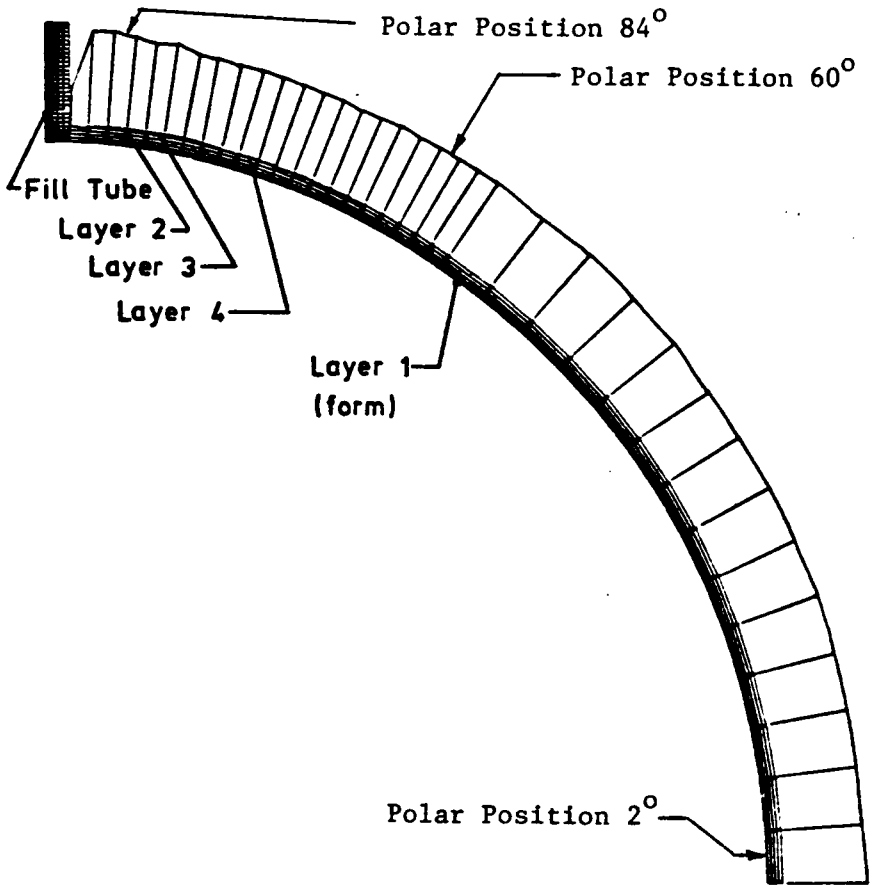

Figure 56. Finite Element Model of Test Case with High-Order Elements

6.3 *Results*

The results from the test case just described are presented from two aspects; i) comparison of the high-order element model results with the conventional finite element solution and ii) computational efficiency of the composite element. The comparison of the high-order element with the conventional element to model a filament-wound sphere will not include a discussion of the accuracy of the solution because of the complexity of the problem for which no known exact elasticity solution exists. However, an isotropic sphere was analyzed to determine if in fact the finite element results were reasonable and if any problems associated with modeling a spherical structure were present before solving a complicated anisotropic structure.

The isotropic sphere was generated with the same mesh as that which modeled the filament-wound structure and was loaded with an internal pressure of 6.89 MPa (1000 psi). Therefore, the sphere has a hole at the pole and the thickness of the sphere is not constant but it does not vary significantly away from the fill tube. The theoretical radial stress, hoop stress and radial displacement on the inside of the sphere made of steel is -6.89 MPa (-1000 psi), 25.40 MPa (3686 psi) and 0.0499 mm (0.000196 in.), respectively. The conventional bi-linear model predicted an average radial stress of 6.72 MPa (-975 psi) in the elements forming the inside of the sphere, the hoop stress was 25.36 MPa (3680 psi) and the radial displacement varied from 0.00517 mm (0.000203 in.) at the fill tube hole to 0.00489 mm (0.000192 in.) at the equator. The high-order results were very similar. Based on these results, the design code was determined to be working satisfactorily and was then used to generate results for a typical filament-wound spherical pressure vessel.

The basic concept of the displacement-based finite element formulation is the order of the assumed displacement function must closely approximate the actual displacement field or enough low-order elements must be used to create such an approximation. There is not an elasticity solution to the filament wound spherical pressure vessel problem with which the finite element results can be compared, therefore, the high-order model results will be compared to the conventional fi-

nite element solution. The displacement field approximations made with the both the conventional element models and the high-order composite element models can be visualized by plotting the deformed structure with exaggerated displacements of the nodes. Figures 57-59 were created by multiplying the nodal point displacements in the r and z directions by 250. Shown in Fig. 57 are two deformed plots superimposed; the blue mesh is the conventional bi-linear model and the red mesh is a model utilizing sixth-order elements to model the filament-wound composite. The 90° sector in Fig. 57 represents the undeformed position of the interior surface of the metal mandrel, indicating that the sphere deforms almost spherically with the greatest variation occuring near the fill tube. Figures 58 and 59 are expanded views of the fill tube region of the sphere, containing the first ten polar positions. Figure 58 contains the deformed bi-linear model, shown in blue, and superimposed is the sixth-order element model shown in red. Again, the two deformed meshes are superimposed so that the undeformed interior of the metal mandrel is aligned in both models. In Fig. 59 the deformed meshes of the third-, fourth-, and sixth-order element models are superimposed. One of the interesting and somewhat surprising results that can be seen in Fig. 59 is that the structure appears to be more stiff when modeled with the sixth-order elements than with the lower-order elements.

Four sets of results for the test model will be presented. The first three are comparisons of the normal stress profiles (normal to the sphere or a spherical radial stress) through the structure at three different polar positions; 2°, 60°, and 84°. The positions on the high-order model are shown in Fig. 56. Figures 60-62 are enlarged section views of the bi-linear model which illustrate the number of linear elements being incorporated into the high-order element. The results are shown in Figs. 63-65 in which the bi-linear results along with fourth-, fifth-, and sixth-order elements results are superimposed. Note that the first four data points on each of the graphs represent the isotropic mandrel and are bi-linear elements for all models. The change in the radial moduli between the filament-wound structure and the metal mandrel causes the distinct piece-wise continuous radial stress profile that was discussed in section 4.2.4. Very good agreement between the high-order element results and the bi-linear solution is shown.

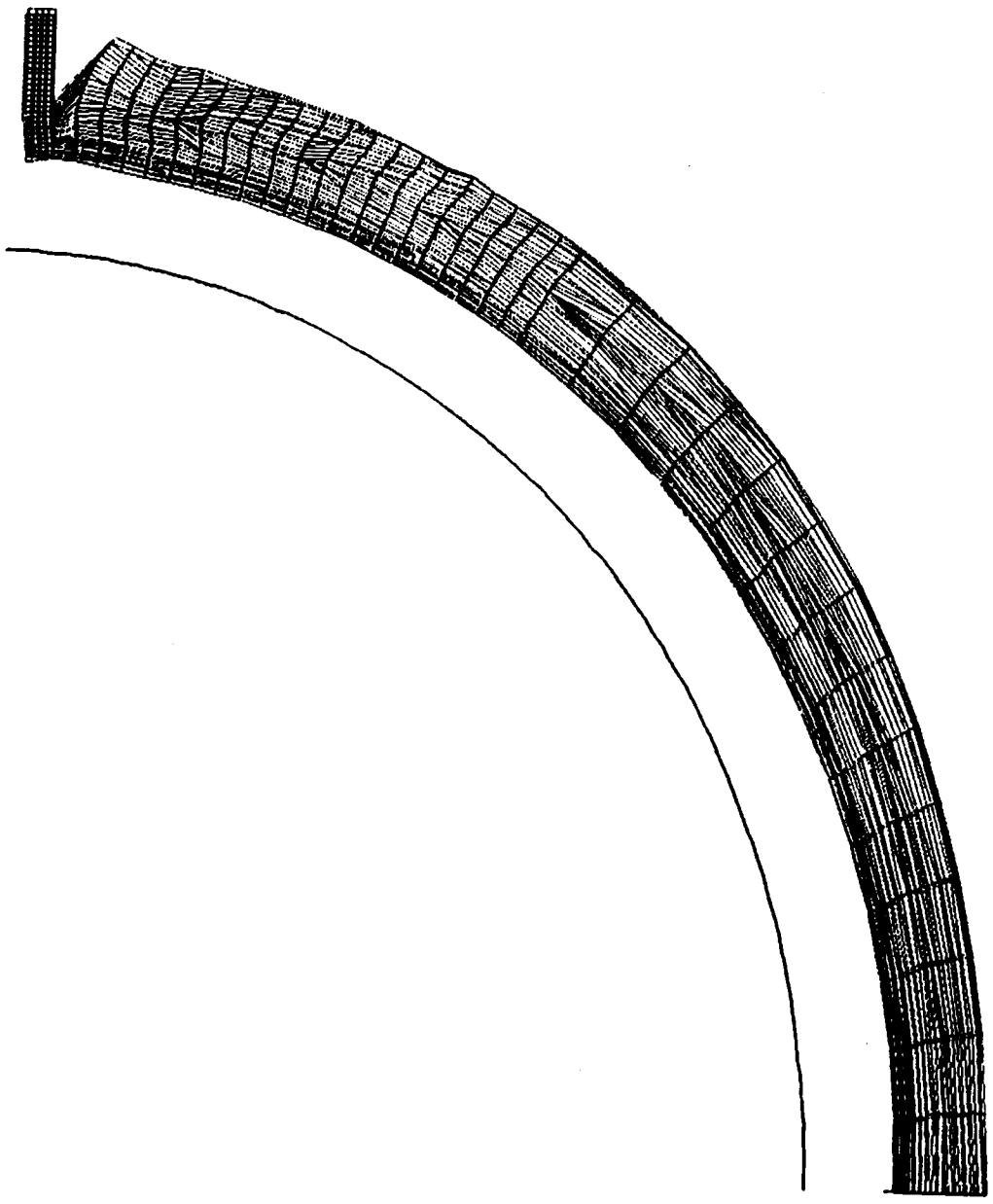

Figure 57. Deformed Meshes of the Conventional and Sixth-Order Element Models of the Filament Wound Spherical Pressure Vessel

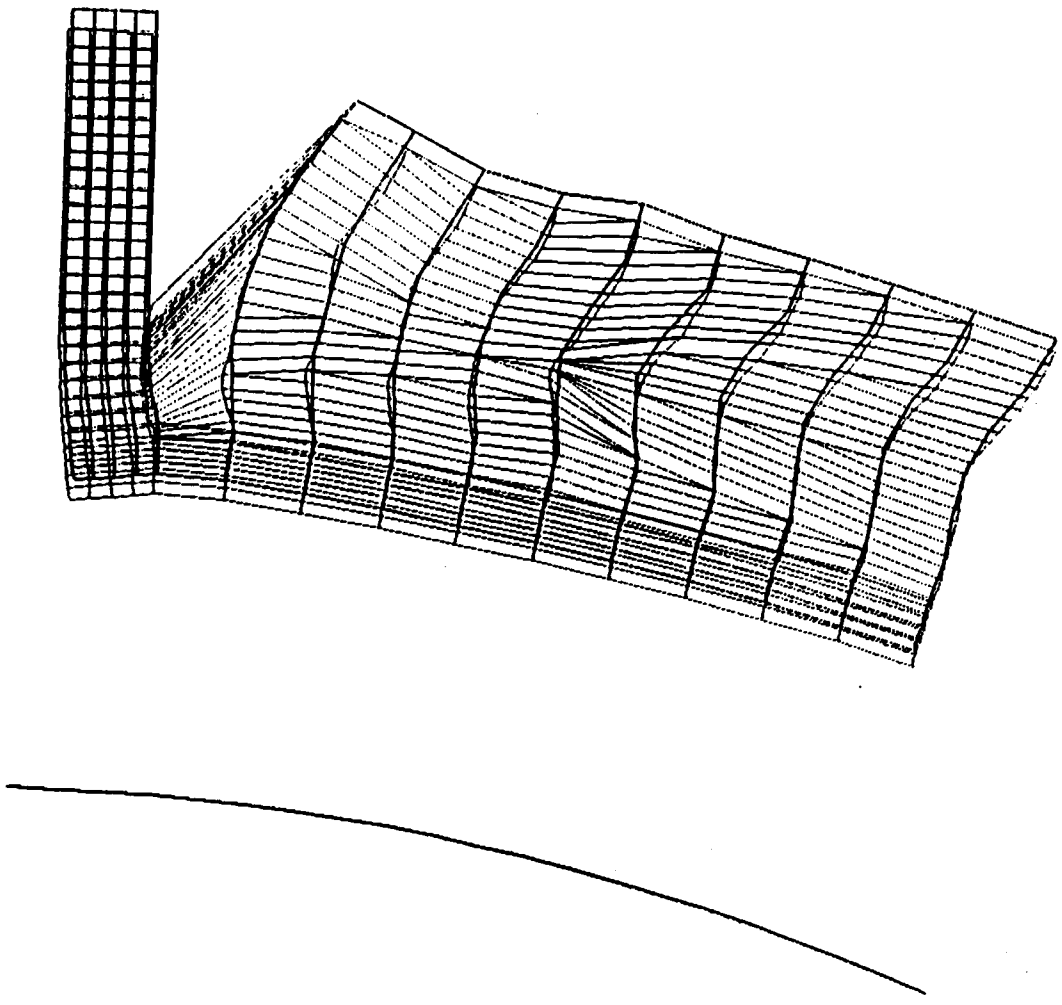

Figure 58. Deformed Meshes of the Conventional and Sixth-Order Element Model at the Fill Tube Region

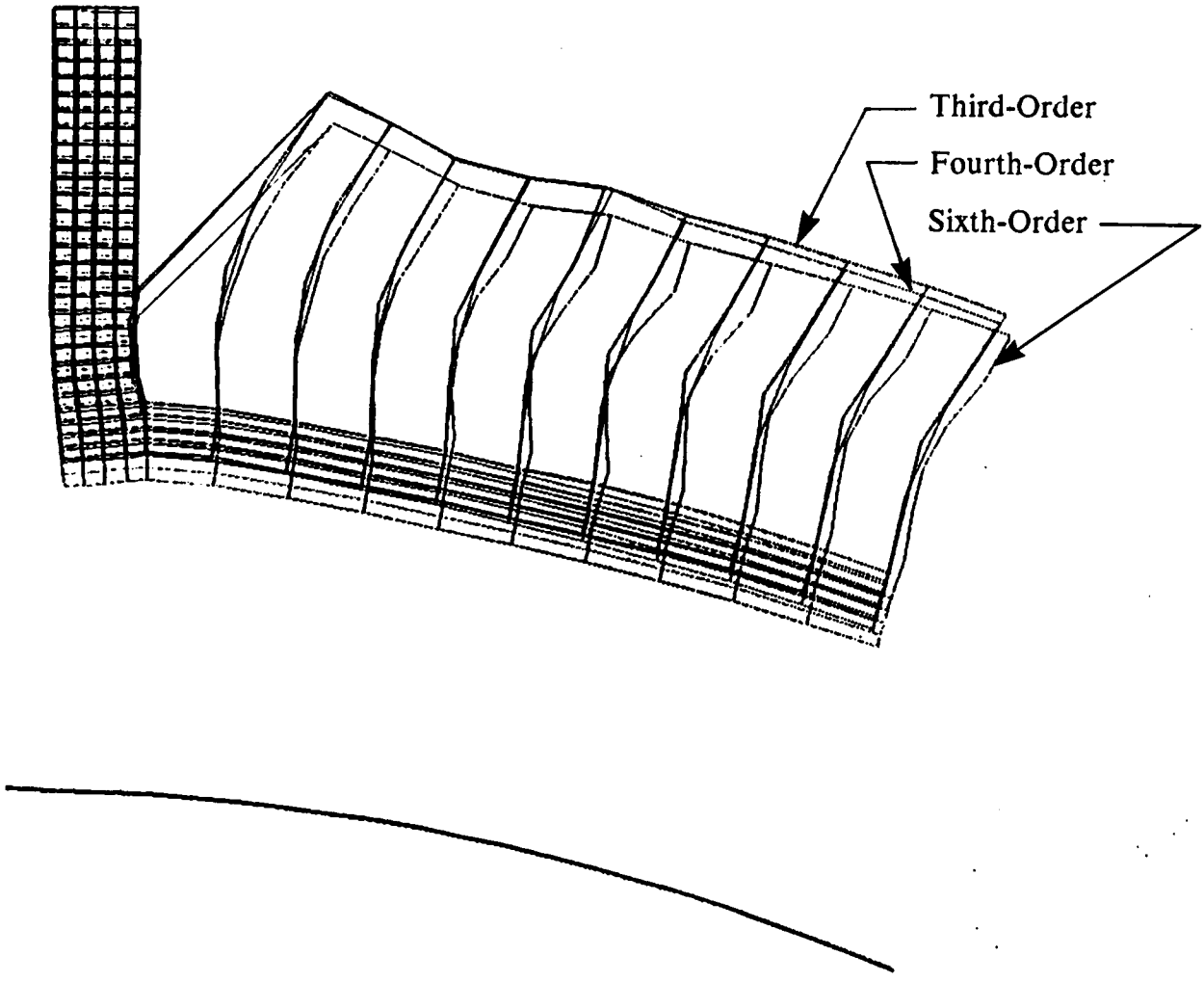

Figure 59. Deformed Meshes of the Fill Tube Region Using Third-, Fourth-, and Sixth-Order Elements

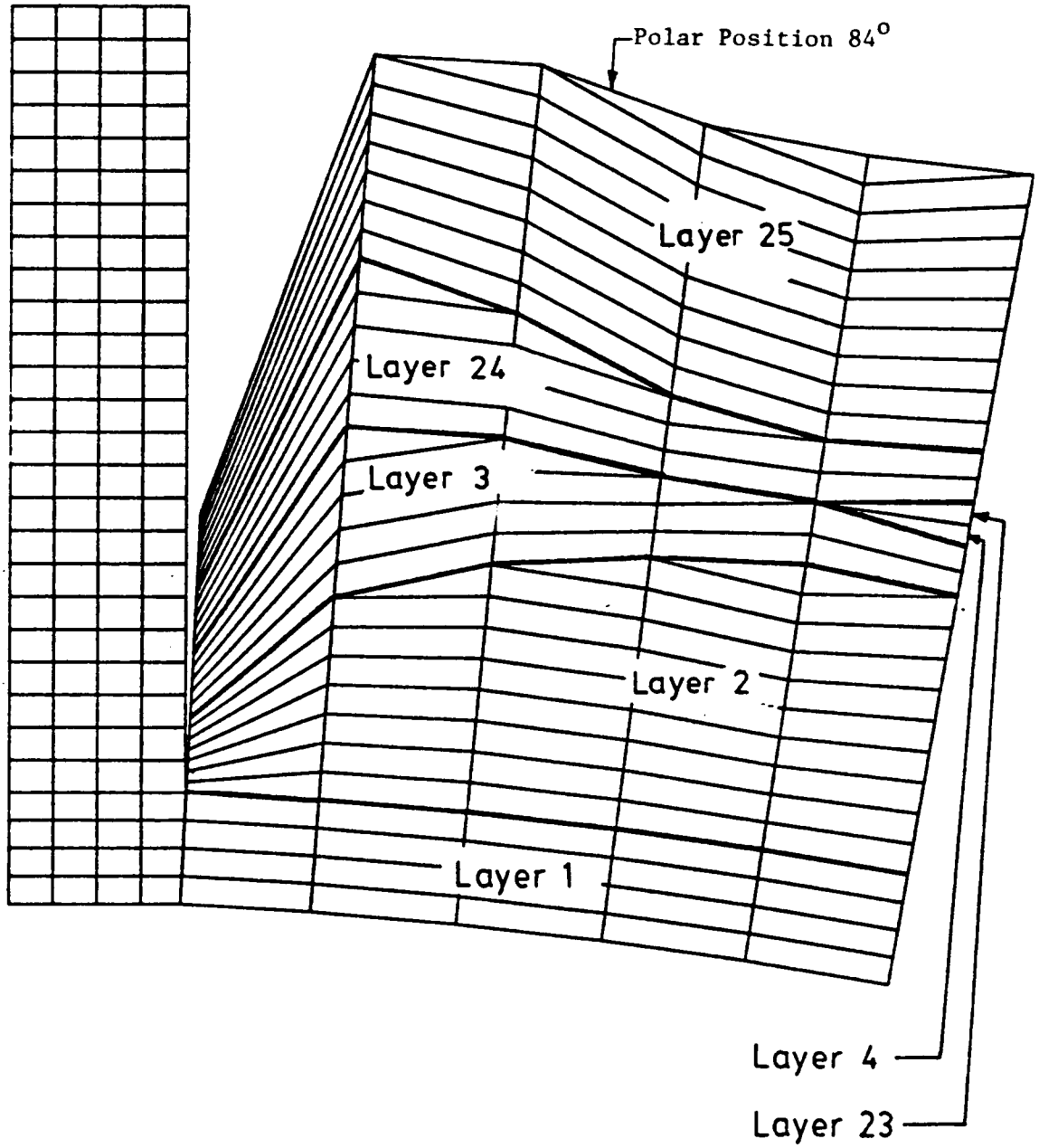

Figure 60. Expanded View of the Mesh around the Fill Tube

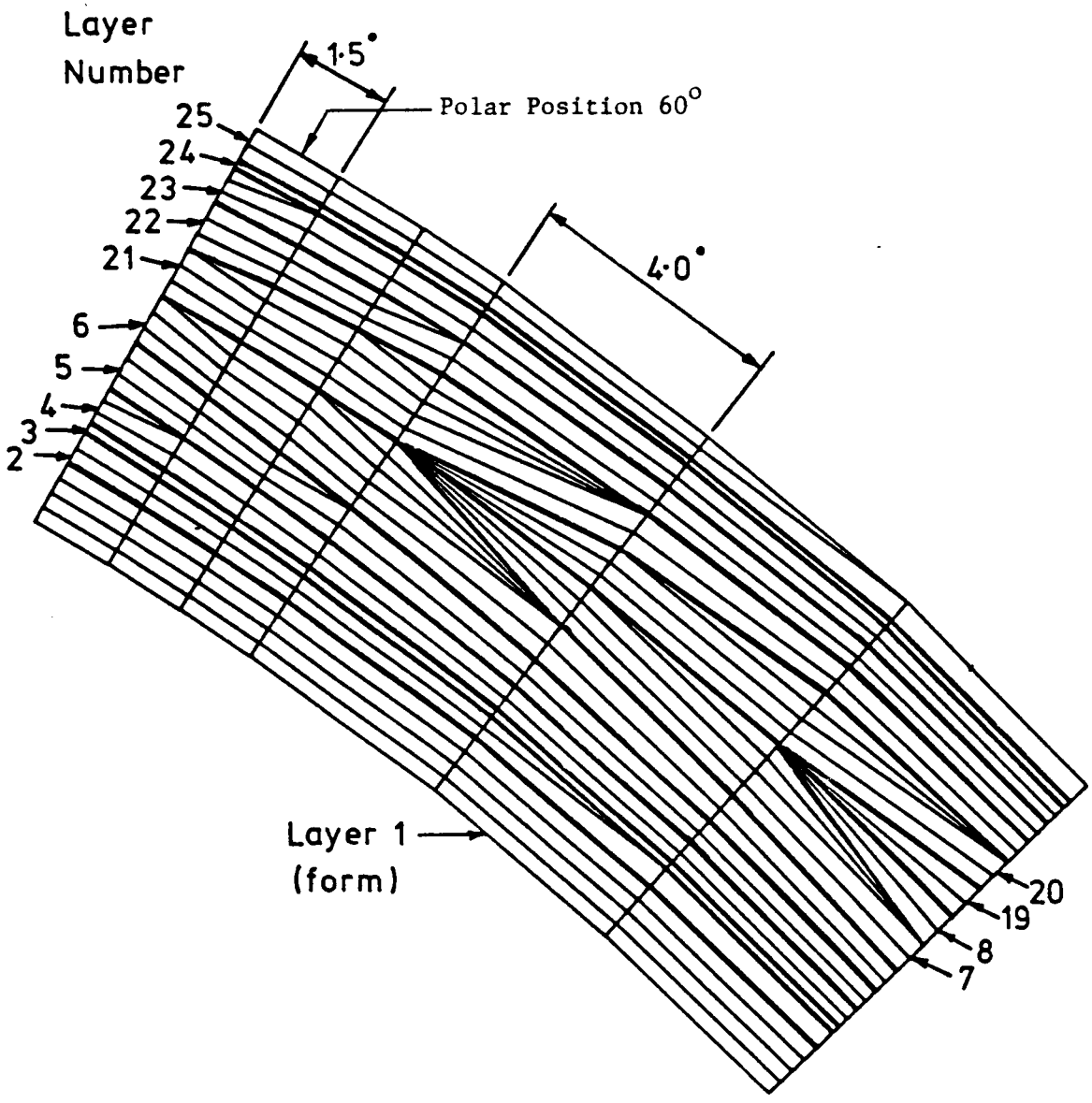

Figure 61. Expanded View of the Mesh at the Change of Element Lengths

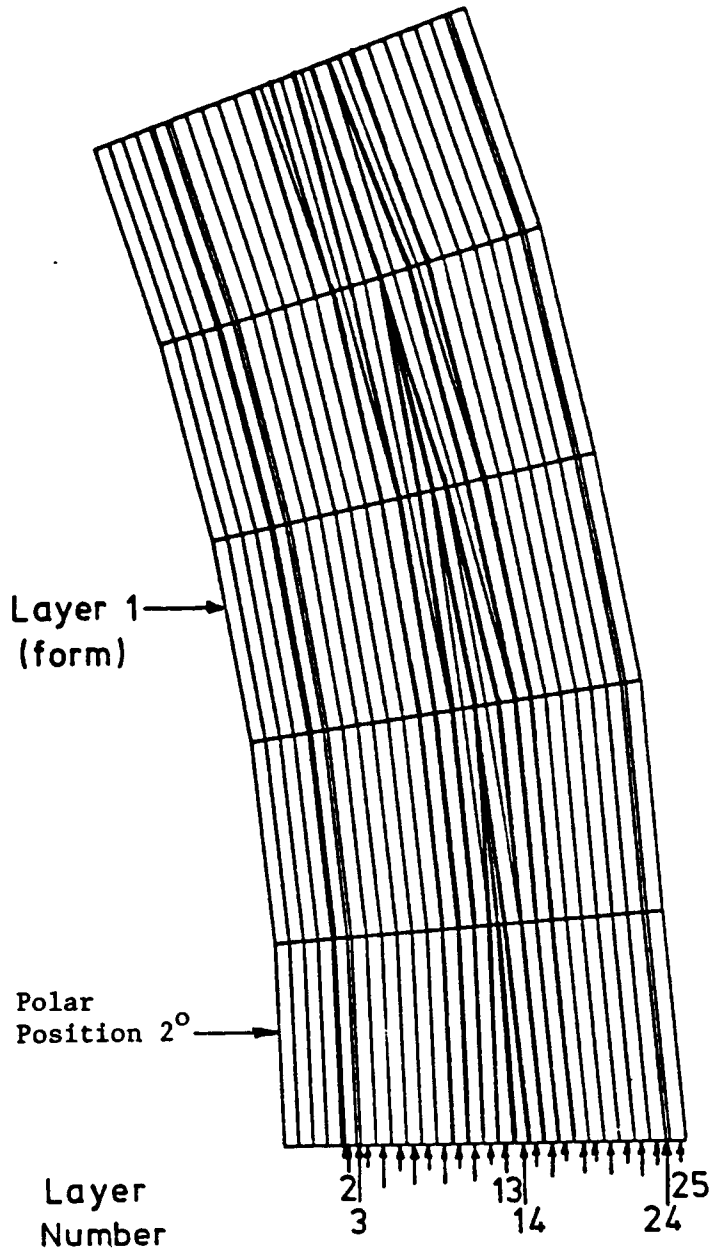

Figure 62. Expanded View of the Mesh at the Equator

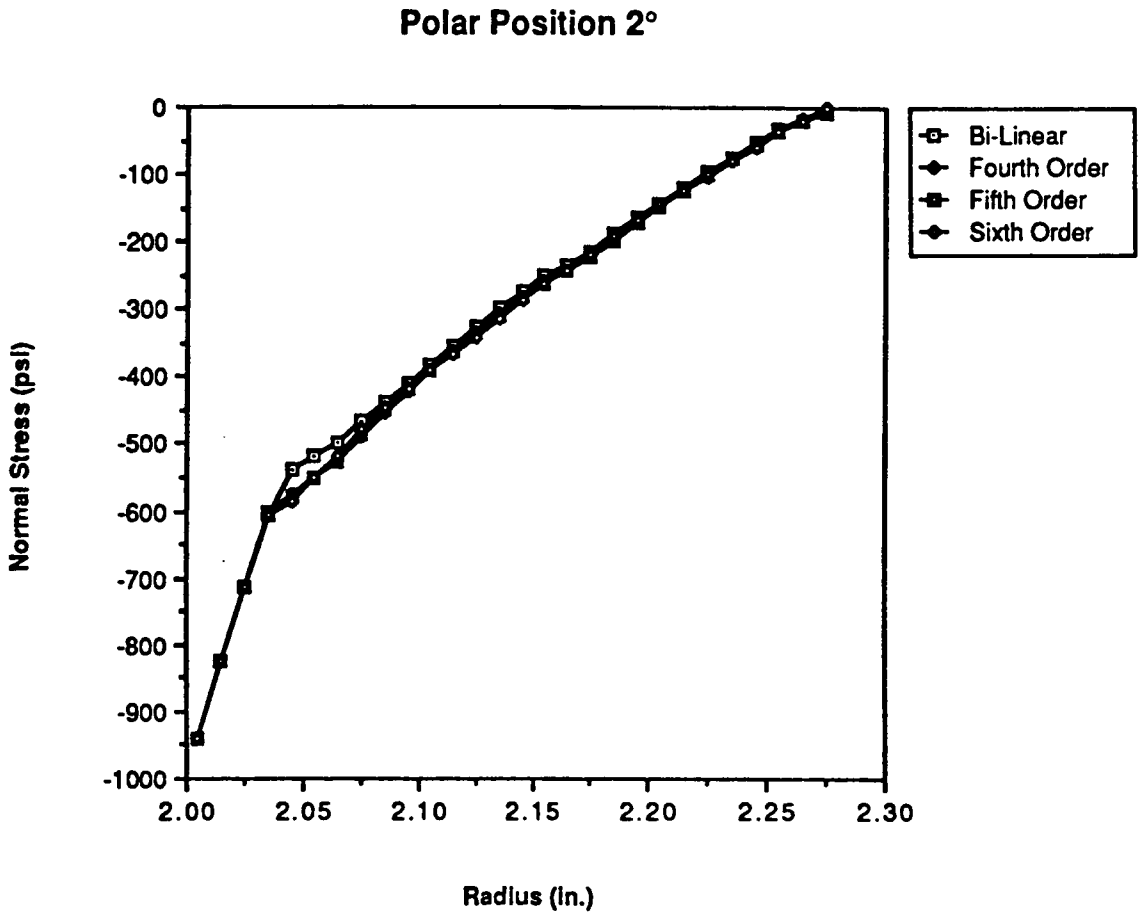

Figure 63. Comparison of Radial Stress Profiles at 2°

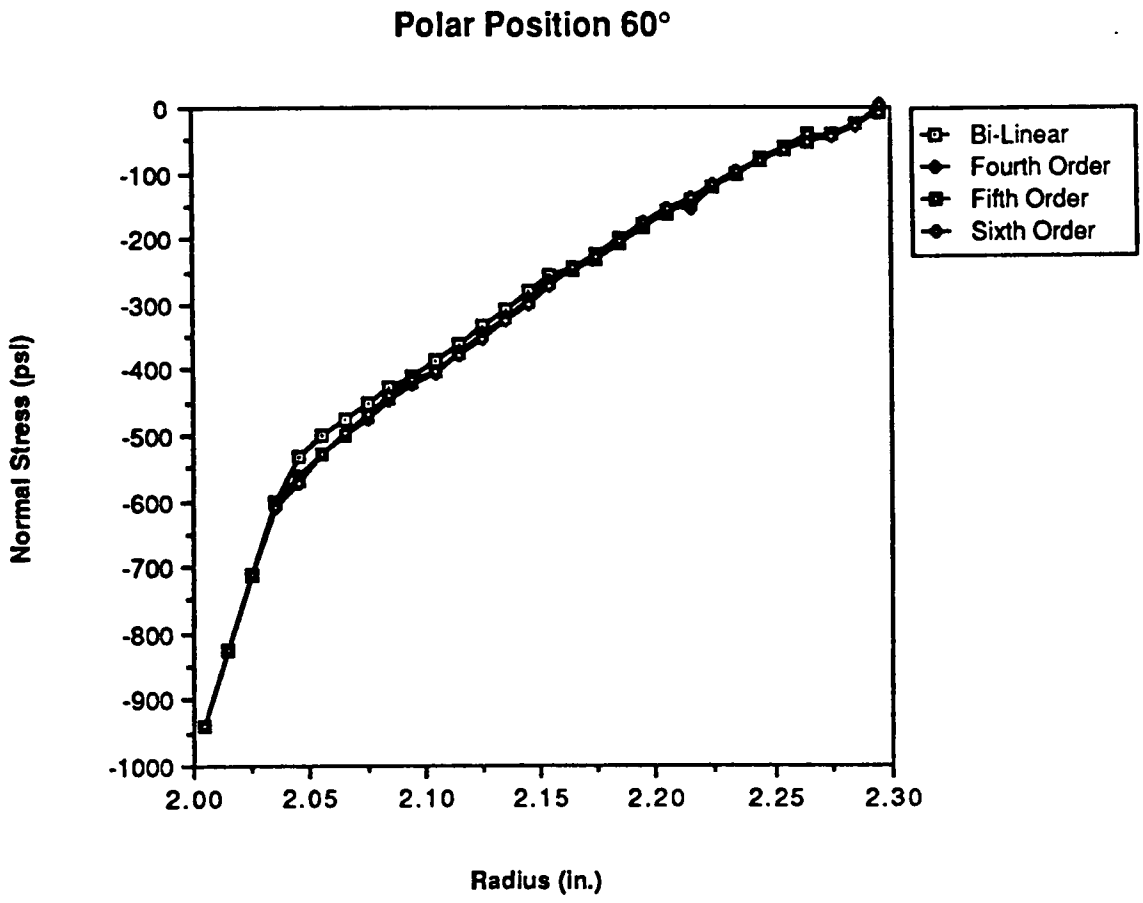

Figure 64. Comparison of Radial Stress Profiles at 60°

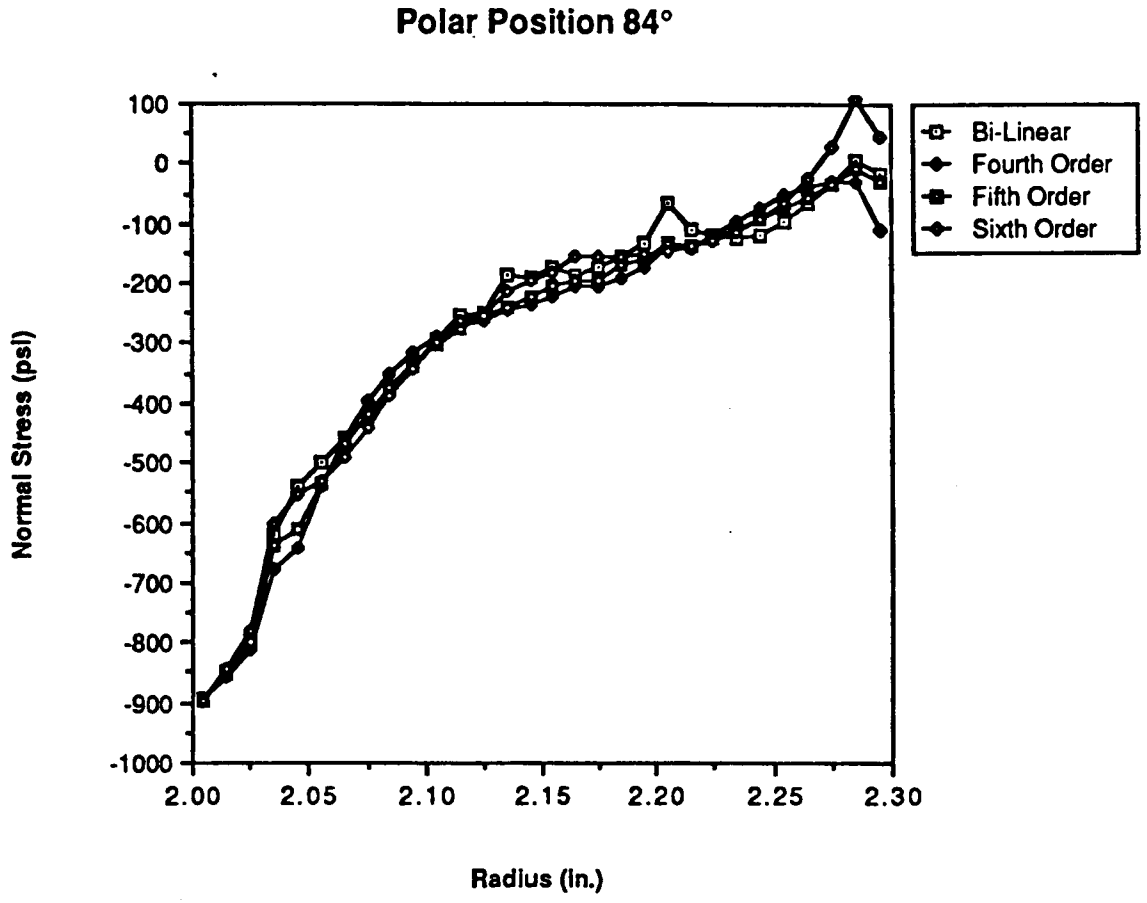

Figure 65. Comparison of Radial Stress Profiles at 84°

One of the most important values in the design of composite structures is the value of the principal fiber stress. Many failure criteria are based on these values. Therefore one of the important capabilities of the finite element program is to output not only the stresses in the global coordinate system, but also in the principal fiber coordinate system. To aid the designer of a filament-wound spherical pressure vessel, post-processing could include information in the form shown in Fig. 66 in which the principal fiber stress (1-direction) for the first layer of fibers on the mandrel is plotted. Figure 66 contains results from the bi-linear model and a sixth-order element model. At the equator, each of the twenty four layers are represented by a single element or intra-element layer depending on the model. However, near the pole, some of the fiber layers become very thick and others are not present at all. Therefore, the state-of-stress can vary significantly throughout the layer at various polar angles. The limits of the stress variation can be easily seen in a figure like Fig. 66, where the maximum and minimum values of the principal stress are plotted. At the fill tube, the first layer is approximately 0.686 mm (0.027 in.) thick which then increases to about 2.06 mm (0.081 in.) at 6° and then decreases gradually to a single band thickness at the equator. Therefore, the value of the principal fiber stress has a large variation at polar positions near the fill tube where the layer is thick. One of the objectives of the designer is to create a vessel in which the variation of the fiber stress from layer-to-layer and within a layer is minimal.

Lastly, the computational efficiency of the high-order elements is presented. Accounting of the number of nodes, elements, and mean bandwidth for the actual test cases that were run is given in Table 11. The actual computation time for high-order elements of order three through ten showing the 'break-even point' with respect to the bi-linear model is shown to be a ninth-order element in Fig. 67. The stress results presented above indicate that depending on the desired accuracy, fourth- through sixth-order elements will generally be acceptable with computational savings ranging from 50 percent to 26 percent when compared to the bi-linear solution.

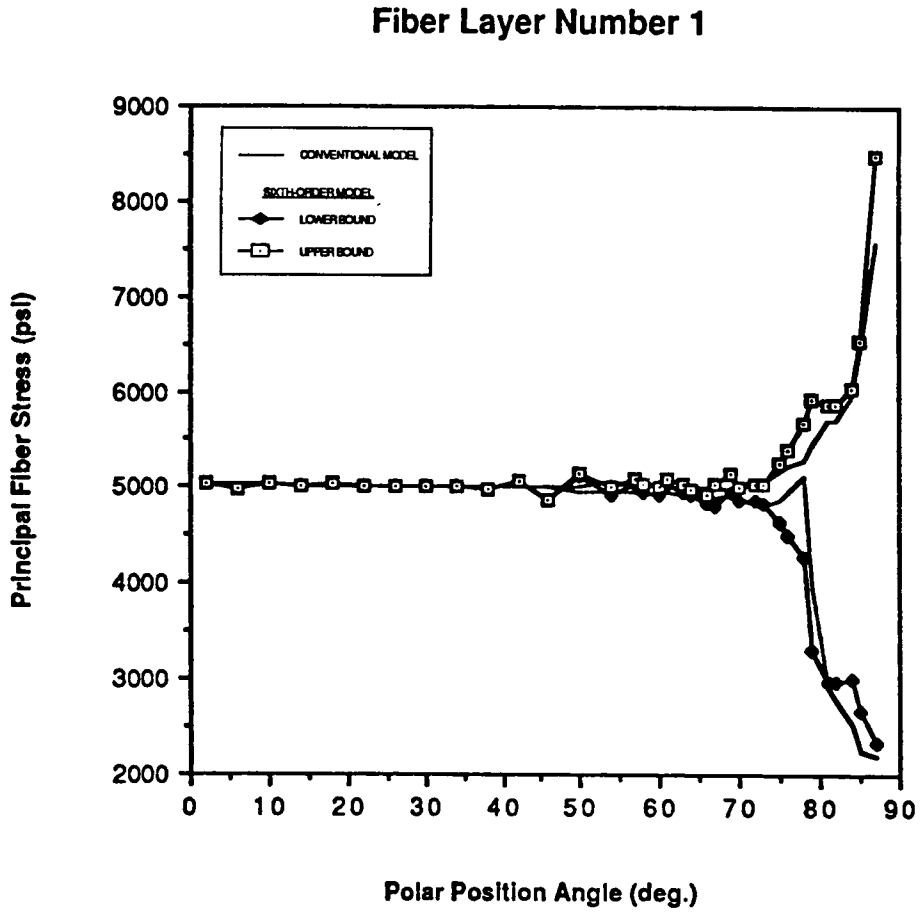

Figure 66. Principal Fiber Stress for the First Fiber Layer as a Function of Polar Position

Table 11. Element and Node Accounting for Conventional and High-Order Elements to Model a Filament-Wound Spherical Vessel

Element Type	Number of Nodes	Number of Elements	Mean Bandwidth
Bi-Linear	1184	1170	58
Third-Order	428	252(Bi-Linear)+35(High-Order)	31
Fourth Order	464	252+35	32
Fifth-Order	500	252+35	33
Sixth-Order	536	252+35	35
Seventh-Order	572	252+35	36
Eighth-Order	608	252+35	38
Ninth-Order	644	252+35	40
Tenth-Order	680	252+35	42

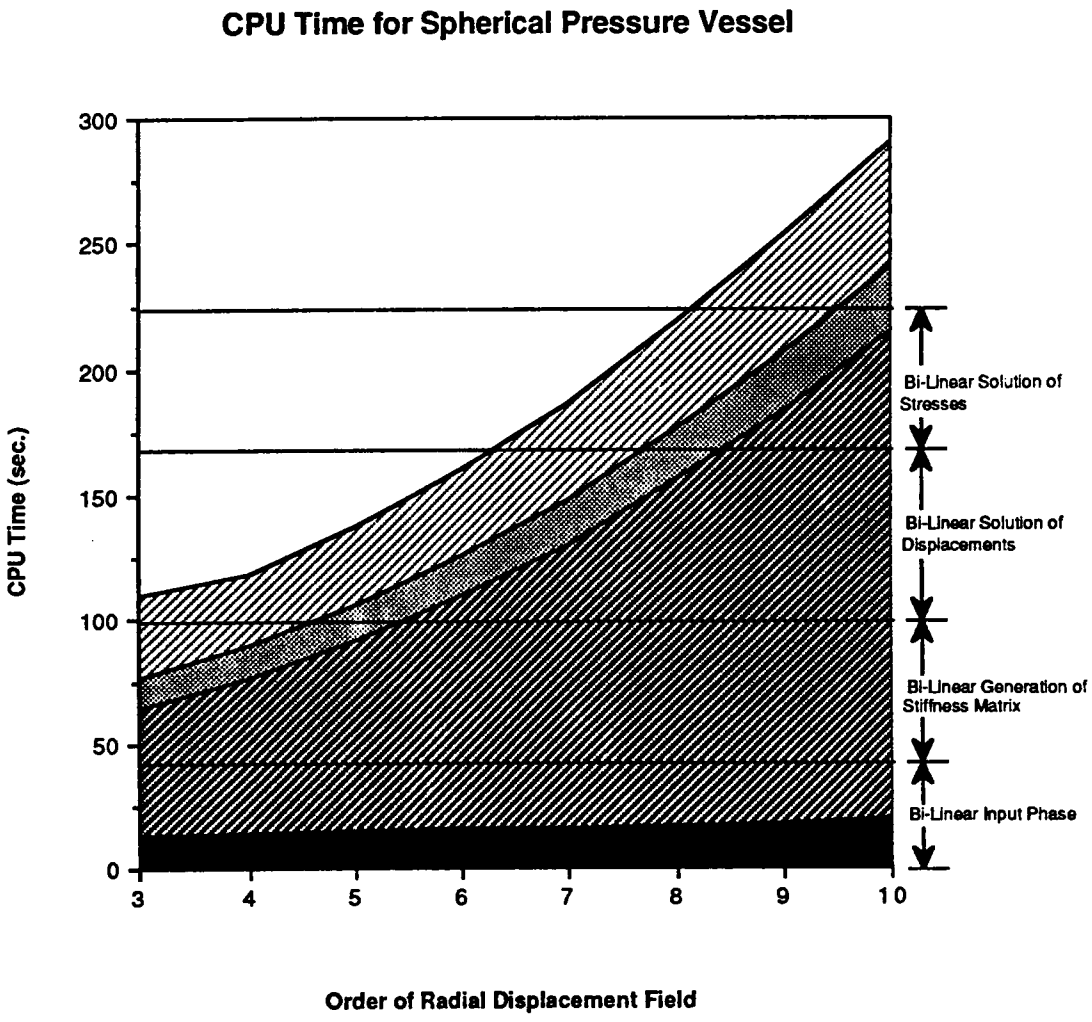

Figure 67. Actual CPU Times for Third- through Tenth-Order Element Models of the Test Model

7.0 Conclusions and Recommendations

7.1 Conclusions

A high-order composite finite element has been developed that can accurately model and simulate the response of thick-wall composite pressure vessels and other axisymmetric structures. Isotropic materials appear to be accurately modeled by a third-order element whereas higher-order elements are necessary for models which have substantial material property variations between adjacent layers. The results seem to indicate that higher order elements are necessary primarily to better fit discontinuous radial strain profiles that are generally caused by discontinuities in the material properties. The magnitudes of the discontinuities are also related to the variation in fiber orientations from layer to layer.

One of the problems that has emerged from the studies presented is how to determine what order element is necessary to accurately model a given system. For the present time it appears that, as is the case with most applications in finite element analysis, practice, experience, engineering intuition and some knowledge of the problem will have to guide the user. However, there do appear to be some indications from observation of the data that has been presented that:

1. For a single-layer isotropic cylinder, a third-order displacement field element models the elastic behavior very well, with an accuracy of approximately ± 0.5 percent.

2. For a single-layer orthotropic cylinder, a third-order element will also predict the displacements, strains, and stresses with an accuracy of approximately ± 1.0 percent.

3. For filament-wound composite cylinders in which the angle of the principal fiber axis varied by 9° from layer to layer, a fourth-order element was needed to sufficiently model the system. In this case, the percent error for the calculated stresses with respect to theoretical elasticity solutions was generally about ± 3 percent. Using higher-order elements, up to a sixth-order, did not reduce the maximum error significantly.

4. For filament-wound composite cylinders in which the angle of the principal axis varied by 18° from layer to layer, a fifth-order element was necessary. A considerable decrease in the error for the fourth- and fifth-order elements as compared to the third-order element was detected. The sixth-order element was slightly more accurate than the fifth-order element but probably not enough to warrant the additional cost of computation time for most applications.

5. Based on these results, it is expected that fourth-order elements will in general model the behavior of the structure with adequate accuracy if the variation of fiber direction is relatively small from layer to layer and if an adequate number of integration points are used.

6. fourth-order elements appear to adequately model the 24 filament layers of the wound composite structure presented.

Unfortunately, it seems unlikely that any 'hard-and-fast' rules for selecting the order of the assumed displacement field will be possible, just as no such rules exist for determining the number of nodes and elements needed to model any system.

The primary motivation for the formulation and implementation of the high-order element was the potential for decreasing the computational time of an analysis. The decrease in computa-

tion time was confirmed with the studies and results presented. Based upon the results presented, the most appropriate modeling strategy to reduce the computation time as much as possible is to use as few integration points as necessary (i.e., one per layer) and then increase the order of the assumed displacement field to verify that 'convergence' has been achieved. Increasing the order of the element is much more economical than increasing the number of integration points. Computational efficiencies of 54 percent were shown without affecting the accuracy of the solution significantly with the use of fourth-order elements. The CPU time savings reduced to 26 percent when using sixth order elements to model the wound composite.

The design of filament-wound spherical pressure vessels often requires the use of materially nonlinear analysis to model the behavior of the metal mandrel as it tends to yield under normal operating conditions which influences the state-of-stress in the filament-wound composite. Using the high-order elements will greatly reduce the computation time when an iterative solution technique is employed, particularly if an incremental approach is used. The results have indicated that the high-order element reduces the solution time to the system equations a great deal but the CPU time for the generation of the structure stiffness matrix is often very large. If a scheme is used in which only the stiffness of the materially-nonlinear elements had to be re-evaluated, the solution of the system equations would become more significant to the overall solution time and the high-order elements would become much more efficient.

Lastly, a design program for filament-wound spherical pressure vessels has been developed which includes the high-order composite element. The design code was built with a philosophy of utilizing a pre-existing mesh generator for conventional bi-linear elements and generating the data necessary for either a bi-linear element model or a high-order model. The mesh generator can also accept data from input files created with the pre-existing mesh generator for four-noded quadrilateral models.

7.2 Recommendations

There are two areas in which future work could be very productive. One proposed area of extended research is concerned with increasing the accuracy of the element formulation which also may have a slight affect on the economy of the element. The second area is concerned solely with the computational efficiency of generating the element stiffness matrices.

The present element uses a zeroth-order numerical integration to evaluate the stiffness of a higher order element. A certain amount of the overall error is created by the numerical integration procedure alone. Early in this research program, discussions focused on how the numerical integration should be evaluated. At that time, a decision was made to sacrifice some amount of accuracy (at that time an unknown amount) in order to create what was thought to be the most economical element possible. However, after generating and evaluating the results that have been presented, it appears that the accuracy may be greatly increased if the integration is carried out on a layer-by-layer basis with a user-selected order of integration. By using a method similar to Reddy's refined high-order shear deformation theory [39-40], Murakami's zig-zag theory [38], and Natarajan's integration method [24], the user could select the order of the assumed displacement field for the entire element and the order of the numerical integration accuracy (number of integration points per layer). The Gauss quadrature method could be used for each layer and the layers' influence summed together to determine the overall stiffness of the element if this theory was implemented. As an example, a third-order element that contains two integration points per layer could integrate the stiffness expressions exactly with Gauss quadrature. In the current formulation, the zeroth-order integration will only be exact for linear functions of displacement. Increasing the order of the element hopefully creates a better approximation of the displacement field. However, if the number of integration points used to integrate the higher-order displacement field is constant, then the potential error in the zeroth-order numerical integration also increases. Nevertheless, the increased error in the numerical integration is generally going to be much less than the increase in accuracy associated with a better approximation to the displacement form. The hypothesis is, by

using a more accurate integration scheme, the error will be reduced and convergence established for as low or lower order element as with the current method and may, therefore, actually decrease the computational time for a given accuracy level.

The results of the computational studies indicated that the evaluation of the element stiffness matrices is the most intensive computation phase of the finite element analysis. Gupta and Mohraz [60] presented a method of formulating and computing numerically integrated stiffness matrices by using the indicial notation and operations of evaluating the integral of $[B][D][B]^T$. Their formulation resulted in a 80 percent reduction in the computational effort for homogeneous elements. The reduction in the computational time for elements in which the material properties are functions of position coordinates is not nearly as significant as for isotropic materials, but is still 40 percent.

References

1. Smith,C. B., "Some New Types of Orthotropic Plates Laminated of Orthotropic Materials," *J. App. Mech.,* Vol. 20, pp. 286-288, June 1953.

2. Lekhnitskii, S. G., *Anisotropic Plates,* Gordon and Breach Science Publishers, New York, 1968.

3. Reissner, E., Stavsky, Y., "Bending and Stretching of Certain Types of Heterogeneous Aeolotropic Elastic Plates," *J. Appl. Mech.,* Vol. 28, pp. 402-408, Sept. 1961.

4. Ashton, J. E., and Whitney, J. M., *Theory of Laminated Plates,* Technomic Publishing Company Inc., Stamford, Conn., 1970.

5. Jones, R. M., *Mechanics of Composite Materials,* Harper & Row, New York, 1975.

6. Pipes, R. B., and Pagano, N. J., "Interlaminar Stresses in Composite Laminates Under Uniform Axial Extension," *J. Comp. Mat.,* Vol. 4, pp. 538-548, Oct. 1970.

7. Pipes, R. B., and Pagano, N. J., "Interlaminar Stresses in Composite Laminates - An Approximate Elasticity Solution," *J. App. Mech.,* Vol. 41, pp. 668-672, Sept. 1974.

8. Isakson, G., and Levy, A., "Finite Element Analysis of Interlaminar Shear in Fibrous Composites," *J. Comp. Mat.,* pp. 273-276, April 1971.

9. Puppo, A. H., and Evensen, H. A., "Strength of Anisotropic Materials Under Combined Stresses," *AIAA/ASME 12th SDM Conf.,* Anaheim, CA., AIAA Paper No. 71-368, April 19-21, 1971.

10. Levy, A., Armen, H., and Whiteside, J., "Elastic and Plastic Interlaminar Shear Deformation in Laminated Composites Under Generalized Plane Stress," *3rd Conf. Wright-Patterson,* Oct. 19-21, 1971, Grumman Research Dept., Memorandum RM-535J, Feb. 1972.

11. Herakovich, C. T., and Brooks, E. W., Jr., "Tensile Strength Behavior of Composite Reinforced Metals," VPI-E-73-5, Virginia Polytechnic Institute and State University, Blacksburg, VA, Jan. 1973.

12. Herakovich, C. T., "On Thermal Edge Effects in Composite Laminates," *Int. J. Mech. Sci.,* Vol. 18, pp. 129-134, 1976.

13. Lin, F. T., *The Finite Element Analysis of Laminated Composites,* Ph.D. Dissertation, Engineering Science & Mechanics Dept., Virginia Polytechnic Institute and State University, Blacksburg, VA, 1972

14. Dana, J. R., *Three Dimensional Finite Element Analysis of Thick Laminated Composites - Including Interlaminar and Boundary Effects Near Circular Holes,* Ph.D. Dissertation, Engineering Science & Mechanics Dept., Virginia Polytechnic Institute and State University, Blacksburg, VA, 1974

15. Dana, J. R., and Barker, R. M., "Three-Dimensional Finite-Element Computer Program - User's Guide," VPI-E-74-19, Engineering Science & Mechanics Dept., Virginia Polytechnic Institute and State University, Blacksburg, VA, Aug. 1974.

16. Rybicki, E. F., and Schmit, Jr., L. A., "An Incremental Complementary Energy Method of Nonlinear Stress Analysis," *AIAA J.,* Vol. 8, pp. 1805-1812, Oct. 1970.

17. Rybicki, E. F., "Approximate Three-Dimensional Solutions for Symmetric Laminates Under Inplane Loading," *J. Composite Materials,* Vol. 5, pp. 354-360, July 1971.

18. Rybicki, E. F., and Kanninen, M. F., "A Finite Element Calculation of Stress Intensity Factors by a Modified Crack Closure Integral," *Engr. Fract. Mech.,* Vol. 9, 1977, pp. 931-938, 1977.

19. Rybicki, E. F., Schmueser, D. W., and Fox, J., "An Energy Release Rate Approach for Stable Crack Growth in the Free-Edge Delamination," *J. Composite Materials,* Vol. 11, pp.470-487, Oct. 1977.

20. Rybicki, E. F., and Schmueser, D. W., "Three-Dimesional Finite Element Stress Analysis of Laminated Plates Containing a Circular Hole," AFML-TR-76-92, August 1976.

21. Stanton, E. L., Crain, L. M., and Neu, T. F., "A Parametric Cubic Modelling System for General Solids of Composite Material," *Int. J. Num. Meth. Eng.,* Vol. 11, pp. 653-670, 1977.

22. Wang, S. S., Mandell, J. F., and McGarry, F. J., "Three-Dimensional Solution for a Through-Thickness Crack with Crack Tip Damage in a Cross-Plied Laminate," *Fracture Mechanics of Composites,* ASTM STP 593, pp. 61-85, 1975.

23. Pian, T. H. H., and Tong, P., "Finite Element Methods in Continuum Mechanics," *Advances in Applied Mechanics,* Vol. 12, Academic Press, N. Y., 1972.

24. Natarajan, R., "Development of a Finite Element to Analyse Anisotropic Multi-Layered Thick Shells," *ASME Int. Computers in Engr. Conf.,* Vol. 2, 1985.

25. Portnov, G. G., and Spridzans, Y. B., "Winding Glass-Reinforced Plastic RingsUnder Programmed Tension," *Polym. Mech.,* Vol. 2, pp. 361-364, March-April, 1971.

26. Dobie, M. J., Leavesley, P. J., and Knight, C. E., Jr., "Residual Strain and Strength Loss in Filament Wound Rings," Union Carbide Research Contract Y01 Report, August, 1982.

27. Leavesley, P. J., *An Analytical Model of Strength Loss in Filament Wound Spherical Vessels,* Ph.D. Dissertation, Department of Mechanical Engineering, Virginia Polytechnic Institute and State University, Blacksburg, VA, Oct. 1983.

28. Reissner, E., "On the Theory of Bending of Elastic Plates," *J. Math. Phy.,* Vol. 23, pp. 184-191, 1944.

29. Reissner, E., "The Effect of Transverse Shear Deformation on the Bending of Elastic Plates," *J. Appl. Mech.,* Vol. 12 (1), pp. 69-77, 1945.

30. Reissner E., "On Bending of Elastic Plates," *Q. Appl. Math.,* Vol. 5, pp. 55-68, 1947.

31. Basset, A. B., "On the Extension and Flexure of Cylindrical and Spherical Thin Elastic Shells," *Phil. Trans. Royal Soc.,* (London), Ser. A, Vol. 181 (6), pp. 433-480, 1890.

32. Hildebrand, F. B., Reissner, E. and Thomas, G. B., "Note on the Foundations of the Theory of Small Displacements of Orthotropic Shells," NACA Technical Note No. 1833, March 1949.

33. Mindlin, R. D., "Influence of Rotary Inertia and Shear on Flexural Motions of Isotropic, Elastic Plates," *J. Appl. Mech.* Vol. 18, pp. 31-38, 1951.

34. Gol'denveizer, A. L., "O Terii zgiba Plastinok Reissnera (On Reissner's Theory of the Bending of Plates)," *Izvestiya AN SSSR, OTN,* No. 4, pp. 102-109, 1958 (translation of the paper is available as NASA Technical Translation F-27, May 1960).

35. Librescu, L. "On the Thermoelastic Problem of Shells Treated by Eliminating the Love-Kirchhoff Hypothesis," *Non-Classical Shell-Problems,* North-Holland Publ. Co., Amsterdam, P. W. N., Warsaw, 1964.

36. Librescu, L., "The Thermoelastic Problem of Shells and Plates Approached by Eliminating the Love-Kirchhoff hypothesis," *St. Cer. Mech. Apl.,* Vol. 21, pp. 351-365, 1966.

37. Levinson, M., "A New Rectangular Beam Theory," *J. Sound and Vibration,* Vol. 75, pp. 81-87, 1981.

38. Murthy, M. V. V., "An Improved Transverse Shear Deformation Theory for Laminated Anisotropic Plates," NASA TP-1903, Nov. 1981.

39. Reddy, J. N., "A Refined Nonlinear Theory of Plates with Transverse Shear Deformation," *Int. J. Solids Struct.,* Vol. 20, No. 9/10, pp. 881-896, 1984.

40. Reddy, J. N., "A Simple Higher-Order Theory for Laminated Composite Plates," *J. Appl. Mech,* Vol. 51, pp. 745-752, 1984.

41. Reddy, J. N., "A Generalization of Two-Dimesional Theories of Laminated Composite Plates," *Comm. Appl. Numer. Meth.,* Vol. 3, pp. 173-180, 1987.

42. Librescu, L., and Schmidt, R., "Higher-Order Moderate Rotation Theories for Elastic Anisotropic Plates," *Proc. Euromech-Colloquium 197, Finite Rotations in Structural Mechanics,* Jablona, 1985, Ed. W. PietraszKiewicz, Springer-Verlag, Berlin, 1986.

43. Murakami, H., "Laminated Composite Plate Theory with Improved In-Plane Responses," *Proc. 1985 Pressure Vessels and Piping Conf., Pressure Vessel Components and Design,* PVP-Vol. 98-2, ASME, 1985.

44. Toledano, A., and Murakami, H., "A High-Order Laminated Plate Theory with Improved In-Plane Responses," *Int. J. Solids Struct.*, Vol. 23, No. 1, pp. 111-131, 1987.

45. Pagno, N. J., "Exact Solutions for Composite Laminates in Cylindrical Bending," *J. Composite Materials,* Vol 3, p.398, 1969.

46. Rogers, C. A., Knight, C. E., Jr., and Dodge, W. G., "Development of High-Order Finite Elements to Model Filament Wound Composites," *Proc. 1985 Pressure Vessels and Piping Conf., Pressure Vessel Components and Design,* PVP-Vol. 98-2, ASME, 1985.

47. Babuska, I., Szabo, B. A., and Katz, I. N., "The *p*-version of the Finite Element Method," *SIAM J. Numer. Anal,* Vol. 18, pp. 515-545, 1981.

48. Babuska, I., and Dorr, M. R., "Error Estimates for the Combined *h* and *p* Versions of the Finite Element Method," *Numer. Math,* Vol. 37, pp. 252-277, 1981.

49. Dorr, M. R., "The Approximation Theory for the *p*-Version of the Finite Element Method," *SIAM J. Numer. Anal.,* Vol. 21, pp. 1180-1207, 1984.

50. Babuska, I., Gui, W., Guo, B., and Szabo, B., "Theory and Performance of the *h-p* Versions of the Finite Element Method," *SIAM J. Numer. Anal.,* 1986.

51. Babuska, I., and Aziz, A. K., "Survey Lectures on the Mathematical Foundations of the Finite Element Method," *The Mathematical Foundations of the Finite Element Method with Applications to Partial Differential Equations,* Aziz, A. K. (Ed.), Academic Press, New York, pp. 3-359, 1972.

52. Babuska, I., Zienkiewicz, O. C., Gago, J., and de A. Oliveira, E. R., (Editors), *Accuracy Estimates and Adaptive Refinements in Finite Element Computations,* John Wiley & Sons Ltd., New York, 1986.

53. Cook, R. D., *Concepts and Applications of Finite Element Analysis, 2nd Ed.,* John Wiley & Sons, Inc., New York, 1981.

54. Bathe, K., Wilson, E. L., *Numerical Methods in Finite Element Analysis,* Prentice-Hall, Inc., Englewood Cliffs, NJ, 1976.

55. Bathe, K., *Finite Element Procedures in Engineering Analysis,* Prentice-Hall, Inc., Englewood Cliffs, NJ, 1982.

56. Reddy, J. N., *An Introduction to the Finite Element Method,* McGraw-Hill, Inc., New York, 1984.

57. Rao, S. S., *The Finite Element Method in Engineering,* Pergamon Press, Inc., New York, 1982.

58. Carnahan, B., Luther, H. A., and Wilkes, J. O., *Applied Numerical Methods,* John Wiley & Sons, Inc., New York, 1969.

59. Rogers, C. A., and Knight, C. E., "User's Guide for Filament Wound Spherical Pressure Vessel Design Code," Mechanical Engineering Department, Virginia Polytechnic Institute and State University, Blacksburg, VA, Sept. 1987.

60. Gupta, A. K., and Mohraz, B., "A Method of Computing Numerically Integrated Stiffness Matrices," *Int. J. Num. Meth. Eng.,* Vol. 5, pp. 83-89, 1972.

Appendix A. Elasticity Solution for Multi-Layer Thick Wall Cylinders

A.1.1 Isotropic Material - Plane Stress

A thick wall cylinder subjected to external and/or internal pressure, has both radial and tangential (hoop) stresses that are dependent upon radial position. A thick wall cylinder may also be stressed longitudinally, such as in pipes. However, in determining the radial and tangential stresses using a plane stress formulation for the continuum, the assumption is made that the longitudinal stress is zero throughout the cylinder wall.

The derivation of the following plane-stress equations may be found in numerous engineering texts.

Radial Stress:

$$\sigma_r = \frac{a^2 p_i - b^2 p_o}{(b^2 - a^2)} - \frac{(p_i - p_o)a^2 b^2}{r^2(b^2 - a^2)} \qquad [A.1]$$

Tangential (Hoop) Stress:

$$\sigma_t = \frac{a^2 p_i - b^2 p_o}{(b^2 - a^2)} + \frac{(p_i - p_o)a^2 b^2}{r^2(b^2 - a^2)} \qquad [A.2]$$

Radial Displacement:

$$u = \frac{(1 + \nu)(1 - 2\nu)}{E}\left[\frac{a^2 p_i - b^2 p_o}{b^2 - a^2}\right] r + \frac{(1 + \nu)}{E}\left[\frac{a^2 b^2 (p_i - p_o)}{b^2 - a^2}\right]\frac{1}{r} \qquad [A.3]$$

in which a = the inside radius of the cylinder

b = the outside radius of the cylinder

p_i = the inside pressure

p_o = the outside pressure

r = the radius to any point between a and b

E = Young's Modulus of elasticity

ν = Poisson' ratio

In order to analyze multi-layer cylinders of varying isotropic materials, a set of equations must be solved which match the interface displacements and interface pressures. As an example, consider the cylindrical pressure vessel shown in Fig. 68., where q_i represents interface pressures. For layer 1, the stress and displacement equations can be easily written from those derived above.

Radial Stress:

$$\sigma_r = \frac{a^2 p - a_1^2 q_1}{(a_1^2 - a^2)} - \frac{(p - q_1)a^2 a_1^2}{r^2(a_1^2 - a^2)} \qquad [A.4]$$

Tangential Stress:

$$\sigma_t = \frac{a^2 p - a_1^2 q_1}{(a_1^2 - a^2)} + \frac{(p - q_1)a^2 a_1^2}{r^2(a_1^2 - a^2)} \qquad [A.5]$$

Radial Displacement:

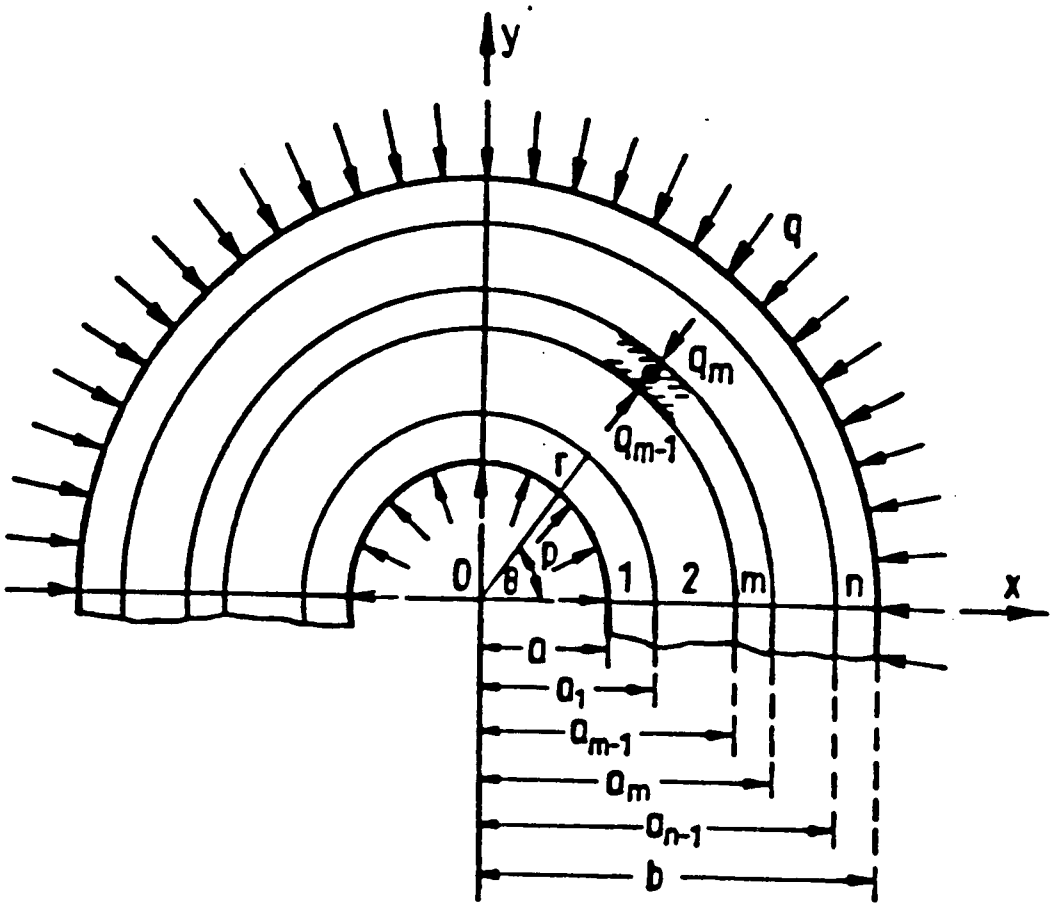

Figure 68. Multi-Layered Thick Wall Cylinder

$$u = \frac{(1+\nu)(1-2\nu)}{E}\left[\frac{a^2p - a_1^2q_1}{(a_1^2 - a^2)}\right]r + \frac{(1+\nu)}{E}\left[\frac{a^2b^2(p-q_1)}{(a_1^2-a^2)}\right]\frac{1}{r} \qquad [A.6]$$

However, in eqs. A.4, A.5, and A.6, the interface pressure q_1 is unknown. In order to solve the stress and displacement equations the interface pressures must first be solved. The procedure is to set up the displacement equations for each layer at both interfaces. This set of equations is then solved in order to find the unknown interface pressures, $q_1, q_2, q_3, ..., q_{n-1}$. At each interface, the sum of the absolute displacement values must equal zero. Equating the expressions for the displacements at an interface of the two layers and collecting the coefficients of the interface pressures result in a system of linear equations. These equations may be solved for the interface pressures. Once the interface pressures have been calculated, the radial and tangential stresses may be calculated by the following expressions.

Radial Stress:

$$\sigma_r^{(m)} = \frac{a_{m-1}^2 q_{m-1} - a_m^2 q_m}{(a_m^2 - a_{m-1}^2)} - \frac{(q_{m-1} - q_m)a_{m-1}^2 a_m^2}{r^2(a_m^2 - a_{m-1}^2)} \qquad [A.7]$$

Tangential (Hoop) Stress:

$$\sigma_t^{(m)} = \frac{a_{m-1}^2 q_{m-1} - a_m^2 q_m}{(a_m^2 - a_{m-1}^2)} + \frac{(q_{m-1} - q_m)a_{m-1}^2 a_m^2}{r^2(a_m^2 - a_{m-1}^2)} \qquad [A.8]$$

Radial Displacement:

$$u^{(m)} = \frac{(1+\nu^{(m)})(1-2\nu^{(m)})}{E^{(m)}}\left[\frac{a_{m-1}^2 p_{m-1} - a_m^2 p_m}{a_m^2 - a_{m-1}^2}\right]r + \frac{+(1+\nu^{(m)})}{E^{(m)}}\left[\frac{(p_{m-1} - p_m)a_{m-1}^2 a_m^2}{(a_m^2 - a_{m-1}^2)}\right]\frac{1}{r} \qquad [A.9]$$

A.1.2 Orthotropic Material - Plane Stress

For an orthotropic body with cylindrical anisotropy the stress strain relations may be written as

$$\begin{aligned}
\varepsilon_r &= \frac{1}{E_r}\sigma_r - \frac{\nu_{\theta r}}{E_\theta}\sigma_\theta - \frac{\nu_{zr}}{E_z}\sigma_z \quad , \quad \gamma_{\theta z} = \frac{1}{G_{\theta z}}\tau_{\theta z} \\
\varepsilon_\theta &= -\frac{\nu_{r\theta}}{E_r}\sigma_r + \frac{1}{E_\theta}\sigma_\theta - \frac{\nu_{z\theta}}{E_z}\sigma z \quad , \quad \gamma_{rz} = \frac{1}{G_{rz}}\tau_{rz} \\
\varepsilon_z &= -\frac{\nu_{rz}}{E_r}\sigma r - \frac{\nu_{(\theta z)}}{E_\theta}\sigma_\theta + \frac{1}{E_z}\sigma_z \quad , \quad \gamma_{r\theta} = \frac{1}{G_{r\theta}}\tau_{r\theta}
\end{aligned} \qquad [A.10]$$

A plane stress assumption would of course mean that σ_z would be equal to zero as well as $\tau_{\theta z}$ and τ_{rz}. Where the constants in Eq. A.10, E_r, E_θ, E_z are the Young's moduli in the r, θ, z directions (radial, tangential, and axial directions respectively) which are also the principal directions of elasticity. The Poisson's ratio, $\nu_{r\theta}$, defines the compression strain in the θ-direction when the tension strain is applied in the r-direction.

Lekhnitskii [2] solved the elasticity problem of "Stress Distribution in a Composite Curvilinear Anisotropic Ring". Using Lekhnitskii's stress functional approach, the solution for a single layer orthotropic pressure vessel may be found. Please note that there are several typographical errors in reference [2] that have been corrected before being included in this discussion. The stress and displacement equations are:

Radial Stress:

$$\sigma_r = \frac{pc^{k+1} - q}{1 - c^{2k}}\left(\frac{r}{b}\right)^{k-1} - \frac{p - qc^{k-1}}{1 - c^{2k}}c^{k+1}\left(\frac{b}{r}\right)^{k+1} \qquad [A.11]$$

Tangential Stress:

$$\sigma_\theta = \frac{pc^{k+1} - q}{1 - c^{2k}}k\left(\frac{r}{b}\right)^{k-1} + \frac{p - qc^{k-1}}{1 - c^{2k}}kc^{k+1}\left(\frac{b}{r}\right)^{k+1} \qquad [A.12]$$

Radial Displacement:

$$u_r = \frac{b}{E_\theta(1-c^{2k})}\left[(pc^{k+1}-1)(k-\nu_\theta)\left(\frac{r}{b}\right)^k + (p-qc^{k-1})c^{k+1}(k+\nu_\theta)\left(\frac{b}{r}\right)^k\right] \qquad [A.13]$$

Using Eqs. A.11, A.12, and A.13, the solution of the multi-layer orthotropic cylinder is very much like the isotropic problem outlined in the previous section. In this problem, it is assumed that each layer is orthotropic, the anisotropy poles of all the layers are located at the center and all layers are rigidly connected, i.e., bonded along the layer interfaces. The following notation will be used: n is the number of layers; a and b are the internal and external radii of the composite ring as in the previous section; p and q are the internal and external pressures per unit area; a_{m-1}, a_m are the internal and external radii of layer m; $\sigma_r^{(m)}$, $\sigma_\theta^{(m)}$, $\tau_{r\theta}^{(m)}$, $u_r^{(m)}$, and $u_\theta^{(m)}$ are stress and displacement components; and $E_r^{(m)}$, $E_\theta^{(m)}$, $\nu_\theta^{(m)}$ are the elastic moduli in the principal material directions, r and θ. Also,

$$c_m = \frac{a_{m-1}}{a_m} \quad , \quad k_m = \sqrt{\frac{E_\theta^{(m)}}{E_r^{(m)}}} \qquad [A.14]$$

Therefore, the expressions for stress and displacement at any point , r , in the multi-layer cylinder becomes:

Radial Stress:

$$\sigma_r^{(m)} = \frac{q_{m-1}c_m^{k_m+1}}{1-c_m^{2k_m}}\left[\left(\frac{r}{a_m}\right)^{k_m-1} - \left(\frac{a_m}{r}\right)^{k_m+1}\right] + \frac{q_m}{1-c_m^{2k_m}}\left[-\left(\frac{r}{a_m}\right)^{k_m-1} + c_m^{2k_m}\left(\frac{a_m}{r}\right)^{k_m+1}\right] \qquad [A.15]$$

Tangential (Hoop Stress):

$$\sigma_\theta^{(m)} = \frac{q_{m-1}c_m^{k_m+1}}{1-c_m^{2k_m}}\left[\left(\frac{r}{a_m}\right)^{k_m-1} + \left(\frac{a_m}{r}\right)^{k_m+1}\right] - \frac{q_m k_m}{1-c_m^{2k_m}}\left[-\left(\frac{r}{a_m}\right)^{k_m-1} + c_m^{2k_m}\left(\frac{a_m}{r}\right)^{k_m+1}\right] \qquad [A.16]$$

Radial Displacement:

$$u_r^{(m)} = \frac{q_{m-1}a_m c_m^{k_m+1}}{E_\theta^{(m)}\left(1-c_m^{2k_m}\right)}\left[\left(k_m - \nu_\theta^{(m)}\right)\left(\frac{r}{a_m}\right)^{k_m} + \left(k_m + \nu_\theta^{(m)}\right)\left(\frac{a_m}{r}\right)^{k_m}\right]$$
$$- \frac{q_m a_m}{E_\theta^{(m)}\left(1-c_m^{2k_m}\right)} \times \left[\left(k_m - \nu_\theta^{(m)}\right)\left(\frac{r}{a_m}\right)^{k_m} + \left(k_m + \nu_\theta^{(m)}\right)c_m^{2k_m}\left(\frac{a_m}{r}\right)^{k_m}\right] \qquad [A.17]$$
$$(m = 1,2,\ldots,n; \quad q_o = p, q_n = q)$$

The set of equations used to determine the interface pressures, assuming no interference fits between layers are

$$q_{m+1}a_{m+1}\alpha_{m+1} + q_m a_{m+1} + q_{m-1}a_{m-1}\alpha_m = 0 \qquad [A.18]$$

where

$$\alpha_m = \frac{2k_m}{E_\theta^m}\ \frac{c_m^{k_m}}{1-c_m^{2k_m}} \qquad [A.19]$$

and

$$\beta_m = \frac{1}{E_\theta^{(m)}}\left[\nu_\theta^{(m)} - k_m\frac{1+c_m^{2k_m}}{1-c_m^{2k_m}}\right] - \frac{1}{E_\theta^{(m+1)}}\left[\nu_\theta^{(m+1)} + k_{m+1}\frac{1+c_{m+1}^{2k_{m+1}}}{1-c_{m+1}^{2k_{m+1}}}\right] \qquad [A.20]$$

Equations A.18,A.19 and A.20 may be written in matrix form as:

$$[M]\{P\} = \{I\} \qquad [A.21]$$

Once the interface pressures have been solved, then Eqs. A.15, A.16, and A.17 can be solved to yield the stresses and the radial displacement.

A.1.3 Orthotropic Material - Plane Strain

The expressions for the stresses in a pipe (cylinder with plane strain) which has cylindrical anisotropy have the same form as Eqs. A.15, A.16, and A.17 except that

$$k = \frac{E_\theta\left(E_z - E_r\nu_{zr}^2\right)}{E_r\left(E_z - E_\theta\nu_{z\theta}^2\right)} \qquad [A.22]$$

In addition, a longitudinal stress is present which is given by the expression

$$\sigma_z = \frac{1}{E_z}\left(\frac{\nu_{rz}}{E_r}\sigma_r + \frac{\nu_{\theta z}}{E_\theta}\sigma_\theta\right) \qquad [A.23]$$

The vita has been removed from the scanned document